

**ENVIRONMENTAL FACTORS IMPACTING THE FORMATION AND
KINETICS OF FE(II) LAYERED HYDROXIDES ON MINERALS AND SOILS**

by

Autumn Nichole Starcher

A dissertation submitted to the Faculty of the University of Delaware in partial fulfillment of the requirements for the degree of Doctor of Philosophy in Plant and Soil Sciences

Summer 2016

© 2016 Autumn Nichole Starcher
All Rights Reserved

ProQuest Number: 10191230

All rights reserved

INFORMATION TO ALL USERS

The quality of this reproduction is dependent upon the quality of the copy submitted.

In the unlikely event that the author did not send a complete manuscript and there are missing pages, these will be noted. Also, if material had to be removed, a note will indicate the deletion.



ProQuest 10191230

Published by ProQuest LLC (2016). Copyright of the Dissertation is held by the Author.

All rights reserved.

This work is protected against unauthorized copying under Title 17, United States Code
Microform Edition © ProQuest LLC.

ProQuest LLC.
789 East Eisenhower Parkway
P.O. Box 1346
Ann Arbor, MI 48106 - 1346

**ENVIRONMENTAL FACTORS IMPACTING THE FORMATION AND
KINETICS OF FE(II) LAYERED HYDROXIDES ON MINERALS AND SOILS**

by

Autumn Nichole Starcher

Approved: _____
D. Janine Sherrier, Ph.D.
Chair of the Department of Plant and Soil Sciences

Approved: _____
Mark Rieger, Ph.D.
Dean of the College of Agriculture and Natural Resources

Approved: _____
Ann Ardis, Ph.D.
Senior Vice Provost for Graduate and Professional Education

I certify that I have read this dissertation and that in my opinion it meets the academic and professional standard required by the University as a dissertation for the degree of Doctor of Philosophy.

Signed:

Donald L. Sparks, Ph.D.
Professor in charge of dissertation

I certify that I have read this dissertation and that in my opinion it meets the academic and professional standard required by the University as a dissertation for the degree of Doctor of Philosophy.

Signed:

Evert J. Elzinga, Ph.D.
Member of dissertation committee

I certify that I have read this dissertation and that in my opinion it meets the academic and professional standard required by the University as a dissertation for the degree of Doctor of Philosophy.

Signed:

Clara S. Chan, Ph.D.
Member of dissertation committee

I certify that I have read this dissertation and that in my opinion it meets the academic and professional standard required by the University as a dissertation for the degree of Doctor of Philosophy.

Signed:

Angelia L. Seyfferth, Ph.D.
Member of dissertation committee

ACKNOWLEDGMENTS

Donald L. Sparks, Ph.D., for his support, resources, generosity, and encouragement to complete my research and pursue my passion for science education and outreach.

My dissertation committee, Dr. Clara Chan, Dr. Eef Elzinga, and Dr. Angelia Seyfferth, for their valuable suggestions, assistance, and encouragement in class and in my research projects.

The University of Delaware Department of Plant and Soil Science, for receiving the Donald L. and Joy G. Sparks Graduate Fellowship Award.

Jerry Hendricks, for his encouragement throughout my graduate student career and for his invaluable laboratory support.

The University of Delaware Environmental Soil Chemistry Research Group, for sharing their knowledge and expertise, for offering support and encouragement, and for being treasured friends and comrades.

Delaware Environmental Institute and staff, for their support during my graduate program.

The University of Delaware Soil Testing and the Advanced Materials Characterization Laboratories, specifically Karen Gartley, Cathy Olsen, and Jerry Poirier, for their assistance with data collection and analysis.

Dr. Ravi Kukkadapu, Dr. Wei Li, Dr. Kaumudi Pandya, and Dr. Matthew Siebecker, for their invaluable assistance with data collection, analysis, and interpretation.

Delaware Wild Lands, specifically Kate Hackett, Andrew Martin, Ronald Haas, and Stroud Water Research Center, specifically Dr. Lou Kaplan and Dr. Anthony Aufdenkampe, for access to their properties and for assistance with soil sampling.

Delaware 4-H, for the opportunity to share my passion for science with youth.

My teachers and mentors, for sharing their knowledge and love of science and for inspiring me to do the same.

My family, friends, and Penny, for always believing in me, being supportive of my aspirations, for encouraging me to try new things, and for loving me unconditionally.

TABLE OF CONTENTS

LIST OF TABLES	xi
LIST OF FIGURES	xiii
ABSTRACT	xvi
Chapter	
1 INTRODUCTION	1
1.1 Layered Double Hydroxide Formation in Soil Chemistry and Geochemistry.....	1
1.1.1 Introduction to Layered Double Hydroxides.....	3
1.1.2 Crystal Structure of Layered Double Hydroxides	4
1.1.2.1 Brucite-like layers	4
1.1.2.2 Metal Cation Substitution.....	4
1.1.2.3 Layered Double Hydroxide Interlayers	6
1.1.2.4 Layered Double Hydroxide Hydration: Intrinsic and Extrinsic Water.....	8
1.2 Wetland Soils.....	8
1.3 Iron in Anoxic Environments	9
1.4 Fe(II) Sorption Reactions	10
1.5 Dissertation Objectives.....	12
REFERENCES	15
2 FE(II) SORPTION ON PYROPHYLLITE: EFFECT OF STRUCTURAL FE(III) (IMPURITY) IN PYROPHYLLITE ON NATURE OF LAYERED DOUBLE HYDROXIDE (LDH) SECONDARY MINERAL FORMATION	28
2.1 Abstract.....	28
2.2 Introduction	29
2.3 Materials and Methods	32
2.3.1 Pyrophyllite Preparation and Characterization.....	32
2.3.2 Maintaining an Anoxic Atmosphere	33
2.3.3 Sorption Experiments	34

2.3.3.1	Macroscopic Studies.....	34
2.3.4	Fe Speciation of Sorption Samples and Fe Standards.....	35
2.3.4.1	Preparation of Fe Sorption Samples.....	35
2.3.4.2	Preparation of Fe Standards.....	36
2.3.5	Bulk Extended X-Ray Absorption Fine Structure Spectroscopy (EXAFS).....	36
2.3.6	⁵⁷ Fe Mössbauer Spectroscopy.....	38
2.4	Results.....	40
2.4.1	Pyrophyllite Characterization.....	40
2.4.2	Batch Kinetics.....	41
2.4.3	XAS Data.....	42
2.4.4	⁵⁷ Fe Mössbauer Data.....	45
2.5	Discussion.....	48
2.5.1	Spectroscopic Studies.....	48
2.5.2	Environmental Implications.....	50
REFERENCES.....		57
3	FORMATION OF A MIXED FE(II)-ZN-AL LAYERED HYDROXIDE: EFFECTS OF ZN CO-SORPTION ON FE(II) LAYERED HYDROXIDE FORMATION AND KINETICS.....	64
3.1	Abstract.....	64
3.2	Introduction.....	65
3.3	Materials and Methods.....	67
3.3.1	Mineral Characterization.....	67
3.3.2	Maintaining an Anoxic Atmosphere.....	67
3.3.3	Macroscopic Sorption Experiments.....	68
3.3.4	Speciation of Sorption Samples and Standards.....	69
3.3.4.1	Preparation of Sorption Samples.....	69
3.3.4.2	Preparation of Standards.....	70
3.3.4.3	Bulk Extended X-Ray Absorption Fine Structure Spectroscopy (EXAFS).....	71
3.4	Results.....	73

3.4.1	Sorption Kinetics	73
3.4.2	Standards Characterization	75
3.4.3	XAS Data.....	77
3.4.3.1	Fe EXAFS	77
3.4.3.2	Zn EXAFS	79
3.5	Discussion.....	82
3.5.1	Macroscopic Study	82
3.5.2	Spectroscopic Study	82
3.5.3	Environmental Implications	86
REFERENCES		97
4	INHIBITION OF FE(II)-AL-LAYERED DOUBLE HYDROXIDE PHASE FORMATION FROM REDUCTIVE DISSOLUTION OF TWO SOIL SOLUTIONS: EFFECTS OF ENVIRONMENTAL VARIABLES	103
4.1	Abstract.....	103
4.2	Introduction	104
4.3	Materials and Methods	106
4.3.1	Site Selection and Sampling Procedures	106
4.3.1.1	Great Cypress Swamp	106
4.3.1.2	Stroud Water Research Center	108
4.3.2	Soil Characterization	108
4.3.2.1	Standard Methods.....	108
4.3.2.2	Chemical Treatments to Determine Principal Forms of Soil Fe	109
4.3.2.3	X-Ray Diffraction Analysis.....	110
4.3.3	Determination of LDH Phase Formation from Reductive Dissolution of Soil Fe Species.....	110
4.3.3.1	Sorption Experiment.....	110
4.3.3.2	X-Ray Fluorescence	113
4.3.3.3	Bulk Extended X-Ray Absorption Fine Structure Spectroscopy (EXAFS)	113
4.4	Results	114

4.4.1	Soil Characterization	114
4.4.2	Chemical Extractions for Fe	115
4.4.3	XRD Data	116
4.4.4	Soil Dissolution Data.....	117
4.4.5	XRF Data.....	118
4.4.6	XAS Data.....	119
4.4.7	Visual Examination of Sorption Samples.....	119
4.5	Discussion.....	120
4.6	Environmental Implications and Future Directions	126
REFERENCES	143
5	CONCLUSIONS, ENVIRONMENTAL IMPLICATIONS, AND FUTURE DIRECTIONS	152
5.1	Introduction	152
5.2	Effects of Structural Fe(III) on Sorption Product.....	152
5.3	Effects of Sorbent Type.....	153
5.4	Effects of Potentially Competing and Complexing Elements	154
5.5	Conclusion.....	155
REFERENCES	156
Appendix		
A	SUPPORTING INFORMATION FROM CHAPTER 2.....	159
A.1	Pyrophyllite Preparation and Characterization.....	159
A.1.1	Clay Fractionation	159
A.1.2	Iron Oxide Determination.....	160
A.1.3	X-ray Diffraction Analysis	160
A.2	Accidental Oxidation.....	161
REFERENCES	172
B	PERMISSIONS	174
C	SUPPORTING INFORMATION FROM CHAPTER 4.....	182
C.1	Chemical Treatments to Determine Principal Forms of Soil Fe	182
C.2	Saturation Procedures for X-Ray Diffraction Analysis.....	183
C.3	Site Descriptions.....	183

REFERENCES 186

LIST OF TABLES

Table 2.1:	Fe K-Edge EXAFS Fitting Results of Fe(II) Sorption and Reference Samples ^a	56
Table 3.1:	Fe K-edge EXAFS fitting results of Fe(II)/Zn co-sorption and reference samples ^a	95
Table 3.2:	Zn K-edge EXAFS fitting results of Fe(II)/Zn co-sorption and reference samples ^a	96
Table 4.1:	Physicochemical properties of composite soil samples from the Great Cypress Swamp in Frankford, DE, (GCS1 and GCS2) and Stroud Water Research Center in Avondale, PA (SWRC).	128
Table 4.2:	Mehlich 3 chemical extraction concentrations for composite soils taken from the Great Cypress Swamp, Frankford, DE, (GCS1, GCS2) and Stroud Water Research Center in Avondale, PA (SWRC).....	129
Table 4.3:	DCB chemical extraction concentrations for composite soil from Stroud Water Research Center in Avondale, PA (SWRC).	129
Table 4.4:	Maximum soil solution [Fe] at 50 g/L from reductive dissolution estimated from DCB and Tamm's extractions for soils from the Great Cypress Swamp, Frankford, DE, (GCS1, GCS2) and Stroud Water Research Center in Avondale, PA (SWRC).....	131
Table 4.5:	Soil solution Fe concentrations and pH for reactions with γ -Al ₂ O ₃ solutions at the initial reaction time and final sampling point.....	134
Table 4.6:	Great Cypress Swamp (GCS1, GCS2) and Stroud Water Research Center (SWRC) soil solution elemental concentrations at reaction start.	137
Table 4.7:	Elemental concentrations of γ -Al ₂ O ₃ sorption samples after reaction with reductive dissolution soil solutions from acid digestion.	138
Table 4.8:	Elemental concentrations of γ -Al ₂ O ₃ sorption samples after reaction with reductive dissolution soil solutions from XRF.....	138

Table 4.9: Fe K-Edge EXAFS Fitting Results of γ -Al ₂ O ₃ Sorption Samples During Reductive Dissolution of SWRC soil ^a	141
Table A.1: Modeled 77 K Mössbauer spectral parameters	163
Table A.2: Results of principal component analysis performed by SixPack with the bulk-EXAFS k ³ -weighted χ functions of Fe sorption reactions with pyrophyllite for 30 minutes to 4 weeks of reaction time.....	168
Table A.3: Target transformation SPOIL values of selected standard spectra obtained by SixPack PCA with EXAFS spectra of Fe sorption reactions with pyrophyllite. SPOIL values indicate the following fits: <1.5 is excellent, 1.5-3 is good, 3-4.5 is fair, 4.5-6 is poor, and >6 is unacceptable (Malinowski, 1978).	169
Table A.4: Fit parameters determined from linear combination fits of Fe-pyrophyllite sorption samples from 3-11 Å ⁻¹ . Fits were only included if they improved the R-factor or reduced chi square by 20% (Singh and Grafe, 2010).....	170
Table C.1: Locations and site descriptions of soil samples from the Great Cypress Swamp in Frankford, DE, (GCS1 and GCS2) and Stroud Water Research Center in Avondale, PA (SWRC). Asterisks (*) indicate the field-oxidized soil samples.....	185

LIST OF FIGURES

- Figure 1.1: Fe oxidation state changes in reducing environments, known Fe(II) phases of importance, and potential factors impacting the formation of Fe(II)-Al-LDH phases in natural environments. 14
- Figure 2.1: Kinetics of Fe(II) sorption to pyrophyllite containing structural Fe impurities by a 0.8 mM Fe(II) solution and a 3 mM Fe(II) solution at pH=7.5 expressed as aqueous concentration of Fe(II) and Si where the symbols ● and ▲ denote 0.8 mM Fe(II) and 3 mM Fe(II) concentrations, respectively, while the symbols ◆ and ■ denote Si concentrations during reactions of 0.8 mM Fe(II) or 3 mM Fe(II), respectively..... 52
- Figure 2.2: Fe K edge EXAFS spectra of Fe(II) sorption samples with pyrophyllite containing structural Fe impurities reacted at pH 7.5 under anoxic conditions and of reference Fe standards. 53
- Figure 2.3: Fe K edge raw $k^3 \cdot \chi$ functions (a) and radial structure functions (RSF) (b) of Fe(II) sorption samples with pyrophyllite containing structural Fe impurities reacted at pH 7.5 under anoxic conditions and of reference Fe standards. 54
- Figure 2.4: ^{57}Fe Mössbauer spectra of a) Fe(II)-pyrophyllite 28 d sorption sample and Fe(II)-Al(III)-LDH and hydroxychloride green rust standards measured at $T = 77\text{ K}$; b) fits of 28 d sorption sample measured at $T = 77\text{ K}$; c and d) Fe(II)-pyrophyllite 28 d sorption sample and Fe(II)-Al(III)-LDH standard measured at $T = 12\text{ K}$; and e) Fe(II)-pyrophyllite 28 d and 1 d sorption samples measured at $T = 77\text{ K}$ 55
- Figure 3.1: Comparison of Fe(II) and Zn co-sorption kinetics (% relative removal) with Fe(II) sorption only to a) natural pyrophyllite containing Fe(III) impurities and b) $\gamma\text{-Al}_2\text{O}_3$. Pyrophyllite co-sorption systems contained either high (3 mM) or low (0.8 mM) Fe concentrations and 0.8 mM Zn, while $\gamma\text{-Al}_2\text{O}_3$ co-sorption systems contain 3 mM Fe(II) and 0.8 mM Zn. Fe(II)-pyrophyllite sorption data was previously reported in Starcher et al. (2016). 88

Figure 3.2: Si release during Fe(II)-Zn co-sorption and Fe(II) sorption reaction with pyrophyllite. Data from Fe(II) sorption to pyrophyllite was previously reported in Starcher et al. (2016).....	89
Figure 3.3: Powder XRD data of Fe(II)-Zn-Al layered hydroxide standard	90
Figure 3.4: Fe <i>K</i> edge raw $k^3 \cdot \chi$ functions (a) and radial structure functions (RSF) (b) of Fe(II)-Zn co-sorption samples with either pyrophyllite or γ -Al ₂ O ₃ reacted at pH 7.5 under anoxic conditions and of reference Fe standards. Diagnostic LDH “beat” pattern is circled in 3.4a.....	91
Figure 3.5: Wavelet transform (WT) analyses of Fe EXAFS data with $\eta=5.5$ and $\sigma=1$ of the first metal shell for Fe references, a) Fe(OH) ₂ , b) nikischerite, and c) Fe/Zn/Al-LDH, and Fe/Zn co-sorption samples, d) high Fe/Zn-pyrophyllite at 28 d, e) low Fe/Zn-pyrophyllite at 28 d, f) Fe/Zn- γ -Al ₂ O ₃ at 28 d, g) high Fe/Zn-pyrophyllite at 7 d, h) low Fe/Zn-pyrophyllite at 7 d, and i) Fe/Zn- γ -Al ₂ O ₃ at 7 d.	92
Figure 3.6: Zn <i>K</i> edge raw $k^3 \cdot \chi$ functions (a) and radial structure functions (RSF) (b) of Fe(II)-Zn co-sorption samples with either pyrophyllite or γ -Al ₂ O ₃ reacted at pH 7.5 under anoxic conditions and of reference Zn standards. Diagnostic LDH “beat” pattern is circled in 3.6a.....	93
Figure 3.7: Wavelet transform (WT) analyses of Zn EXAFS data with $\eta=5.5$ and $\sigma=1$ of the first metal shell for Zn references, a) Zn(OH) ₂ , b) Zn/Al-LDH, and c) Fe/Zn/Al-LDH, and Fe/Zn co-sorption samples, d) high Fe/Zn-pyrophyllite at 28 d, e) low Fe/Zn-pyrophyllite at 28 d, f) Fe/Zn- γ -Al ₂ O ₃ at 28 d, g) high Fe/Zn-pyrophyllite at 7 d, h) low Fe/Zn-pyrophyllite at 7 d, and i) Fe/Zn- γ -Al ₂ O ₃ at 7 d.	94
Figure 4.1: Soil Fe concentrations from DCB, Tamm’s reagent (acid ammonium oxalate), and Mehlich 3 chemical extraction for composite soils taken from the Great Cypress Swamp, Frankford, DE, (GCS1, GCS2) and Stroud Water Research Center in Avondale, PA (SWRC).	130
Figure 4.2: Powder XRD data of Great Cypress Swamp Sites 1 (GCS1) and 2 (GCS2) sand/silt and K ⁺ - and Mg ²⁺ -clay fractions at 298 K (RT) and 823 K.	132
Figure 4.3: Powder XRD data of Stroud Water Research Center soil sand/silt and K ⁺ - and Mg ²⁺ -clay fractions at 298 K (RT) and 823 K.	133

Figure 4.4:	Fe concentration in soil solution during reductive dissolution of soils from the Great Cypress Swamp, Frankford, DE, (GCS1, GCS2) and Stroud Water Research Center in Avondale, PA (SWRC).	135
Figure 4.5:	Change in soil solution pH during reductive dissolution of soil from the Stroud Water Research Center in Avondale, PA (SWRC).....	136
Figure 4.6:	Fe <i>K</i> edge XANES spectra of SWRC reductive dissolution and γ -Al ₂ O ₃ sorption samples	139
Figure 4.7:	Fe <i>K</i> edge raw $k^3 \cdot \chi$ functions (a) and radial structure functions (RSF) (b) of SWRC reductive dissolution and γ -Al ₂ O ₃ sorption samples and Fe standards.	140
Figure 4.8:	Image of dark precipitate formed during sorption of Stroud soil solutions to γ -Al ₂ O ₃ in dialysis tubing with the following initial reaction conditions in soil solution: a) soil present in solution, pH 7.4; b) no soil in solution, pH 7.0; and c) no soil in solution, pH 7.5.	142
Figure A.1:	Powder X-ray diffraction data of K ⁺ - (solid line) and Mg ²⁺ -saturated (dashed line) pyrophyllite at 298 K.	164
Figure A.2:	Near-edge Fe <i>K</i> edge XAS spectra of pyrophyllite (with structural Fe(III)) and the Fe(II) standards Fe(II) solution and nikischerite (an Fe(II)-Al(III)-LDH).....	165
Figure A.3:	Fe <i>K</i> edge EXAFS raw $k^3 \cdot \chi$ function of 4 week Fe(II)-Zn- γ -Al ₂ O ₃ co-sorption sample (solid black line) and its corresponding linear combination fit (dashed red line). The LCF was performed on a chi region of 3 to 10 Å ⁻¹ , and yielded an R-factor of 0.0440. Standards used in fit contain no Fe(III).....	166
Figure A.4:	Near-edge Fe <i>K</i> edge XAS spectra for the first and last (tenth) scans of Fe(II) sorption reaction with pyrophyllite at 30 minutes sample time. .	167
Figure A.5:	Fe <i>K</i> edge EXAFS raw $k^3 \cdot \chi$ functions of 3 mM Fe-pyrophyllite sorption samples (solid black lines) and their corresponding linear combination fits (dashed red lines).	171

ABSTRACT

Fe(II)-Al(III)-layered double hydroxide (LDH) phases have been shown to form from reactions of aqueous Fe(II) with Fe-free Al-bearing minerals (phyllosilicate/clays and Al-oxides); however, these phases have not been observed in the natural environment due to limited data and technical limitations on Fe(II) solid phase speciation in anoxic environments. Potential locations of Fe(II)-Al-LDH phases in nature include areas with suboxic and anoxic conditions. Because these areas can be environments of significant contaminant and nutrient accumulation, it is important to understand the possible interactions and impacts of redox-sensitive and contaminant elements on LDH phase formation. One such contaminant, Zn, can also form as an LDH and has been found to form as a mixed divalent layered hydroxide phase. The effect of small amounts of structural Fe(III) impurities in natural clays and the effect of the environmental contaminant Zn on Fe(II)-Al-LDH phase formation were examined. The potential for Fe(II)-Al-LDH phase formation from the reductive dissolution of soil Fe(II)-oxides was also examined to better understand if and how these phases may exist in the natural environment.

Understanding the kinetics and sorption products of other Al-bearing minerals becomes especially important when impurities such as Fe(III) are present in the mineral due to the changes in phase stability and redox processes that may occur. The goal of the first study was to examine the kinetics and characterize sorption products of Fe(II) sorption to an Al-bearing phyllosilicate with Fe(III) impurities in anoxic conditions. To understand the role of structural Fe(III) impurity in clay, laboratory

batch studies with pyrophyllite (10 g/L), an Al-bearing phyllosilicate, containing small amounts of structural Fe(III) impurities and 0.8 mM and 3 mM Fe(II) (both natural and enriched in ^{57}Fe) were carried out at pH 7.5 under anaerobic conditions (4% H_2 – 96% N_2 atmosphere). Samples were taken up to 4 weeks for analysis by Fe-X-ray absorption spectroscopy (XAS) and ^{57}Fe Mössbauer spectroscopy. In addition to the precipitation of Fe(II)-Al(III)-LDH phases as observed in earlier studies with pure minerals (no Fe(III) impurities in the minerals), the ^{57}Fe Mössbauer analysis indicated the formation of small amounts of Fe(III) containing solids, most probably a hybrid Fe(II)-Al(III)/Fe(III)-LDH phase. The mechanism of Fe(II) oxidation was not apparent but most likely was due to interfacial electron transfer from the sorbed Fe(II) to the structural Fe(III) and/or surface-sorption-induced electron-transfer from the sorbed Fe(II) to the clay lattice. Increase in the Fe(II)/Al ratio of the LDH with reaction time further indicated the complex nature of the samples. This research provides evidence for the formation of both Fe(II)-Al(III)-LDH and Fe(II)-Fe(III)/Al(III)-LDH-like phases during reactions of Fe(II) in systems that mimic the natural environments.

Previous studies demonstrated the formation of single divalent metal (Co-, Ni-, and Zn-Al) and mixed divalent metal (Ni-Zn-Al) layered double hydroxide (LDH) phases from reactions of the divalent metal with Al-bearing substrates and soils in both laboratory experiments and in the natural environment. Because Fe(II) ions are of similar size to the other divalent metal ions that form LDH phases, it is important to understand if and how these ions are incorporated into the LDH structure together. The objective of the second study was to examine Fe(II) and Zn co-sorption to an Al-bearing oxide and phyllosilicate to determine the effects of Zn on sorption products

and kinetics, and ultimately determine if formation of a mixed divalent metal (Fe(II)-Zn-Al-LDH) phase will form from these reactions. By understanding how Zn may interact with Fe-sorption, we can better understand natural environments in which Fe(II)-Al(III)-LDH phases may occur. To understand how Zn impacts the formation of Fe(II)-Al-LDH phase formation and kinetics, 3 mM or 0.8 mM Fe(II) and 0.8 mM Zn were batch reacted with either 10 g/L pyrophyllite or 7.5 g/L γ -Al₂O₃ for up to three months under anoxic conditions. Aqueous samples were analyzed by inductively coupled plasma optical emission spectrometry (ICP-OES) and solid samples were analyzed with XAS. Shell-by-shell fits of Fe(II) and co-sorption samples with pyrophyllite show the formation of a mixed divalent metal (Fe(II)-Zn-Al) layered hydroxide phase, while Fe(II) and Zn co-sorption samples with γ -Al₂O₃ produce Fe(II)-Al-LDH phases and Zn in inner-sphere complexation with the γ -Al₂O₃. This study demonstrates the formation of a mixed divalent metal layered hydroxide and further iterates the importance of sorbent reactivity on LDH phase formation.

Because of the technical limitations associated with analyzing bulk soils for LDH phases, the potential for Fe(II)-Al-LDH phases to form from the reductive dissolution of soil Fe was examined through a laboratory batch reaction system. Soil solutions of 50 g/L <2 mm size fraction of soil from the Great Cypress Swamp in Delaware (GCS) and the Stroud Water Research Center (SWRC) in Pennsylvania were induced into reductive dissolution inside a glovebox with inert conditions (4% H₂ – 96% N₂ atmosphere) for 21 days or more. During this time, 1 kDa MWCO dialysis tubes with 7.5 g/L γ -Al₂O₃ were submerged in the soil solution. Following the reactions, the γ -Al₂O₃ sorption samples were analyzed with X-ray diffraction (XRD), X-ray fluorescence spectrometry (XRF), XAS, and by acid digestion. The

GCS- γ - Al_2O_3 sorption samples had insufficient Fe sorption to produce usable XAS data. The low concentration of Fe released to the soil solution during reductive dissolution and low soil solution pH were not ideal conditions for LDH phase formation, as seen in other LDH work. Fe(II)-Al-LDH phases were not observed in the EXAFS spectra of SWRC- γ - Al_2O_3 sorption samples; instead, a mononuclear surface species with multiple coordination environments is the most likely sorption product formed. Other elements that complex Fe and Al or that inhibit the dissolution of γ - Al_2O_3 were also included in the sorption products, as observed by acid digestion and XRF. Because EXAFS is a bulk technique, an average of all species of the element of interest (in this case Fe) is taken. Although a mononuclear surface species is likely the dominant sorption form, other Fe phases may have formed with the complexing elements in this system, such as carbonates, P, S, Si, and organic matter. Further systematic research is required to better understand the conditions in the natural environment that are ideal for LDH phase formation.

Chapter 1

INTRODUCTION

1.1 Layered Double Hydroxide Formation in Soil Chemistry and Geochemistry

Ni-, Zn-, and Co-Al-layered double hydroxides (LDHs) have been the most studied LDH phases in soil chemistry and geochemistry (O'Day et al., 1994; Roberts et al., 2003; Scheidegger et al., 1996); however, recently, an Fe(II)-Al(III)-LDH phase was found to form from reactions of Al-oxides and clays with aqueous Fe(II) at circumneutral pH (Elzinga, 2012; Starcher et al., 2016; Zhu and Elzinga, 2014; Zhu and Elzinga, 2015). Layered double hydroxides, or LDHs, have been found to form from model reactions between divalent metals, such as Ni, Co, and Zn, and Al-bearing phyllosilicates and oxides, and they have also been found to occur naturally in the environment (Allada et al., 2006; Elzinga and Sparks, 1999, 2001; Ford and Sparks, 2000; Johnson and Glasser, 2003; Khaokaew et al., 2012; McNear et al., 2007; Nachtegaal et al., 2005; Peltier et al., 2006; Roberts et al., 2003; Scheckel and Sparks, 2000; Scheidegger et al., 1997; Scheinost and Sparks, 2000; Thompson et al., 1999; Towle et al., 1997; Trainor et al., 2000). LDHs have the general formula $\text{Me}^{\text{II}}_{1-x}\text{Al}^{\text{III}}_x(\text{OH})_2(\text{A}^{n-})_{x/n} \cdot n\text{H}_2\text{O}$, with Me being the divalent metal cation and A being one of several possible interlayer anions (de Roy et al., 2001; Reichle, 1986). The structure of LDHs consists of layered edge-sharing octahedra sheets, in which the octahedra contain a mixture of divalent and trivalent metals, and the layered sheets are separated by interlayer anions (Taylor, 1984).

LDHs generally form rapidly (on a timescale of minutes) and are thermodynamically preferred to pure metal hydroxide formation (Allada et al., 2002; Allada et al., 2005; Johnson and Glasser, 2003; McNear et al., 2007; Peltier et al., 2010; Sparks, 2003). They form at near-neutral pH with less than monolayer coverage (Scheidegger et al., 1997; Scheidegger and Sparks, 1996). This pH-range is below that required for the formation of the pure mineral hydroxide as determined by the thermodynamic solubility product (Scheidegger and Sparks, 1996). Aerobic soils that are acidic have an increase in pH due to consumption of H⁺ during Fe and Mn reduction, while those that are more basic see a decrease in pH during anoxic periods. When species change due to redox reaction in flooded soils, the pH tends to be buffered at near neutrality (Ponnamperuma, 1972; Reddy and DeLaune, 2008; Redman and Patrick, 1965). Such pH conditions are required for the formation of LDH phases.

The types of mineral sorbents used in metal sorption reactions are significant factors to consider, as their dissolution ultimately controls the Al and Si available for LDH phase formation and stabilization (Ford et al., 1999; Ford and Sparks, 2000; Johnson and Glasser, 2003; Li et al., 2012; Peltier et al., 2010; Roberts et al., 2003; Scheckel et al., 2000; Scheinost and Sparks, 2000; Scheidegger et al., 1998; Zhu and Elzinga, 2014). The rate of formation of LDH phases is controlled by dissolution of the Al-bearing substrate (Li et al., 2012; McBride, 1994; Scheidegger et al., 1998), and these phases become more stable over time due to silication of the interlayer space (Scheckel et al., 2000). With aging, these phases become less soluble, which aids in reducing contaminant mobility (Sparks, 2003).

1.1.1 Introduction to Layered Double Hydroxides

A LDH is a mineral composed of brucite-like layers separated by interlayers. Unlike brucite ($\text{Mg}(\text{OH})_2$), LDHs have mixed-valence metal cations within the layers, yielding positively charged layers. These layers are separated by charge-balancing interlayers composed of negatively charged anions and water. As a result, these minerals are considered anionic clays since most clays contain cations, rather than anions, in their interlayers (de Roy et al., 2001). LDHs have the general chemical formula $\text{Me}^{\text{II}}_{1-x}\text{Al}^{\text{III}}_x(\text{OH})_2(\text{A}^{n-})_{x/n} \cdot n\text{H}_2\text{O}$, where Me^{II} is a divalent metal cation, and A is one of several possible interlayer anions (de Roy et al., 2001; Reichle, 1986).

LDHs can form via a variety of processes. Synthetic preparation can occur through several methods. The most commonly utilized method of LDH preparation is coprecipitation from an aqueous solution containing the desired divalent and trivalent metal cations at a specified pH (de Roy et al., 2001). A two-step method of LDH preparation is induced hydrolysis, in which a trivalent metal hydroxide (precipitated during the first step of the process) is added to a divalent metal salt solution in the second step, releasing some of the trivalent metal hydroxide to form an LDH (Allman and Jepsen, 1969). Another method, the salt-oxide method, is most often used in the preparation of Zn-bearing LDHs (de Roy et al., 2001). LDH minerals are also widespread in nature and have been found to form from reactions between divalent metals, such as Ni, Co, and Zn, and Al-bearing phyllosilicates and oxides (Allada et al., 2006; Elzinga and Sparks, 1999, 2001; Ford and Sparks, 2000; Johnson and Glasser, 2003; Peltier et al., 2006; Roberts et al., 2003; Scheckel and Sparks, 2000; Scheidegger et al., 1997; Scheinost and Sparks, 2000; Thompson et al., 1999; Towle et al., 1997; Trainor et al., 2000).

1.1.2 Crystal Structure of Layered Double Hydroxides

1.1.2.1 Brucite-like layers

It is well known that LDHs are composed of positively charged brucite-like layers and interlayers composed of anions and water. The basic structure of LDHs is based on the structure of brucite ($\text{Mg}(\text{OH})_2$) in which the metal is octahedrally coordinated with the hydroxide ions and edge-sharing among the octahedra forms sheets. In this arrangement, the hydroxide ions are situated perpendicular to the plane in which the layers lie (Catti et al., 1995). The sheets stack to form a triangular lattice in which metal cations occupy holes in the octahedra between alternate pairs of hydroxide planes. As a result of this distortion in LDHs, octahedra are compressed and layer thickness is significantly decreased (Greaves and Thomas, 1986). Although distorted, the hexagonal symmetry still remains. LDH minerals, like many layered minerals, are also prone to stacking faults from weaknesses within the interlayers (Drits and Bookin, 2001).

1.1.2.2 Metal Cation Substitution

One of the most important differences between the various LDHs is substitution of cations within the layers. Within the brucite-like layers, some divalent cations are substituted with trivalent cations, giving the layers a positive charge. This positive charge is balanced by negatively charged anions and water molecules in the interlayer. The relative proportions of divalent and trivalent cations in conjunction with anions in the interlayer produces the general chemical formula Me^{II}_1 .

${}_x\text{M}^{\text{III}}{}_x(\text{OH})_2(\text{A}^{n-})_{x/n} \cdot n\text{H}_2\text{O}$, where M^{II} is a divalent metal cation, M^{III} is a trivalent metal cation, and A is one of several possible interlayer anions (de Roy et al., 2001; Reichle,

1986). Some common divalent cations are Co, Cu, Fe, Mg, Mn, Ni, and Zn, while common trivalent cations are Al, Co, Cr, Fe, Ga, Mn, and Ni (de Roy et al., 2001).

Stoichiometries for pure LDHs have been the topic of debate for some time. The general consensus is that they can only be formed for stoichiometries in the range of $0.20 < x < 0.33$ or for M^{II}/M^{III} ratios ranging from 2 to 4 (Bravo-Suárez et al., 2004a; Cavani et al., 1991; Khan and O'Hare, 2002; Takagi et al., 1999). Stoichiometries with $x > 0.33$ have been found for some LDHs; however, for $x > 0.33$, $M^{III}-O-M^{III}$ bonds would need to be formed. Such bonding is highly unlikely in most situations as a result of charge repulsion (Bellotto et al., 1996; Bourrié et al., 2004; Vucelic et al., 1997). High values of x are suggested to result from M^{II} leaching at low pH values (Alberti and Costantino, 1996; de Roy et al., 2001; Gago et al., 2004; Labajos et al., 2001; Legrand et al. 2001; Pausch et al., 1986; Thevenot et al., 1989; Tsuji et al., 1993). Values of $x < 0.20$ have also been reported (López-Salinas et al., 1997). It is expected that values outside of the $0.20 < x < 0.33$ range are most likely not a pure single LDH phase, but may contain mixtures of other M^{II} or M^{III} hydroxides or oxyhydroxides (Evans and Slade, 2006).

Determining the exact amount of each metal cation has been the primary source of difficulty in determining the range of stoichiometries for LDHs. Whenever other metal hydroxides or oxyhydroxides are present, they are detected along with the divalent and trivalent metals in LDHs during elemental analyses, producing inaccurate values of x (Bourrié et al., 2004). This is expected for values of x that fall outside of the narrow range of 0.20 to 0.33 (Evans and Slade, 2006). Other techniques, such as X-ray diffraction (XRD), Fourier-transform infrared spectroscopy (FTIR), inductively coupled plasma (ICP) spectroscopy, Mössbauer spectroscopy, and high resolution

scanning transmission electron microscopy (HRSTEM), have been successfully used to examine some LDHs but have significant limitations (Basile et al., 2003; Brindley and Kikkawa, 1979; Kaneyoshi and Jones, 1999; Kooli et al., 1996; Kumbhar et al., 2000; Pausch et al., 1986; Sanchez-Valente et al., 2000; Thevenot et al., 1989; Turco et al., 2004; Vucelic et al., 1995; Xu and Zheng, 2001; Zheng et al., 1999). These techniques depend on certain chemical properties, such as the presence of particular elements, or significant crystallinity that may not be present or available in all LDH phases.

The ability of various metal cations to form LDHs has been the topic of numerous studies. The size of the metal cation was determined to be significant. It is important that the ionic radii of the divalent and trivalent metals are similar; if the radius of any given cation is too large, then it cannot be incorporated into the LDH structure (Alberti and Costantino, 1996; de Roy et al., 2001; Khan and O'Hare, 2002; Newman and Jones, 2001; Prakash et al., 2000; Takagi et al., 1999). The common range for divalent cationic radii is 0.65 to 0.80 Å, while for trivalent cationic radii the range is 0.62 to 0.69 Å, with Al (trivalent cationic radius of 0.50 Å) being the main exception. Monovalent-trivalent and divalent-tetravalent combinations have also been observed in LDHs containing minor elements (de Roy et al., 2001).

1.1.2.3 Layered Double Hydroxide Interlayers

Another significant difference between brucite and LDHs is the presence of interlayers between the brucite-like layers of LDHs whereas brucite lacks this interlayer space. Due to the presence of interlayers, LDHs have a significantly larger basal spacing, or distance between similar faces of adjacent layers, than brucite. The spacing distance will vary depending on the types and sizes of anions in the interlayer

and the extent of hydration (Alberti and Costantino, 1996; Cavani et al., 1991; Newman and Jones, 2001). Within these interlayers are anions that balance the positive charge caused by cation substitution within the layers as well as water molecules. Some of the most common LDH interlayer anions include halides, oxo-anions, oxo- and polyoxo-metallates, anionic complexes, and organic anions (de Roy et al., 2001). The complex bonding scheme between the octahedral layers and interlayers within LDHs results from electrostatic forces and hydrogen bonding between the anions, water, and layer hydroxyl groups (Khan and O'Hare, 2002).

Due to the complex nature of interlayers, multiple techniques have been used to address the question of which anions are present and how they are arranged. Some techniques that have been utilized include XRD; Rietveld refinements; X-ray absorption spectroscopy (XAS), including extended X-ray absorption fine structure spectroscopy (EXAFS) and X-ray absorption near-edge spectroscopy (XANES); IR spectroscopy; Raman spectroscopy; nuclear magnetic resonance (NMR), including ^{13}C , ^2H , and ^{35}Cl ; Mössbauer spectroscopy; photophysical and photochemical responses; and theoretical modeling (Beaudot et al., 2001; Beaudot et al., 2004; Bellotto et al., 1996; Braithwaite et al., 1994; Costantino et al., 1999; Costantino et al., 2000; del Arco et al., 2004; Gago et al., 2004; Hansen and Koch, 1994; Hou and Kirkpatrick, 2002; Klopogge, 2005; Klopogge and Frost, 1999; Klopogge and Frost, 2001; Maxwell et al., 1999; Moggridge et al., 1994; Moggridge et al., 1995; Morlat-Thérias et al., 1999; Raki et al., 1995; Roussel et al., 2000; Simon et al., 2003; Wang et al., 2003). In a theoretical molecular model for estimating textural properties of LDHs, good agreement has been found between experimental and calculated results

for well-crystallized samples, but was less successful for poorly crystalline ones (Bravo-Suárez, 2004b).

1.1.2.4 Layered Double Hydroxide Hydration: Intrinsic and Extrinsic Water

LDHs contain water within their interlayers, but they can also have water sorbed to their external surfaces. Water within the layered double hydroxide interlayers is considered intrinsic water, while water adsorbed on external surfaces of LDHs are considered extrinsic water. The maximum amount of water that can be incorporated into interlayer spaces is $(1 - Nx/n)$ where N is the number anion-occupied sites where the anion's charge is n (Hibino and Tsunashima, 1997). In many studies, the amount of water experimentally determined has exceeded $(1 - Nx/n)$, in which it is assumed that both intrinsic and extrinsic water are present (Yun and Pinnavaia, 1995).

Intrinsic and extrinsic water are both important to the structure of LDHs. Several studies have been conducted using a variety of techniques to examine the local environment and behavior of intrinsic water within LDH interlayers. From molecular dynamics calculations, it has been determined that water molecules within interlayers behave differently than bulk water, which exhibits distorted local tetrahedral arrangements (Wang et al., 2004). Intrinsic and extrinsic water can cause a variety of swelling and sorption behaviors in LDHs, ranging from essentially no expansion and little intrinsic water replacement to significant basal spacing expansion (0.15-0.30 nm) (Hou et al., 2003).

1.2 Wetland Soils

Wetlands play a critical role in regulating the biogeochemical cycles of many elements in the natural environment, with productivity exceeding that of the terrestrial

and aquatic systems surrounding them. Due to their intermediate position between uplands and aquatic ecosystems, wetlands can function as filters of terrestrial system runoff that would otherwise directly enter aquatic ecosystems, altering element bioavailability and mobility through a number of biogeochemical processes. In this way, wetlands can serve as sinks, sources, or transformers of pollutants and nutrients, making them highly influential in the health of the other systems around them. Transformations are greatly affected by oxidation-reduction processes that occur in wetland soils, and such processes are largely responsible for the cycling of elements and changes in heavy metal availability (Reddy and DeLaune, 2008).

1.3 Iron in Anoxic Environments

Iron (Fe) is an important element in environmental systems. Cycling of Fe affects many other important elements, including sulfur, nitrogen, carbon, and phosphorus, and because of its redox capacity, it often affects the speciation of other elements, including metal(loid)s (Stumm and Sulzberger, 1992). In anoxic environments, such as wetlands and riparian zones, Fe is often present in its more soluble form, Fe(II), which is released as a result of reductive dissolution (Kirk, 2004). When soils become saturated with water, O₂ availability is depleted, resulting in the microbial use of other sources of electron acceptors. Electron acceptors follow the order of O₂ > NO₃⁻ > Fe(III)/Mn(III) > SO₄²⁻ > CO₂ to provide the greatest energy upon reduction by microbes (Reddy and DeLaune, 2008). This transformation of Fe oxidation state results in increased concentrations of soluble Fe(II) in the system initially (Kirk, 2004), followed by adsorption and precipitation of the Fe with increased time under anoxic conditions (Ponnamperuma, 1972).

Limited data exist on the solid phase speciation of Fe(II) in these environments. Species of known importance in such environments have been determined from ferrihydrite ($\text{Fe}(\text{OH})_3$) microbial reduction model reactions and include green rust ($\{\text{Fe}^{\text{II}}_{(6-x)}\text{Fe}^{\text{III}}_x(\text{OH})_{12}\}^{x+}\{\text{A}^{2-}\}_{x/2}\cdot y\text{H}_2\text{O}\}^{x-}$), ferrihydrite ($\text{Fe}(\text{OH})_3$), siderite (FeCO_3), magnetite ($\text{Fe}^{\text{II}}\text{Fe}^{\text{III}}_2\text{O}_4$), and vivianite ($\text{Fe}(\text{PO}_4)_2\cdot n\text{H}_2\text{O}$) (Abdelmoula et al., 1998; Cooper et al., 2000; Feder et al., 2005; Fredrickson et al., 1998; Hansel et al., 2003; Inskeep and Bloom, 1986; Lovley et al., 1987; Lovley and Phillips, 1988; Mortimer and Coleman, 1997; Roden and Lovley, 1993; Trolard et al., 1997; Zachara et al. 2002). Green rusts have been observed in reduced soils that undergo periodic changes in redox conditions and are considered to be important Fe(II) phases in the environment (Abdelmoula et al., 1998; Christiansen et al., 2009; Feder et al., 2005; Refait et al., 2001; Trolard et al., 1997). As green rusts are exposed to oxidizing conditions, they transform to magnetite, goethite, lepidocrocite ($\gamma\text{-FeO}(\text{OH})$), akaganeite ($\beta\text{-Fe}^{\text{III}}\text{O}(\text{OH},\text{Cl})$), ferric-green rust ($\text{Fe}^{\text{III}}_4\text{O}_3(\text{OH})_5\text{Cl}\cdot 2\text{H}_2\text{O}$), or ferrihydrite (Génin et al., 2006a, 2006b; Hansen, 2001; Refait and Génin, 1997; Refait et al., 2003; Schwertmann and Fechter, 1994). It is important that solid phase distribution of Fe(II) in wetlands be examined and better understood because of the importance of wetlands as an intermediate between terrestrial and aquatic systems (Kirk, 2004). Dissolution of Fe(III)-minerals, which can serve as sinks for metal(loid)s, could affect the mobility of the metal(loid)s in these systems.

1.4 Fe(II) Sorption Reactions

Fe(II) sorption reactions to Al-bearing substrates, including phyllosilicates and oxides, have been previously examined over a range of reaction times, pH values,

Fe(II) concentrations, and ionic strengths. Studies of Fe(II) sorption to Al-oxides (γ - Al_2O_3 and γ - AlOOH) found evidence of slow sorption processes occurring at circum-neutral pH that exhibited low sorption reversibility (Hiemstra and van Riemsdijk, 2007; Nano and Strathmann, 2006); however, reactions of Fe(II) with corundum (Al_2O_3) formed reversible adsorbed phases (Jeon et al., 2003). Greater than monolayer coverage was reported for Fe(II) sorption to γ - Al_2O_3 at near-neutral pH suggesting precipitation, even though the solution was undersaturated with respect to the formation of a pure metal hydroxide (Mikutta et al., 2009). Sorption of ferrous iron to Al-bearing phyllosilicates (nontronite and montmorillonite) was observed to increase at near-neutral pH (Jaisi et al., 2008; Schultz and Grundl, 2000). In a recent study by Elzinga (2012), it was determined by XAS that an Fe(II)-Al(III)-LDH phase forms from reactions of γ - Al_2O_3 with Fe(II) at near-neutral pH under anoxic conditions. Further evidence of LDH phase formation has been reported by XAS analysis of reaction between Fe(II) with γ - Al_2O_3 and mica-montmorillonite suspensions at $\text{pH} \geq 7.0$, while Fe(II)-phyllosilicates formed in presence of SiO_2 (Zhu and Elzinga, 2014). The study by Zhu and Elzinga (2014) highlights the importance of pH and mineral substrate solubility on the formation of LDH phases. Other studies have examined the impacts of competing or redox-sensitive elements in these systems on LDH formation (Starcher et al., 2016; Zhu and Elzinga, 2015).

In substrates that also contain structural Fe(III), electron transfer has been observed by attenuated total reflectance Fourier transform infrared spectroscopy (ATR-FTIR) and ^{57}Fe Mössbauer spectroscopy between sorbed Fe(II) and the structural Fe(III) of phyllosilicates (Merola et al., 2007; Schaefer et al., 2011). Almost complete oxidation of $^{57}\text{Fe(II)}$ to $^{57}\text{Fe(III)}$ was observed with Mössbauer spectroscopy

during sorption reactions of $^{57}\text{Fe}(\text{II})$ to goethite and hydrous ferric oxide (Silvester et al., 2005). Fe atom exchange has also been reported for reactions of $^{57}\text{Fe}(\text{II})$ with isotopically normal magnetite (Gorski et al., 2012).

Fe(II)-Al(III)-LDHs may act as a significant sink in the environment, and they could also be highly reactive towards redox-sensitive elements and divalent metals. It is essential to understand the formation of these phases because of the impact they can have on other elements, including trace metals. Anoxic soils, such as those in wetlands, frequently have nearer to neutral pH values than aerobic soils as a result of changes that occur during reductive dissolution and could lead to the formation of Fe(II)-Al(III)-LDH phases.

1.5 Dissertation Objectives

The overarching objective of this dissertation is to better understand what environmental factors may limit the formation of Fe(II)-Al-LDH phases in natural systems (Figure 1.1). Fe(II)-Al(III)-layered double hydroxide (LDH) phases have been shown to form from reactions of aqueous Fe(II) with Fe-free Al-bearing minerals (phyllosilicate/clays and Al-oxides). Understanding the kinetics and sorption products of other Al-bearing minerals becomes especially important when impurities such as Fe(III) are present in the mineral due to the changes in phase stability and redox processes that may occur. The goal of the first study was to examine the kinetics and characterize sorption products of Fe(II) sorption to an Al-bearing phyllosilicate with Fe(III) impurities in anoxic conditions.

Although Fe(II)-Al-LDHs have been observed in laboratory conditions, they have not been observed in the natural environment due to limited data and technical limitations on Fe(II) solid phase speciation in anoxic environments. Potential

locations of Fe(II)-Al-LDH phases in nature include areas with suboxic and anoxic conditions. The objective of the third study was to determine if Fe(II)-Al-LDH phases can form in natural soils using two soils with different physicochemical properties. The potential for Fe(II)-Al-LDH phase formation from the reductive dissolution of soil Fe(II)-oxides was also examined to better understand if and how these phases may exist in the natural environment.

Because wetland areas can be environments of significant contaminant and nutrient accumulation, it is important to understand the possible interactions and impacts of redox-sensitive and contaminant elements on LDH phase formation. One such contaminant, Zn, can also form as an LDH and has been found to form as a mixed divalent layered hydroxide phase. Because Fe(II) ions are of similar size to the other divalent metal ions that form LDH phases, it is important to understand if and how these ions are incorporated into the LDH structure together. The objective of the second study was to examine Fe(II) and Zn co-sorption to an Al-bearing oxide and phyllosilicate to determine the effects of Zn on sorption products and kinetics, and ultimately determine if formation of a mixed divalent metal (Fe(II)-Zn-Al-LDH) phase will form from these reactions. By understanding how Zn may interact with Fe-sorption, we can better understand natural environments in which Fe(II)-Al(III)-LDH phases may occur.

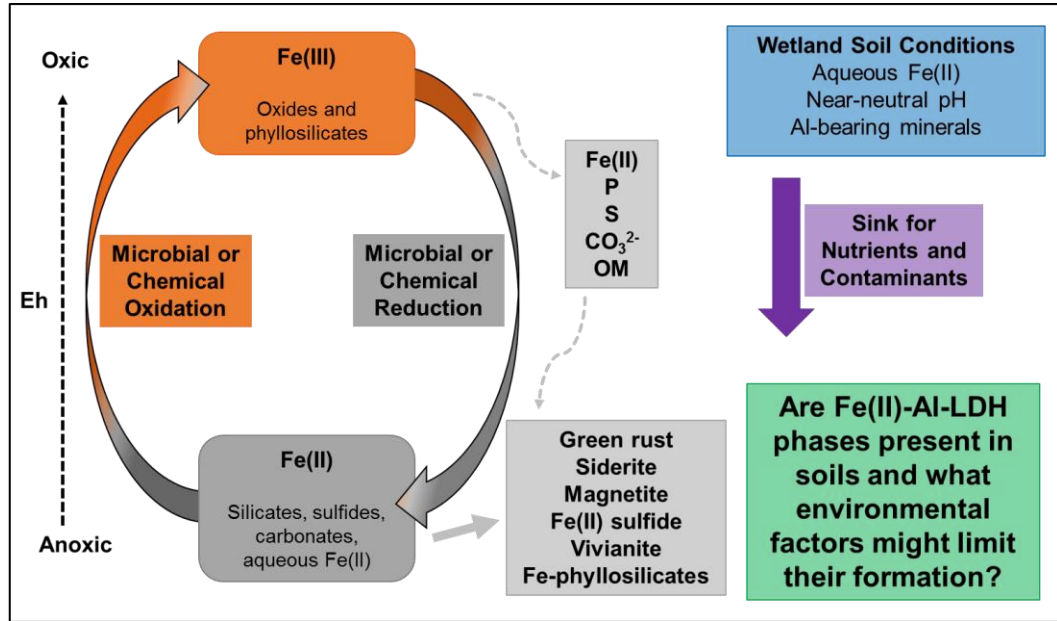


Figure 1.1: Fe oxidation state changes in reducing environments, known Fe(II) phases of importance, and potential factors impacting the formation of Fe(II)-Al-LDH phases in natural environments.

REFERENCES

- Abdelmoula, M.; Trolard, F.; Bourrie, G.; Génin, J.M.R. Evidence for the Fe(II)-Fe(III) green rust "Fougerite" mineral occurrence in a hydromorphic soil and its transformation with time and depth. *Hyperfine Interact.*, **1998**, 112:235-238; DOI 10.1023/A:1010802508927.
- Alberti, G.; Costantino, U. Solid state supramolecular chemistry: Two- and three-dimensional inorganic networks, In *Comprehensive Supramolecular Chemistry*, Vol. 7, Alberti, G.; Bein, T., Ed. Pergamon and Elsevier Science: Oxford, UK, 1996.
- Allada, R.K.; Navrotsky, A.; Berbeco, H.T.; Casey, W.H. Thermochemistry and aqueous solubilities of hydrotalcite-like solids. *Science*, **2002**, 296:721-723; DOI 10.1126/science.1069797.
- Allada, R.K.; Navrotsky, A.; Boerio-Goates, J. A thermochemistry of hydrotalcite-like phases in the MgO-Al₂O₃-CO₂-H₂O system: A determination of enthalpy, entropy, and free energy. *Am. Mineral.*, **2005**, 90:329-335; DOI 10.2138/am.2005.1737.
- Allada, R.K.; Peltier, E.; Navrotsky, A.; Casey, W.H.; Johnson, C.A.; Berbeco, H.T.; Sparks, D.L. Calorimetric determination of the enthalpies of formation of hydrotalcite-like solids and their use in the geochemical modeling of metals in natural waters. *Clay Clay Miner.*, **2006**, 54(4):409-417; DOI 10.1346/CCMN.2006.0540401.
- Allman, R.; Jepsen H.P. Die struktur des hydrotalkits. *Neues Jahrb. Mineral. Monatsh.*, **1969**, 12:544-551
- Basile, F.; Fornasari, G.; Gazzano, M.; Kiennemann, A.; Vaccari, A. Preparation and characterization of a stable Rh catalyst for the partial oxidation of methane. *J. Catal.*, **2003**, 217:245-252; DOI 0.1016/S0021-9517(03)00021-6.
- Beaudot, P.; de Roy, M.E.; Besse, J.P. Intercalation of platinum complex in LDH compounds. *J. Solid State Chem.*, **2001**, 161:332-340; DOI 10.1006/jssc.2001.9322

- Beaudot, P.; de Roy, M.E.; Besse, J.P. Preparation and characterization of intercalation compounds of layered double hydroxides with metallic oxalate complexes. *Chem. Mater.*, **2004**, 16:935-945; DOI 10.1021/cm0311067.
- Bellotto, M.; Rebours, B.; Clause, O.; Lynch, J.; Bazin, D.; Elkaïm, E. A reexamination of hydrotalcite crystal chemistry. *J. Phys. Chem.-US*, **1996**, 100:8527-8534; DOI 10.1021/jp960039j.
- Bourrié, G.; Trolard, F.; Refait, P.; Feder, F. A solid-solution model for Fe(II)-Fe(III)-Mg(II) green rusts and fougérite and estimation of their Gibbs free energies of formation. *Clay Clay Miner.*, **2004**, 52:382-394; DOI 10.1346/CCMN.2004.0520313.
- Braithwaite, R.S.W.; Dunn, P.J.; Pritchard, R.G.; Paar, W.H. Iowaite, a re-investigation. *Mineral. Mag.*, **1994**, 58:79-85; DOI 10.1180/minmag.1994.058.390.08.
- Bravo-Suárez, J.J.; Páez-Mozo, E.A.; Oyama, S.T. Microtextural properties of layered double hydroxides: a theoretical and structural model. *Micropor. Mesopor. Mat.*, **2004**, 67:1-17; DOI 10.1016/j.micromeso.2003.10.003.
- Bravo-Suárez, J.J.; Páez-Mozo, E.A.; Oyama, S.T. Models for the estimation of thermodynamic properties of layered double hydroxides: Application to the study of their anion exchange characteristics. *Quím. Nova*, **2004**, 27:601-614; DOI 10.1590/S0100-40422004000400011.
- Brindley, G.W.; Kikkawa, S. A crystal-chemical study of Mg,Al and Ni,Al hydroxyl-perchlorates and hydroxyl-carbonates. *Am. Mineral.*, **1979**, 64:836-843.
- Catti, M.; Ferraris, G.; Hull, S.; Pavese, A. Static compression and H-disorder in brucite, Mg(OH)₂, to 11 GPa – a powder neutron-diffraction study. *Phys. Chem. Miner.*, **1995**, 22:200-206; DOI 10.1007/BF00202300.
- Cavani, F.; Trifirò, F.; Vaccari, A. Hydrotalcite-type anionic clays: preparation, properties and applications. *Catal. Today*, **1991**, 11:173-301; DOI 10.1016/0920-5861(91)80068-K.
- Christiansen, B.C.; Balic-Zunic, T.; Petit, P.O.; Frandsen, C.; Morup, S.; Geckeis, H.; Katerinopoulou, A.; Stipp, S.L.S. Composition and structure of an iron-bearing, layered double hydroxide (LDH) – Green rust sodium sulphate. *Geochim. Cosmochim. Acta*, **2009**, 73:3579-3592; DOI 10.1016/j.gca.2009.03.032.

- Costantino, U.; Coletti, N.; Nocchetti, M.; Aloisi, G.G.; Elisei, F. Anion exchange of methyl orange into Zn-Al synthetic hydrotalcite and photophysical characterization of the intercalates obtained. *Langmuir*, **1999**, 15:4454-4460; DOI 10.1021/la981672u.
- Costantino, U.; Coletti, N.; Nocchetti, M.; Aloisi, G.G.; Elisei, F.; Latterini, L. Surface uptake and intercalation of fluorescein anions into Zn-Al-hydrotalcite. Photophysical characterization of materials obtained. *Langmuir*, **2000**, 16:10351-10358; DOI 10.1021/la001096d.
- Cooper, D.C.; Picardal, F.; Rivera, J.; Talbot, C. Zinc immobilization and magnetite formation via ferric oxide reduction by *Shewanella putrefaciens*. *Environ. Sci. Technol.*, **2000**, 34:100-106; DOI 10.1021/es990510x.
- de Roy, A.; Forano, C.; Besse, J.P. Layered double hydroxides: Synthesis and post-synthesis modification, In *Layered Double Hydroxides: Present and Future*, Rives, V., Ed. Nova Science Publishers, Inc.: New York, 2001.
- del Arco, M.; Gutierrez, S.; Martin, C.; Rives, V.; Rocha, J. Synthesis and characterization of layered double hydroxides (LDH) intercalated with non-steroidal anti-inflammatory drugs (NSAID). *J. Solid State Chem.*, **2004**, 177:3954-3962; DOI 10.1016/j.jssc.2004.08.006.
- Drits, V.A.; Bookin, A.S. Crystal structure and X-ray identification of layered double hydroxides, In *Layered Double Hydroxides: Present and Future*, Rives, V. Ed. Nova Science Publishers, Inc.: New York. Publishers, New York, 2001.
- Elzinga, E.J. Formation of layered Fe(II)-Al(III)-hydroxides during reaction of Fe(II) with aluminum oxide. *Environ. Sci. Technol.*, **2012**, 46:4894-4901; DOI 10.1021/es2044807.
- Elzinga, E.J.; Sparks, D.L. Nickel sorption mechanisms in a pyrophyllite-montmorillonite mixture. *J. Colloid Interface Sci.*, **1999**, 213:506-512; DOI 10.1006/jcis.1999.6161.
- Elzinga, E.J.; Sparks, D.L. Reaction condition effects on nickel sorption mechanisms in illite-water suspensions. *Soil Sci. Soc. Am. J.*, **2001**, 65:94-101; DOI 10.2136/sssaj2001.65194x.
- Evans, D.G.; Slade, R.C.T. Structural aspects of layered double hydroxides. *Struct. Bond.*, **2006**, 119:1-87; DOI 10.1007/430_005.

- Feder, F.; Trolard, F.; Klingelhöffer, G.; Bourrie, G. In situ Mössbauer spectroscopy: Evidence for green rust (fougerite) in a gleysol and its mineralogical transformations with time and depth. *Geochim. Cosmochim. Acta*, **2005**, 69:4463-4483; DOI 10.1016/j.gca.2005.03.042.
- Ford, R.G.; Scheinost, A.C.; Scheckel, K.G.; Sparks, D.L. The link between clay mineral weathering and the stabilization of Ni surface precipitates. *Environ. Sci. Technol.* **1999**, 33(18):3140-3144, DOI 10.1021/es990271d.
- Ford, R.G.; Sparks, D.L. The nature of Zn precipitates formed in the presence of pyrophyllite. *Environ. Sci. Technol.*, **2000**, 34:2479-2483; DOI 10.1021/es991330q.
- Fredrickson, J.K.; Zachara, J.M.; Kennedy, D.W.; Dong, H.L.; Onstott, T.C.; Hinman, N.W.; Li, S.M. Biogenic iron mineralization accompanying the dissimilatory reduction of hydrous ferric oxide by a groundwater bacterium. *Geochim. Cosmochim. Acta*, **1998**, 62:3239-3257; DOI 10.1016/S0016-7037(98)00243-9.
- Gago, S.; Pillinger, M.; Valente, A.A.; Santos, T.M.; Rocha, J.; Gonçalves, I.S. Immobilization of oxomolybdenum species in a layered double hydroxide pillared by 2,2'-bipyridine-5,5'-dicarboxylate anions. *Inorg. Chem.*, **2004**, 43:5422-5431; DOI 10.1021/ic049755n.
- Génin, J.-M.R.; Abdelmoula, M.; Ruby, C.; Upadhyay, C. Speciation of iron; characterization and structure of green rusts and Fe^{II-III} hydroxycarbonate fougerite. *C. R. Geosci.*, **2006**, 338:402-419; DOI 10.1016/j.crte.2006.04.005.
- Génin, J.-M.R.; Ruby, C.; Upadhyay, C. Structure and thermodynamics of ferrous, stoichiometric and ferric oxyhydroxycarbonate green rusts: redox flexibility and fougerite mineral. *Solid State Sci.*, **2006**, 8:1330-1343; DOI 10.1016/j.gca.2009.10.030.
- Gorski, C.A.; Handler, R.M.; Beard, B.L.; Pasakarnis, T.; Johnson, C.M.; Scherer, M.M. Fe atom exchange between aqueous Fe²⁺ and magnetite. *Environ. Sci. Technol.*, **2012**, 46:12399-12407; DOI 10.1021/es204649a.
- Greaves, C.; M.A. Thomas. Refinement of the structure of deuterated nickel hydroxide, Ni(OD)₂, by powder neutron diffraction and evidence for structural disorder in samples with high surface area. *Acta Crystallogr. B.*, **1986**, 42:51-55; DOI 10.1107/S0108768186098592.

- Hansel, C.M.; Benner, S.G.; Neiss, J.; Dohnalkova, A.; Kukkadapu, R.K.; Fendorf, S. Secondary mineralization pathways induced by dissimilatory iron reduction of ferrihydrite under advective flow. *Geochim. Cosmochim. Acta*, **2003**, 67:2977-2992; DOI 10.1016/S0016-7037(03)00276-X.
- Hansen, H.C.B. Environmental chemistry of iron(II)-iron(III) LDHs (green rusts), In *Layered Double Hydroxides: Present and Future*, Rives, V., Ed. Nova Science Publishers, Inc.: New York, 2001.
- Hansen, H.C.B.; Koch, C.B. Synthesis and properties of hexacyanoferrate interlayered in hydrotalcite. I. Hexacyanoferrate(II). *Clay Clay Miner.*, **1994**, 42:170-179.
- Hibino, T.; Tsunashima, A. Synthesis of paramolybdate intercalates of hydrotalcite-like compounds by ion exchange in ethanol/water solution. *Chem. Mater.*, **1997**, 9:2082-2089; DOI 10.1021/cm970115a.
- Hiemstra, T.; van Riemsdijk, W.H. Adsorption and surface oxidation of Fe(II) on metal (hydr)oxides. *Geochim. Cosmochim. Acta*, **2007**, 71:5913-5933; DOI 10.1016/j.gca.2007.09.030
- Hou, X.Q.; Kirkpatrick, R.J. Interlayer structure and dynamics of ClO₄⁻ layered double hydroxides. *Chem. Mater.*, **2002**, 14:1195-1200; DOI 10.1021/cm0107474.
- Hou, X.Q.; Bish, D.L.; Wang, S.L.; Johnston, C.T.; Kirkpatrick, R.J. Hydration, expansion, structure and dynamics of layered double hydroxides, *Am. Mineral.*, **2003**, 88:167-179; DOI 10.2138/am-2003-0120.
- Huminicki, D.M.C.; Hawthorne, F.C. The crystal structure of nikischerite, NaNaFe²⁺₆Al₃(SO₄)₂(OH)₁₈(H₂O)₁₂, a mineral of the shigaite group. *Can. Mineral.*, **2003**, 41:79-82, DOI 10.2113/gscanmin.41.1.79.
- Inskeep, W.P.; Bloom, P.R. Kinetics of calcite precipitation in the presence of water-soluble organic-ligands. *Soil Sci. Soc. Am. J.*, **1986**, 50:1167-1172; DOI 10.2136/sssaj1986.03615995005000050015x.
- Jaisi, D.P.; Liu, C.; Dong, H.; Blake, R.E.; Fein, J.F. Fe²⁺ sorption onto nontronite (Nau-2). *Geochim. Cosmochim. Acta*, **2008**, 72:5361-5371; DOI 10.1016/j.gca.2008.08.022.
- Jeon, B.H.; Dempsey, B.A.; Burgos, W.D. Kinetics and mechanisms for reactions of Fe(II) with iron(III) oxides. *Environ. Sci. Technol.*, **2003**, 37:3309-3315; DOI 10.1021/es025900p.

- Johnson, C.A.; Glasser, F.P. Hydrotalcite-like minerals ($M_2Al(OH)_6(CO_3)_{0.5}.XH_2O$ where M)Mg, Zn, Co, Ni) in the environment: synthesis, characterization and thermodynamic stability. *Clay Clay Miner.*, **2003**, 51:1–8; DOI 10.1346/CCMN.2003.510101.
- Kaneyoshi, M.; Jones, W. Formation of Mg-Al layered double hydroxides intercalated with nitrilotriacetate anions. *J. Mater. Chem.*, **1999**, 9:805-811; DOI 10.1039/A808415G.
- Khan, A.I.; O'Hare, D. Intercalation chemistry of layered double hydroxides: recent developments and applications. *J. Mater. Chem.*, **2002**, 12:3191-3198; DOI 10.1039/b204076j.
- Kirk, G. *The Biogeochemistry of Submerged Soils*. John Wiley & Sons, Ltd: Chichester, 2004.
- Kloprogge, J.T. (ed). *The Application of Vibrational Spectroscopy to Clay Minerals and Layered Double Hydroxides*. Clay Minerals Society: Aurora, CO, 2005.
- Kloprogge, J.T.; Frost, R.L. Fourier transform infrared and Raman spectroscopic study of the local structure of Mg-, Ni-, and Co-hydrotalcites. *J. Solid State Chem.*, **1999**, 146:506-515; DOI 10.1006/jssc.1999.8413.
- Kloprogge, J.T.; Frost, R.L. Infrared and Raman spectroscopic studies of layered double hydroxides (LDHs), In *Layered Double Hydroxides: Present and Future*, Rives, V., Ed., Nova Science Publishers, Inc.: New York, 2001.
- Kooli, F.; Chisem, I.C.; Vucelic, M.; Jones, W. Synthesis and properties of terephthalate and benzoate intercalates of Mg-Al layered double hydroxides possessing varying layer charge. *Chem. Mater.*, **1996**, 8:1969-1977; DOI 10.1021/cm960070y.
- Kumbhar, P.S.; Sanchez-Valente, J.; Millet, J.M.M.; Figueras, F. Mg-Fe hydrotalcite as catalyst for reduction of aromatic nitro compounds with hydrazine hydrate. *J. Catal.*, **2000**, 191:467-473; DOI 10.1006/jcat.2000.2827.
- Labajos, F.M.; Sánchez-Montero, M.J.; Holgado, M.J.; Rives, V. Thermal evolution of V(III)-containing layered double hydroxides. *Thermochim. Acta*, **2001**, 370:99-104; DOI 10.1016/S0040-6031(00)00780-2.
- Legrand, L.; Abdelmoula, M.; Géhin, A.; Chaussé, A.; Génin, J.M.R. Electrochemical formation of a new Fe(II)-Fe(III) hydroxy-carbonate green rust: Characterisation and morphology. *Electrochim. Acta*, **2001**, 46:18151822; DOI 10.1016/S0013-4686(00)00728-3.

- Li, W.; Livi, K.J.; Xu, W.; Siebecker, M.G.; Wang, Y.; Phillips, B.L.; Sparks, D.L. Formation of crystalline Zn-Al layered double hydroxide precipitates on γ -alumina: the role of mineral dissolution. *Environ. Sci. Technol.*, **2012**, 46(21):11670-11677, DOI 10.1021/es3018094.
- López-Salinas, E.; García-Sánchez, M.; Montoya, J.A.; Acosta, D.R.; Abasolo, J.A.; Schifter, I. Structural characterization of synthetic hydrotalcite-like $[\text{Mg}_{1-x}\text{Ga}_x(\text{OH})_2](\text{CO}_3)_{x/2}\cdot m\text{H}_2\text{O}$. *Langmuir*, **1997**, 13:4748-4753; DOI 10.1021/la970192k.
- Lovley, D.R.; Phillips, E.J.P. Novel mode of microbial energy metabolism: Organic carbon oxidation coupled to dissimilatory reduction of iron or manganese. *Applied Env. Microbiol.*, **1988**, 54:1472-1480.
- Lovley, D.R.; Stolz, J.F.; Nord Jr., G.L.; Phillips, E.J.P. Anaerobic production of magnetite by a dissimilatory iron-reducing microorganism. *Nature*, **1987**, 330:252-254; DOI 10.1038/330252a0.
- Maxwell, R.S.; Kukkadapu, R.K.; Amonette, J.E.; Cho, H. ^2H solid-state NMR investigation of terephthalate dynamics and orientation in mixed-anion hydrotalcite-like compounds. *J. Phys. Chem. B*, **1999**, 103:5197-5203; DOI 10.1021/jp990459j.
- McBride, M.B. *Environmental Chemistry of Soils*. Oxford University Press: New York, 1994.
- McNear, D.H.; Chaney, R.L.; Sparks, D.L. The effects of soil type and chemical treatment on nickel speciation in refinery enriched soils: A multi-technique investigation. *Geochim. Cosmochim. Acta*, **2007**, 71(9):2190–2208; DOI 10.1016/j.gca.2007.02.006.
- Merola, R.B.; Fournier, E.D.; McGuire, M.M. Spectroscopic investigations of Fe^{2+} complexation on nontronite clay. *Langmuir*, **2007**, 23:1223-1226; DOI 10.1021/la062467e.
- Mikutta, C.; Wiederhold, J.G.; Cirpka, O.A.; Hoffstetter, T.B.; Bourdon, B.; Von Gunten, U. Iron isotope fractionation and atom exchange during sorption of ferrous iron to mineral surfaces. *Geochim. Cosmochim. Acta*, **2009**, 73:1795-1812; DOI 10.1016/j.gca.2009.01.014.
- Moggridge, G.D.; Parent, P.; Tourillon, G. A NEXAFS study of the orientation of benzoate intercalated into a layer double hydroxide. *Clay Clay Miner.*, **1994**, 42:462-472.

- Moggridge, G.D.; Parent, P.; Tourillon, G. A NEXAFS study of the orientation of benzoate intercalated into a layer double hydroxide. *Physica B*, **1995**, 209:269-270; DOI 10.1016/0921-4526(94)00843-K.
- Morlat-Thérias, S.; Mousty, C.; Palvadeau, P.; Molinié, P.; Léone, P.; Rouxel, J., Taviot-Guého, C.; Ennaoui, A.; de Roy, A.; Besse, J.P. Concomitant intercalation and decomplexation of ferrocene sulfonates in layered double hydroxide. *J. Solid State Chem.*, **1999**, 144:143-151; DOI 10.1006/jssc.1999.8134.
- Mortimer, R.J.G.; Coleman, M.L. Microbial influence on the oxygen isotopic composition of diagenetic siderite. *Geochim. Cosmochim. Acta*, **1997**, 61:1705-1711; DOI 10.1016/S0016-7037(97)00027-6.
- Nano, G.V.; Strathmann, T.J. Ferrous iron sorption by hydrous metal oxides. *J. Colloid Interface Sci.*, **2006**, 297:443-454; DOI 10.1016/j.jcis.2005.11.030.
- Newman, S.P.; Jones, W. Layered double hydroxides as templates for the formation of supramolecular structures, In *Supramolecular Organization and Materials Design*, Jones, W.; Rao, C.N.R., Eds. Cambridge University Press: Cambridge, UK, 2001.
- O'Day, P. A.; Rehr, J. J.; Zabinsky, S. I.; Brown, G. E. Extended X-ray absorption fine structure (EXAFS) analysis of disorder and multiple-scattering in complex crystalline solids. *J. Am. Chem. Soc.*, **1994**, 116:2938-2949, DOI 10.1021/ja00086a026.
- Pausch, I.; Lohse, H.H.; Schürmann, K.; Allmann, R. Synthesis of disordered and Al-rich hydrotalcite-like compounds. *Clay Clay Miner.*, **1986**, 34:507-510.
- Peltier, E.; Allada, R.; Navrotsky, A.; Sparks, D. L. Nickel solubility and precipitation in soils: A thermodynamic study. *Clay Clay Miner.* **2006**, 54(2):153-164; DOI 10.1346/CCMN.2006.0540202.
- Peltier, E.; Van Der Lelie, D.; Sparks, D.L. Formation and stability of Ni-Al hydroxide phases in soils. *Environ. Sci. Technol.*, **2010**, 44:302-308; DOI 10.1021/es902332b.
- Ponnamperuma, F. N. The chemistry of submerged soils. *Adv. Agron.* **1972**, 24:29-96.
- Prakash, A.S.; Kamath, P.V.; Hedge, M.S. Synthesis and characterization of the layered double hydroxides of Mg with Cr. *Mater. Res. Bull.*, **2000**, 35:2189-2197; DOI 10.1016/S0025-5408(00)00419-0.

- Raki, L.; Rancourt, D.G.; Detellier, C. Preparation, characterization, and Mössbauer spectroscopy of organic anion intercalated pyroaurite-like layered double hydroxides. *Chem. Mater.*, **1995**, 7:221-224; DOI 10.1021/cm00049a034.
- Reddy, K.R.; DeLaune, R.D. *Biogeochemistry of Wetlands: Science and Applications*. Taylor & Francis Group, LLC: Boca Raton, 2008.
- Redman, F.H.; Patrick, Jr, W.H. *Effects of Submergence on Several Biological and Chemical Properties*. Agricultural Experiment Station, Louisiana State University, Bulletin No. 592, 1965, pp. 1-28.
- Refait, P.; Abdelmoula, M.; Trolard, F.; Génin, J.M.R.; Ehrhardt, J.J.; Bourrié G. Mössbauer and XAS study of green rust mineral; the partial substitution of Fe²⁺ by Mg²⁺. *Am. Mineral.*, **2001**, 86:731-739; DOI 10.2138/am-2001-5-613.
- Refait, P.; Benali, O.; Abdelmoula, M.; Génin, J.-M.R. Formation of “ferric green rust” and/or ferrihydrite by fast oxidation of iron(II-III) hydroxychloride green rust. *Corros. Sci.*, **2003**, 45(11):2435-2449; DOI 10.1016/S0010-938X(03)00073-8.
- Refait, P.; Génin, J.-M.R. The mechanisms of oxidation of ferrous hydroxychloride β -Fe₂(OH)₃Cl in aqueous solution: The formation of akaganeite vs goethite. *Corros. Sci.*, **1997**, 39:539-553; DOI 10.1016/S0010-938X(97)86102-1.
- Reichle, W.T. Synthesis of anionic clay-minerals (mixed metal-hydroxides, hydroxalcite). *Solid State Ionics*, **1986**, 22:135-141; DOI 10.1016/0167-2738(86)90067-6.
- Roberts, D.R.; Ford, R.G.; Sparks, D.L. Kinetics and mechanisms of Zn complexation on metal oxides using EXAFS spectroscopy. *J. Colloid Interface Sci.*, **2003**, 263:364-376; DOI 10.1016/S0021-9797(03)00281-9.
- Roden, E.E.; Lovley, D.R. Dissimilatory Fe(III) reduction by the marine microorganism *Desulfuromonas acetoxidans*. *Applied Env. Microbiol.*, **1993**, 59:734-742.
- Roussel, H.; Briois, V.; Elkaïm, E.; de Roy, A.; Besse, J.P. Cationic ordering and structure of [Zn-Cr-Cl] and [Cu-Cr-Cl] layered double hydroxides: A XRD and EXAFS study. *J. Phys. Chem. B*, **2000**, 104:59150-5923; DOI 10.1021/jp0000735.

- Sanchez-Valente, J.; Millet, J.M.M.; Figueras, F.; Fournes, L. Mössbauer spectroscopic study of iron containing hydrotalcite catalysts for the reduction of aromatic nitro compounds. *Hyperfine Interact.*, **2000**, 131:43-50; DOI 10.1023/A:1011047324479.
- Schaefer, M.V.; Gorski, C.A.; Scherer, M.M. Spectroscopic evidence for interfacial Fe(II)-Fe(III) electron transfer in a clay mineral. *Environ. Sci. Technol.*, **2011**, 45:540-545, DOI 10.1021/es102560m.
- Scheckel, K.G.; Scheinost, A.C.; Ford, R.G.; Sparks, D.L. Stability of layered Ni hydroxide surface precipitates: A dissolution kinetics study. *Geochim. Cosmochim. Acta*, **2000**, 64(16):2727–2735, DOI 10.1016/S0016-7037(00)00385-9.
- Scheckel, K.G.; Sparks, D.L. Kinetics of the formation and dissolution of Ni precipitates in a gibbsite/amorphous silica mixture. *J. Colloid Interface Sci.*, **2000**, 229(1):222-229, DOI 10.1006/jcis.2000.7001.
- Scheidegger, A.M.; Lamble, G.M.; Sparks, D.L. Investigation of Ni sorption on pyrophyllite: An XAFS study. *Environ. Sci. Technol.*, **1996**, 30:548-554, DOI 10.1021/es950293+.
- Scheidegger, A.M.; Sparks, D.L. Kinetics of the formation and the dissolution of nickel surface precipitates on pyrophyllite. *Chem. Geol.* **1996**, 132:157-164, DOI 10.1016/S0009-2541(96)00051-4.
- Scheidegger, A.M.; Strawn, D.G.; Lamble, G.M.; Sparks, D.L. The kinetics of mixed Ni-Al hydroxide formation on clay and aluminum oxide minerals: a time-resolved XAFS study. *Geochim. Cosmochim. Acta*, **1998**, 62(13):2233-2245, DOI 10.1016/S0016-7037(98)00136-7.
- Scheidegger, A.M.; Lamble, G.M.; Sparks, D.L. Spectroscopic evidence for the formation of mixed-cation hydroxide phases upon metal sorption on clays and aluminum oxides. *J. Colloid Interface Sci.*, **1997**, 186:118-128; DOI 10.1006/jcis.1996.4624.
- Scheinost, A.C.; Sparks, D.L. Formation of layered single- and double-metal hydroxides precipitates at the mineral/water interface: A multiple-scattering XAFS analysis. *J. Colloid Interface Sci.*, **2000**, 223:167-178, DOI 10.1006/jcis.1999.6638.
- Schultz, C.A.; Grundl, T. pH dependence on reduction rate of 4-Cl-nitrobenzene by Fe(II)/montmorillonite systems. *Environ. Sci. Technol.*, **2000**, 34:3641-3648; DOI 10.1021/es990931e.

- Schwertmann, U.; Fechter, H. The formation of green rust and its transformation to lepidocrocite. *Clay Miner.*, **1994**, 29:87-92; DOI 10.1180/claymin.1994.029.1.10.
- Silvester, E.; Charlet, L.; Tournassat, C.; Géhin, A.; Grenèche, J.M.; Liger, E. Redox potential measurements and Mössbauer spectrometry of Fe^{II} adsorbed onto Fe^{III}(oxyhydr)oxides. *Geochim. Cosmochim. Acta*, **2005**, 69(20):4801-4815; DOI 10.1016/j.gca.2005.06.013.
- Simon, L.; François, M.; Refait, P.; Renaudin, G.; Lelaurin, M.; Génin, J.M.R. Structure of the Fe^(II-III) layered double hydroxysulphate green rust two from Rietveld analysis. *Solid State Sci.*, **2003**, 5:327-334; DOI 10.1016/S1293-2558(02)00019-5.
- Sparks, D.L. *Environmental soil chemistry*. 2nd ed. Academic Press, San Diego, CA, 2003.
- Starcher, A.N.; Elzinga, E.J.; Kukkadapu, R.K.; Sparks, D.L. Evidence for the formation of Fe-layered hydroxides using spectroscopic techniques. 251st American Chemical Society National Meeting and Exposition, San Diego, CA, March 13-17, **2016**, poster presentation.
- Stumm, W.; Sulzberger, B. The cycling of iron in natural environments considerations based on laboratory studies of heterogeneous redox processes. *Geochim. Cosmochim. Acta*, **1992**, 56:3233-3257; DOI 10.1016/0016-7037(92)90301-X.
- Takagi, K.; Saito, N.; Shichi, T.; Sawaki, Y. Intercalation of aliphatic carboxylates in hydrotalcite interlayers: Selective photochemical hydrogen abstraction by benzophenonecarboxylate. *Chem. Lett.*, **1999**, 4:275-276, DOI 10.1246/cl.1999.275.
- Taylor, R.M. The rapid formation of crystalline double hydroxy salts and other compounds by controlled hydrolysis. *Clay Minerals*, **1984**, 19:591-603; DOI 10.1180/claymin.1984.019.4.06.
- Thevenot, F.; Szymanski, R.; Chaumette, P. Preparation and characterization of Al-rich Zn-Al Hydrotalcite-like compounds. *Clay Clay Miner.*, **1989**, 37:396-402; DOI 10.1346/CCMN.1989.0370502.
- Thompson, H.A.; Parks, G.A.; Brown, G.E. Dynamic interactions of dissolution, surface adsorption, and precipitation in an aging cobalt(II)-clay-water system. *Geochim. Cosmochim. Acta*, **1999**, 63:1767-1779, DOI 10.1016/S0016-7037(99)00125-8.

- Towle, S.N.; Bargar, J.R.; Brown, G.E.; Parks, G.A. Surface precipitation of Co(II)(aq) on Al₂O₃. *J. Colloid Interface Sci.*, **1997**, 187:62-82, DOI 10.1557/PROC-432-237.
- Trainor, T.P.; Brown, G.E.; Parks, G.A. Adsorption and precipitation of aqueous Zn(II) on alumina powders. *J. Colloid Interface Sci.*, **2000**, 231:359-372; DOI 10.1006/jcis.2000.7111.
- Trolard, F.; Génin, J.M.R.; Abdelmoula, M.; Bourrié, G.; Humbert, B.; Herbillon A. Identification of a green rust mineral in a reductomorphic soil by Mössbauer and Raman spectroscopies. *Geochim. Cosmochim. Acta*, **1997**, 61:1107-1111, DOI 10.1016/S0016-7037(96)00381-X.
- Tsuji, M.; Mao, G.; Yoshida, T.; Tamaura, Y. Hydrotalcites with an extended Al³⁺-substitution: Synthesis, simultaneous TG-DTA-MS study, and their CO₂ adsorption behaviors. *J. Mater. Res.*, **1993**, 8:1137-1142; DOI 10.1557/JMR.1993.1137.
- Turco, M.; Bagnasco, G.; Costantino, U.; Marmottini, F.; Montanari, T.; Ramis, G.; Busca, G. Production of hydrogen from oxidative steam reforming of methanol: I. Preparation and characterization of Cu/ZnO/Al₂O₃ catalysts from a hydrotalcite-like LDH precursor. *J. Catal.*, **2004**, 228:43-55; DOI 10.1016/j.jcat.2004.08.026.
- Vucelic, M.; Jones, W.; Moggridge, G.D. Cation ordering in synthetic layered double hydroxides. *Clay Clay Miner.*, **1997**, 45:803-813.
- Vucelic, M.; Moggridge, G.D.; Jones, W. Thermal properties of terephthalate- and benzoate-intercalated LDH. *J. of Phys. Chem.-US*, **1995**, 99:8328-8337; DOI 10.1021/j100020a068.
- Wang, J.W.; Kalinichev, A.G.; Amonette, J.E.; Kirkpatrick, R.J. Interlayer dynamics in Cl-hydrotalcite: far-infrared spectroscopy and molecular dynamics modeling. *Am. Mineral.*, **2003**, 88:398-409; DOI 10.1016/j.gca.2005.10.006.
- Wang, J.; Kalinichev, A.G.; Kirkpatrick, R.J. Molecular modeling of water structure in nano-pores between brucite (001) surfaces. *Geochim. Cosmochim. Acta*, **2004**, 68:3351-3365; DOI 10.1016/j.gca.2004.02.016.
- Xu, Z.P.; Zheng, H.C. Abrupt structural transformation in hydrotalcite-like compounds Mg_{1-x}Al_x(OH)₂(NO₃)_x·nH₂O as a continuous function of nitrate anions. *J. Phys. Chem. B*, **2001**, 105:1743-1749; DOI 10.1021/jp0029257.

- Yun, S.K.; Pinnavaia, T.J. Water content and particle texture of synthetic hydrotalcite-like layered double hydroxides. *Chem. Mater.*, **1995**, 7:348-354; DOI 10.1021/cm00050a017.
- Zachara, J.M.; Kukkadapu, R.K.; Fredrickson, J.K.; Gorby, Y.A.; Smith, S.C. Biomineralization of poorly crystalline Fe(III) oxides by dissimilatory metal reducing bacteria (DMRB). *Geomicrobiol. J.*, **2002**, 19:179-207; DOI 10.1080/01490450252864271.
- Zheng, H.C.; Xu, Z.P.; Qian, M. Synthesis of non-Al-containing hydrotalcite-like compounds $Mg_{0.3}Co^{(II)}_{0.6}Co^{(III)}_{0.2}(OH)_2(NO_3)_{0.2}\cdot H_2O$. *Chem. Mater.*, **1998**, 10:2277-2283; DOI 10.1021/cm9802503.
- Zhu, Y.; Elzinga, E.J. Formation of layered Fe(II)-hydroxides during Fe(II) sorption onto clay and metal-oxide substrates. *Environ. Sci. Technol.*, **2014**, 48:4937-4945, DOI 10.1021/es500579p.
- Zhu, Y.; Elzinga, E.J. Macroscopic and spectroscopic assessment of the cosorption of Fe(II) with As(III) and As(V) on Al-oxide. *Environ. Sci. Technol.*, **2015**, 49:13369-13377; DOI 10.1021/acs.est.5b04525.

Chapter 2

FE(II) SORPTION ON PYROPHYLLITE: EFFECT OF STRUCTURAL FE(III) (IMPURITY) IN PYROPHYLLITE ON NATURE OF LAYERED DOUBLE HYDROXIDE (LDH) SECONDARY MINERAL FORMATION

2.1 Abstract

Fe(II)-Al(III)-LDH (layered double hydroxide) phases have been shown to form from reactions of aqueous Fe(II) with Fe-free Al-bearing minerals (phyllosilicate/clays and Al-oxides). To our knowledge, however, the effect of small amounts of structural Fe(III) in natural clays on such reactions were not studied. In this study to understand the role of structural Fe(III) in clay, laboratory batch studies with pyrophyllite (10 g/L), an Al-bearing phyllosilicate, containing small amounts of structural Fe(III) and 0.8 mM and 3 mM Fe(II) (both natural and enriched in ^{57}Fe) were carried out at pH 7.5 under anaerobic conditions (4% H_2 – 96% N_2 atmosphere). Samples were taken up to 4 weeks for analysis by Fe-X-ray absorption spectroscopy and ^{57}Fe Mössbauer spectroscopy. In addition to the precipitation of Fe(II)-Al(III)-LDH phases as observed in earlier studies with pure minerals (no Fe(III) impurities in the minerals), the analyses indicated the formation of small amounts of Fe(III) containing solids, most probably a hybrid Fe(II)-Al(III)/Fe(III)-LDH phase. The mechanism of Fe(II) oxidation was not apparent but most likely was due to either interfacial electron transfer from the spiked Fe(II) to the structural Fe(III) and/or surface-sorption-induced electron-transfer from the sorbed Fe(II) to the clay lattice. This research provides evidence for the formation of both Fe(II)-Al(III)-LDH and

Fe(II)-Fe(III)/Al(III)-LDH-like phases during reactions of Fe(II) in systems that mimic the natural environments. Better understanding Fe phase formation in complex laboratory studies will improve models of natural redox systems.

2.2 Introduction

A layered double hydroxide (LDH) is a mineral composed of brucite-like octahedral layers separated by interlayers. Unlike brucite ($\text{Mg}(\text{OH})_2$), LDHs have mixed-valence metal cations within the layers due to the substitution of trivalent cations for divalent cations, yielding positively charged layers. These layers are separated by charge balancing interlayers containing negatively charged anions and water. These minerals are referred to as “anionic clays” because they hold exchangeable anions, whereas common phyllosilicates, such as smectite and vermiculite, contain interlayer cations (de Roy et al., 2001). LDHs have the general chemical formula $[\text{M}^{\text{II}}_{1-x}\text{M}^{\text{III}}_x(\text{OH})_2]_x^+[\text{A}^{n-}]_{x/n}\cdot y\text{H}_2\text{O}$, where M^{II} is a divalent metal cation, M^{III} is a trivalent metal cation, and A is one of several possible interlayer anions (de Roy et al., 2001; Reichle, 1986). In most soil and environmentally relevant systems, the trivalent metal cation is Al(III) derived from dissolution of Al-oxides and phyllosilicates. The most common LDH interlayer anion in nature is carbonate; however, other interlayer anions include chloride, nitrate, sulfate, and silicate (de Roy et al., 2001).

Layered double hydroxides occur naturally in soils (Jacquat et al., 2008; Juillot et al., 2003; McNear et al., 2007; Nachtegaal et al., 2005; Voegelin and Kretzschmar 2005). Numerous laboratory studies have shown that LDHs, particularly Fe(II)/Fe(III)-containing, e.g., green rusts, are very reactive towards contaminants (Abdelmoula et al., 1998; Christiansen et al., 2009; Feder et al., 2005; Génin et al.,

2001; Refait et al., 2001; Trolard et al., 1997). In laboratory systems, LDH precipitates have been found to form rapidly from reactions between divalent metals (e.g. Ni, Co, and Zn) and Al-mineral substrates (Ford and Sparks, 2000; Roberts et al., 2003; Scheidegger et al., 1996; Scheidegger et al., 1998; Thompson, et al., 1999; Towle et al., 1997). The kinetics and mechanisms of Fe containing LDH formation, however, under conditions reflective of natural systems are not known. Recently, Elzinga's laboratory (Elzinga, 2012; Zhu and Elzinga, 2014) reported precipitation of Fe(II)-Al(III)-LDH in synthetic γ -Al₂O₃/mica-montmorillonite systems containing [Fe(II)] and circumneutral pHs typical of natural systems. The rapid and extensive formation of these secondary Fe(II) phases suggest that they could be important sinks of Fe(II) in suboxic and anoxic environments, such as wetland soils and sediments.

A factor that has not been considered in these previous studies is the potential impact of structural Fe(III) impurities inside clay sorbents on the precipitation of secondary Fe(II) phases during sorption. Substitution of Fe(III) impurities is ubiquitous in natural clays (Sparks, 2003). These impurities may significantly impact spiked Fe(II) and clay interactions. An understanding of the role Fe in these minerals on the nature of LDH (if any formed), hence, is critical in predicting interplay of Fe redox on LDH formation. This is important because of the possibility of oxidation of spiked Fe(II) by structural Fe(III) via interfacial electron transfer mechanism, as noted in Fe(III)-rich clay systems (Merola et al., 2007; Schaefer et al., 2011) and/or the potential for surface-sorption-induced electron transfer oxidation as noted in synthetic Fe-free clay (Géhin et al., 2007) on the nature of the secondary LDH mineral product.

Another factor that needs to be considered is the effect of time on the nature of the products. Kinetic studies on Co(II)-, Zn(II)-, and Ni(II)-LDH phases formed on

phyllosilicate and Al-oxide substrates have shown increased stability of those precipitates during aging over the course of weeks to months due to Ostwald ripening and silica substitution and polymerization in the anion interlayers (Ford et al. 1999; Ford and Sparks, 2000; Scheckel et al., 2000; Scheckel and Sparks, 2001; Scheckel and Sparks, 2000; Scheidegger and Sparks, 1996; Scheinost et al. 1999; Thompson et al., 1999). Similar processes will likely cause time-dependent changes in the structure of Fe(II)-Al(III)-LDHs as well, but the extent and rate at which these mechanisms operate for Fe(II) phases remain to be determined.

Understanding the kinetics and sorption products of other Al-bearing minerals becomes especially important when impurities such as Fe(III) are present in the mineral due to the changes in phase stability and redox processes that may occur. The goal of this study was to examine the kinetics and characterize sorption products of aqueous Fe(II) and an Al-bearing phyllosilicate with Fe(III) impurities in anoxic conditions. To address these issues, a reference natural pyrophyllite (a 2:1 Al-Si non-expandable phyllosilicate) containing small amounts of Fe(III) “impurity” was reacted with Fe(II) at circumneutral pH under strict anoxic conditions to gain insights into the potential effects of 1) electron transfer between spiked Fe(II) and Fe(III) in the clay, as noted in a Fe(III)-rich clay (Schaefer et al., 2011), 2) surface-sorption-induced electron-transfer oxidation of spiked Fe(II) by the clay lattice, as noted in a synthetic Fe-free pure clay system (Géhin et al., 2007), and 3) clay weathering on the nature of the products. The sorption products were then characterized by Fe-XAS and ⁵⁷Fe Mössbauer spectroscopy. Our study has shown that structural Fe(III) plays a significant role in LDH formations.

2.3 Materials and Methods

2.3.1 Pyrophyllite Preparation and Characterization

Pyrophyllite from Hillsboro, NC, (Ward Natural Science, 46E6430) was used in this study. The pyrophyllite was prepared similar to the method given in Scheidegger et al. (1996) using centrifuge parameters calculated by Jackson (1985) and Gee and Or (2002). To quantify Fe in the pyrophyllite sample that was not in the pyrophyllite structure (i.e. adsorbed Fe or Fe oxides), the pyrophyllite was treated with sodium dithionite-citrate-bicarbonate (Na-DCB) to extract any Fe oxides (Kunze and Dixon, 1986). To determine the total Fe concentration, the untreated pyrophyllite samples were microwave digested in a CEM Mars 5 microwave digestion oven and analyzed by inductively coupled plasma optical emission spectrometry (ICP-OES) by the University of Delaware Soil Testing Laboratory according to procedures in United States Environmental Protection Agency (USEPA) Method 3051 (USEPA, 2007a). Detailed methods for pyrophyllite clay fractionation, X-ray diffraction analysis, and iron oxide determination are provided in the Supporting Information (Appendix A). Microwave digestions of the untreated pyrophyllite indicated a 429 mg Fe per kg pyrophyllite sample concentration, showing the presence of Fe impurities within the pyrophyllite sample. From the ICP analysis of the pyrophyllite Na-DCB extractant, it was determined that the 0.005 Wt% of the pyrophyllite sample was a Na-DCB extractable Fe oxide, and 11.5% of the Fe present in the pyrophyllite was Na-DCB extractable Fe. This indicates that the structural Fe content of the pyrophyllite sorbent was 380 mg Fe per kg pyrophyllite.

The pyrophyllite was characterized with X-ray diffraction (XRD) using Mg^{2+} - and K^+ -saturated Na-DCB-treated clay fractions (Jackson, 1969; Whittig and

Allardice, 1986). As smectites had not been previously observed in the sample (Scheidegger et al., 1996; Livi et al., 2009) and no smectite, vermiculite, or chlorite characteristic d-spacings were observed at 1.4 nm (Brown and Brindley, 1980), further solvation with glycerol was not performed on the Mg²⁺-saturated samples (Whittig and Allardice, 1986).

Diffraction patterns were obtained with a Philips X'Pert PW3040 powder diffractometer using randomly oriented powder mounts and Cu K α radiation (Whittig and Allardice, 1986). Scans were made from 5° to 70° 2 Θ , with a counting time of 3 seconds, and a step size of 0.02° 2 Θ , and these parameters were selected to include relevant peaks for pyrophyllite (Livi et al., 2009). The generator current and voltage were at 44 mA and 40 kV, respectively. Data were background-subtracted and smoothed using Philips X'Pert High Score.

2.3.2 Maintaining an Anoxic Atmosphere

Reactions were conducted anoxically to exclude the possibility of Fe(II) oxidation by O₂(g) using protocols described previously by Elzinga (2012). Samples were prepared in a Coy glovebox containing a 96% N₂ – 4% H₂ atmosphere. A palladium catalyst was utilized to remove trace O₂, and the O₂ levels were monitored throughout the experiment using an O₂-H₂ meter to ensure an atmospheric O₂ concentration of <1 ppm. Humidity was controlled through the implementation of a dehumidifier. Deionized (DI) water utilized in the experiment was boiled under N₂ purging and cooled in the glovebox for 2 d to outgas any remaining O₂.

2.3.3 Sorption Experiments

2.3.3.1 Macroscopic Studies

Reaction kinetics of Fe sorption onto pyrophyllite were examined using a batch reaction method (Elzinga, 2012) for a reaction time of up to 12 weeks. A pyrophyllite suspension with a solid concentration of 10 g/L was prepared in polypropylene tubes inside the glovebox, and the untreated pyrophyllite was hydrated in this solution for 1 day while open to the glovebox atmosphere (Scheidegger et al., 1996). The background electrolytes consisted of 0.1 M NaCl and 50 mM 4-(2-hydroxyethyl)-piperazine-1-ethanesulfonic acid (HEPES) buffer to maintain a pH of 7.5. The pH was adjusted to 7.5 using 1 M and 0.1 M HCl. Fe(II) stock solution (1.0 M) was prepared by dissolving FeCl₂·H₂O salt in anoxic 0.1 M HCl and filtering the solute through a 0.22 μm nitrocellulose filter membrane. Appropriate aliquots of the Fe(II) stock solution were added slowly to the batch reaction vessel under vigorous mixing to achieve final Fe(II) concentrations of 0.8 mM or 3 mM. These concentrations were selected for comparisons to previous works (Elzinga, 2012; Elzinga and Zhu, 2014). After the initial addition of Fe(II), the batch reaction vessels were placed on rotators to ensure mixing throughout the entire experiment. The pH and initial Fe(II) concentrations were selected so that the reactions remained undersaturated with respect to Fe^{II}(OH)₂. The pH of the batch reaction was measured at each sampling point, and it was found to deviate from the initial pH value by <0.35 pH unit over the entire reaction period. Macroscopic kinetic samples were removed from the batch reaction vessel in 10-mL increments and were syringe-filtered with a 0.22 μm nitrocellulose filter.

Samples were prepared for elemental analysis by ICP-OES by adding the appropriate aliquot of anoxic 1 M HCl to achieve a 5% HCl background to prevent precipitation. Blanks along with Fe-Si standards were prepared with a 5% HCl background and included with samples for ICP-OES analysis as quality control measures. The University of Delaware Soil Testing Laboratory uses the USEPA Method 6010C (USEPA, 2007b) for measuring elemental concentrations by ICP-OES.

2.3.4 Fe Speciation of Sorption Samples and Fe Standards

2.3.4.1 Preparation of Fe Sorption Samples

Samples for analysis by X-ray absorption spectroscopy (XAS) were prepared by using similar procedures to that of the macroscopic kinetics experiment. Batch reactions for XAS samples were prepared using identical solid concentrations, background electrolytes, hydration time, pH, and Fe(II) concentrations as the macroscopic kinetics experiments, but were conducted in 50-mL polypropylene tubes for a total sample volume of 30 mL. This volume allowed for a sufficient amount of solid phase to be analyzed by XAS. At the end of the allocated reaction time, the samples were centrifuged for 5 minutes at 8080 rpm (10,000 g) outside the glovebox in airtight centrifuge tubes. Following centrifugation, the samples were immediately transferred back inside the glovebox. After 24 hours, the supernatant was decanted and the wet paste was allowed to air dry for up to 1 hour. The wet pastes were then individually sealed into sample holders using Kapton® tape. Sealed XAS samples remained in the glovebox for less than 2 months before being analyzed.

2.3.4.2 Preparation of Fe Standards

Standards utilized for principal component analysis and linear combination fits of the reaction samples include unreacted Na-saturated pyrophyllite from Hillsboro, NC, (Ward Natural Science, 46E6430) and greenalite ((Fe^{II}, Fe^{III})₂₋₃Si₂O₅(OH)₄), an Fe(II)-Fe(III) phyllosilicate from Salamanca, Spain (Excalibur Mineral Company). Other Fe standards examined in this study are those used in previously published studies: nikischerite (NaFe^{II}₆Al₃(SO₄)₂(OH)₁₈(H₂O)₁₂), an Fe(II)-Al(III)-LDH; 10 mM Fe^{II} solution, “white rust” (Fe^{II}(OH)₂) (Elzinga, 2012); magnetite (Fe^{III}₂Fe^{II}O₄); 2-line ferrihydrite (5Fe^{III}₂O₃·9H₂O); hydroxychloride green rust; Fe(II)-phyllosilicate (Zhu and Elzinga, 2014); goethite (α-FeO(OH)); hematite (Fe₂O₃); lepidocrocite (γ-FeO(OH)); pyrite (FeS₂); vivianite (Fe(PO₄)₂·nH₂O); and siderite (FeCO₃) (Chen, 2013).

2.3.5 Bulk Extended X-Ray Absorption Fine Structure Spectroscopy (EXAFS)

For transportation to the beamline, samples were individually sealed into five ziplock bags (Elzinga, 2012). Bulk-XAS analysis was conducted at the National Synchrotron Light Source (NSLS) at beamline X11-A. Monochromator calibration was performed using an Fe foil, and Fe K edge spectra were recorded at an E₀ of 7112 eV using a Si(111) monochromator. Fluorescence data were collected using a Stern-Heald type Lytle detector or a passivated implanted planar silicon (PIPS) detector. A Mn filter was positioned between the sample and detector to reduce elastic scattering. Harmonics were suppressed by detuning by 50%. Samples were removed from the ziplock bags just prior to analysis, and no signs of visible oxidation were observed. Samples were stored outside the glovebox during transport and data collection for no longer than 44 hours prior to XAS analysis. At least three scans were collected for

each sample to improve the signal-to-noise ratio. After scanning, all samples were visually examined for signs of oxidation, and no oxidation was observed in the surrounding area hit by the X-ray beam.

Raw bulk-EXAFS $\mu(E)$ spectra for each sample were averaged, background subtracted, and normalized in Athena (Demeter 0.9.16), and the $\chi(k)$ functions were then isolated and k^3 -weighted (Ravel and Newville, 2005). Forward Fourier transforms of the k^3 -weighted χ functions were performed in Athena (Demeter 0.9.16) using Hanning windows with a dk of 0.5 to produce radial structure functions (RSF), and backward Fourier transforms were performed using Hanning windows with a dR of 0.2. Shell-by-shell fits of sorption samples and standards EXAFS data was conducted in Artemis (Demeter 0.9.16) using theoretical back-scattering paths calculated from Feff 6.0 (Ravel and Newville, 2005). Paths were calculated based on crystal structure of lizardite ($Mg_3Si_2O_5(OH)_4$) with Fe and Al substituted for Mg in the octahedra. The amplitude reduction factor (S_0^2) was set to equal 0.85 for all fits (O'Day et al., 1994). EXAFS sample data were fitted with Fe-O for the first shell, and Fe-Fe and Fe-Al for the second shell. The total CN for the second shell was fixed at 6, consistent with the LDH structure. When Si was considered in the fits of samples with longer reaction time, an additional path of Fe-Si was incorporated with CN of approximately 2 to account for the additional presence of Si in the local coordination environment of central Fe due to interlayer silication (Charlet and Manceau, 1994). An isotropic expansion-contraction fitting model was used for the second shell; thus constraining Debye-Waller factors (σ^2) and radial distance (R) to remain the same for all elements within the second shell and not adding additional variables (Kelly et al., 2008).

Principal component analysis (PCA) and target transforms (TT) of the k^3 -weighted χ functions of on the 3 mM Fe(II) sorption samples and Fe standards, respectively, were performed in SixPack to determine principal components and SPOIL values (Webb, 2005). Combinatorial linear combination fits (LCF) were performed in Athena (Demeter 0.9.16) on the k^3 -weighted χ functions between k values of 3 to 11 \AA^{-1} using standards (principal components) from TT with low SPOIL values. These techniques are used to determine the speciation of the element of interest within heterogeneous samples (Wasserman et al., 1999; McNear, 2005; Seiter et al., 2008; Jacquat et al., 2008). Standards were only included as sample Fe components if they improved the R-factor or reduced chi square of the LCF by 20% (Singh and Grafe, 2010).

2.3.6 ^{57}Fe Mössbauer Spectroscopy

Batch reactions for Mössbauer samples were prepared using identical solid concentration, background electrolytes, hydration time, pH, and Fe(II) concentrations as the macroscopic kinetics experiment; however, samples for Mössbauer spectroscopy measurements were prepared using FeCl_2 that was enriched in ^{57}Fe (natural abundance of 2.2%; ^{57}Fe is the only Mössbauer sensitive Fe isotope). $^{57}\text{Fe(II)}$ -chloride was prepared by dissolving 98+% $^{57}\text{Fe(0)}$ metal (Cambridge Isotope Laboratory, USA) in HCl solution as described in Peretyazhko et al. (2008). The sorption reactions were carried out in 50-mL polypropylene tubes which had a total sample volume of 20 mL. This volume allowed for a sufficient amount of solid phase to be analyzed with Mössbauer spectroscopy. At the end of the allocated reaction time, the samples were centrifuged outside the glovebox in airtight centrifuge tubes for 5 minutes at 8080 rpm (10,000 g). Following centrifugation, the samples were

immediately transferred back inside the glovebox, and after 24 hours, the supernatant was decanted and the wet paste was allowed to air dry completely (note: Mössbauer spectra of samples spiked with $^{56}\text{Fe}(\text{II})$, a Mössbauer-insensitive isotope that would allow exclusively to track changes to structural Fe environment without any interference from changes to the spiked Fe(II), were not attempted because the structural ^{57}Fe content of the clay [$\sim 2.12\%$ (natural abundance of ^{57}Fe) of the structural natural Fe content, 430 ppm] was not high enough to obtain a reasonable signal-to-noise ratio spectrum).

^{57}Fe Mössbauer analyses were conducted at the Environmental Molecular Sciences Laboratory (EMSL) of Pacific Northwest National Laboratory (PNNL). Samples in air-tight containers were shipped overnight immediately after anoxic drying to EMSL for Mössbauer spectroscopic analysis. For shipment to PNNL, samples were placed inside of airtight anaerobic vials, the vials were individually placed into three ziplock bags with an AnaeroPouch™ O_2 scrubber, and shipped to PNNL inside of an airtight AnaeroPack™ box with three AnaeroPack-Anaero™ O_2 scrubbers to prevent sample oxidation during travel. Mössbauer sample holders were prepared in a 0 ppm oxygen anoxic chamber, as in Peretyazhko et al. (2012), within a day of the shipment. Mössbauer measurements were collected using either WissEl Elektronik (Germany) or Web Research Company (St. Paul, MN) instruments that included a closed-cycle cryostat SHI-850 obtained from Janis Research Company, Inc. (Wilmington, MA), a Sumitomo CKW-21 He compressor unit, and an Ar-Kr proportional counter detector with WissEl setup or a Ritverc (St. Petersburg, Russia) NaI detection system. A $^{57}\text{Co}/\text{Rh}$ source (50 mCi to 75 mCi, initial strength) was used as the gamma energy source. With the WissEl setups, the transmitted counts were

stored in a multichannel scalar (MCS) as a function of energy (transducer velocity) using a 1024-channel analyzer. The setups data were folded to 512 channels to provide a flat background. Calibration spectra were obtained with a 25-micron thick Fe-foil (Amersham, England) placed in the same position as the samples to minimize any geometry errors. The data were modeled with Recoil software (University of Ottawa, Canada), using both a Voigt-based method as reported in Rancourt and Ping (1991). Spectral fitting parameters are given in Table A.1.

2.4 Results

2.4.1 Pyrophyllite Characterization

XRD data (Figure A.1) of the K⁺- and Mg²⁺-saturated pyrophyllite at 298 K, exhibit the characteristic d-spacing of 0.91 nm for pyrophyllite in both diffractograms (Brown and Brindley, 1980; Essington, 2004). Mg²⁺-saturation is used to distinguish expanding 2:1 phyllosilicates from non-expanding 2:1 phyllosilicates. No shifts are observed in the d-spacings between the two saturation treatments, indicating that no expanding phyllosilicates were present. These diffractograms appear similar to those of Livi et al. (2009), except that the material used here shows no evidence for the presence of trace quartz and kaolinite impurities. In the initial application of this pyrophyllite as a sorbent for Ni/Al LDH, it was reported that an XRD analysis of the sample showed pyrophyllite with trace quartz (<5%) (Scheidegger et al., 1996); however, subsequent XRD analysis of the pyrophyllite sample by Livi et al. (2009) indicated the presences of pyrophyllite, kaolinite, and quartz. No quartz was found in this study. The variability in the XRD patterns between the three studies is most likely due to heterogeneity within the sample material.

2.4.2 Batch Kinetics

Figure 2.1 shows the kinetics of Fe(II) removal from solutions containing 0.8 mM and 3 mM Fe(II) and the concurrent dissolution of Si from the pyrophyllite sorbent. These results show that for both systems, there is an initial fast reaction step in which >30% of Fe(II) is removed from solution during the first 24 h. This is followed by a slower step in which >70% is removed by the end of the 12 week reaction time, at which point the reactions do not appear to have reached equilibrium. Zhu and Elzinga (2014) found lower Fe(II) removal (equilibrium reached at ~50%) from Fe(II) sorption to a Fe-free mica-montmorillonite under similar reaction conditions. The Fe and Si solution data were corrected for the Fe and Si concentrations that were released into solution due to pyrophyllite dissolution prior to Fe(II) addition, i.e., during the pyrophyllite hydration period of 24 hours (Scheidegger et al., 1996). The concentrations from pyrophyllite dissolution were approximately 1×10^{-6} M Fe and 1×10^{-4} M Si, which agrees well with the Si dissolution observed by Scheidegger et al. (1996) for the same pyrophyllite (Fe dissolution was not monitored in their study). Similar, yet slightly higher, Si release from a Fe-free mica-montmorillonite at pH 7.5 during Fe(II) sorption was observed by Zhu and Elzinga (2014) during LDH formation; however, at pH 8.0 they observe the formation of Fe(II)-phyllosilicate accompanied by significant removal of Si from solution, relative to Fe-free standards.

The kinetics data shown in Figure 2.1 demonstrate the initial rapid Fe sorption followed by slower sorption, which is similar to the macroscopic reaction kinetics for Fe(II) sorption on Al-bearing minerals under anoxic conditions shown by others (Elzinga, 2012; Hiemstra and van Riemsdijk, 2007; Jaisi et al., 2008; Jeon et al., 2003; Nano and Strathmann, 2006; Zhu and Elzinga, 2014). The kinetics in Figure 2.1 are

also similar to the kinetics of metal(loid)s sorbed to mineral surfaces that has been observed by others (Elzinga, 2012; Ford and Sparks, 2000; Roberts et al., 2003; Scheidegger et al., 1996; Scheidegger et al., 1998; Thompson, et al., 1999; Towle et al., 1997) which resulted in the formation of layered double hydroxide (LDH) phases. The initial fast sorption is often interpreted to represent fast reaction processes, such as adsorption, and the slower sorption is interpreted to represent slower reaction processes, such as co-precipitation; however, mechanistic information cannot be determined from macroscopic data alone.

2.4.3 XAS Data

The pyrophyllite used in this study was analyzed with X-ray absorption spectroscopy (XAS) at the Fe K edge (7112 eV), and the spectra are shown in Figure A.2 with two Fe(II) standards, Fe(II) solution and nikischerite. The edge shift to higher energies exhibited by pyrophyllite is indicative of Fe(III), suggesting that the Fe impurity present in the pyrophyllite sample occurs as Fe(III) (also visible in Figure 2). Figure A.4 shows the first and last (tenth) scan for 3 mM Fe(II) sorption after 30 minutes of reaction time, and this figure demonstrates that there was no beam-induced change in sample Fe oxidation state. The K edge EXAFS spectra (Figure 2.2) shows the edge shifts observed for the two Fe oxidation states, +II or +III. Figure 2.3 shows the k^3 -weighted χ functions and radial structure functions (RSF) of Fe(II) sorption samples with pyrophyllite reacted at pH 7.5 under anoxic conditions and of reference Fe standards pyrophyllite, Fe(II) solution, greenalite, nikischerite, Fe(II)-phyllosilicate, and green rust. When comparing the 7-8 Å⁻¹ fingerprint regions of the k^3 -weighted χ functions for samples and standards in Figure 2.3, the sorption samples appear similar to greenalite, nikischerite, and green rust. This region is a diagnostic for Ni-, Zn-, and

Co-Al-LDH phases due to the destructive interference of Al neighbors (Scheinost and Sparks, 2000). The presence of this “beat” pattern is also consistent with χ spectra of Fe(II)-Al(III)-LDH phase formation found recently by Elzinga (2012) and Zhu and Elzinga (2014) from reactions of Fe(II) with γ -Al₂O₃ and a mica-montmorillonite.

Sorption sample RSFs show the first Fe coordination shell at ~ 1.6 Å (uncorrected for phase shift), which represent O ligands in the first shell surrounding Fe. This shell was fitted with 5.0-6.3 O atoms at radial distance of 2.05-2.11 Å (Table 2.1), which is consistent with octahedral coordination of the O atoms around the central Fe(II) atom (Elzinga, 2012; Huminicki and Hawthorne, 2003; Olszewski et al., 2011; Parise et al., 2000; Shannon, 1976). A growth in the second coordination shell (~ 2.8 Å) of the sorption samples can be observed with an increase in reaction time for both Fe and Al, indicating an increasing Fe-Fe/Al backscattering contribution over time. The second shell was fitted with Fe and Al atoms at a distance of 3.14-3.16 Å (Table 2.1), which is consistent with the structure of nikischerite (Huminicki and Hawthorne, 2003). The LDH fingerprint (oscillation) is missing from the 7-8 Å⁻¹ region of the 28 d 0.8 mM Fe(II) sorption sample, but was present in the 7 d 0.8 mM Fe(II) sample.

Results of the PCA for 3 mM Fe(II) system show that the first four components contributed up to 92% of the total variance of the Fe-sorption samples and the empirical indicator function suggests that two components are required for fitting (Table A.2). Target transformation SPOIL values of the standards (Table A.3) were used to select the standards to be used during the combinatorial linear combination fitting (LCF) of the Fe-sorption samples. Several standards had excellent to good SPOIL values (2-line ferrihydrite, FeCl₂ aqueous solution, goethite, hydroxychloride

green rust, hematite, nikischerite, and pyrophyllite) and were included in the combinatorial LCFs. PCA could not be performed for the 0.8 mM Fe(II) system because only two XAS samples were taken over the reaction time. Although the Fe(II)-phyllosilicate had a very high TT value for the 3 mM Fe(II) system, it was used in fitting of the 0.8 mM Fe(II)-pyrophyllite 28 day sorption sample due to the appearance of the 7-8 Å⁻¹ region.

Combinatorial fitting was used to compare fits using combinations of up to two standards from the standards pool, as suggested by an empirical indicator function in PCA. Results of the LCFs are shown in Figure A.5, and fit parameters are given in Table A.4. The sorption product was predominately Fe/Al-LDH (nikischerite) as indicated by the standard weights in Table A.4, which is in agreement with the EXAFS shell-by-shell fits and the ⁵⁷Fe Mössbauer data (below). The trend in decreasing Fe concentration from pyrophyllite and increasing Fe concentration from Fe(II)-Al(III)-LDH sorption product with reaction time is consistent with the results of the macroscopic kinetics study. Sorption sample LCF produced several fits that were not statistically significant (R-factors were not different by ≥20%). This likely results from the similarities in structure and k³-weighted χ functions for the standards used. The Athena program can constrain the data enough to demonstrate the formation of layered hydroxide-like phases; however, it cannot fully distinguish between the standards due to the similarity in their spectra. Furthermore, the sorption product may also be a hybrid LDH-like phase with elemental substitutions, thus convoluting the results of the LCF.

2.4.4 ^{57}Fe Mössbauer Data

Since a) unambiguous identification of Fe(III) in LDHs can be realized from Mössbauer spectroscopy (Kukkadapu et al., 2004), b) it is possible to detect small amounts of Fe phases by this technique, and c) the data acquisition is time consuming. ^{57}Fe Mössbauer spectroscopy measurements were carried out on only one sample in this study. Only spectral features due to spiked ^{57}Fe are prominent in the spectra; greater than 99% of the signal for Mössbauer in the sorption samples comes from spiked ^{57}Fe sorbed to the pyrophyllite surface (the natural abundance of ^{57}Fe in the clay is miniscule compared to the sorbed ^{57}Fe). The spectrum of 3 mM $^{57}\text{Fe(II)}$ reacted with pyrophyllite for 28 d at 77 K is shown in Figure 2.4a (red trace) as an example. The spectrum displayed, in addition to doublet peaks attributed to Fe(II) (* in the figure), features due to Fe(III) (+ in the figure); the relative spectral areas of the Fe(II) and Fe(III) doublets in the spectrum was based on a fit of the spectrum (Figure 2.4b). The Fe(III) presence in the spectrum unambiguously indicated partial oxidation of the spiked $^{57}\text{Fe(II)}$, which was not evident from the EXAFS data. This observation is in line with the noted oxidation of spiked $^{57}\text{Fe(II)}$ by structural Fe(III) in $\square\text{-Al}_2\text{O}_3$ sample (Peretyazhko et al., 2008). The presence of oxidized Fe(III) in the sample was likely due to oxidation of the spiked $^{57}\text{Fe(II)}$ by structural Fe(III), as noted in a nontronite clay system (Schaefer et al., 2011) based on the difference in “doublet” contents between room temperature (not shown) and 77 K spectra. The model-derived Fe(III) content, however, is somewhat higher (15% vs. 4-6%) expected due solely to electron transfer from sorbed $^{57}\text{Fe(II)}$ to the structural Fe(III) in the pyrophyllite structure. The additional $^{57}\text{Fe(II)}$ oxidation could be due to surface-sorption-induced electron-transfer from the sorbed Fe(II) to the clay lattice, as noted in the Fe(II) sorbed montmorillonite system that was free of structural Fe(III) (Géhin et al., 2007).

Alternatively, the discrepancy (to a certain extent) could be 1) a combination of variation in Fe content between the subsamples, which would be in accordance with XRD variation noted in the three different studies (see Section 3.1), 2) different recoilless fractions of the Fe species (Murad and Cashion, 2004), 3) semi-quantitative since the measurement was carried on only a single sample, and 4) the errors associated in determining relative spectral areas. Relatively low Fe(III) content in the 1 d sample, implies that the oxidation process is rather slow. From the present data, however, it was not possible to hypothesize the relative rates of Fe(III) oxidation by interfacial electron transfer and surface sorption induced mechanisms.

The precise nature of the Fe species was not readily apparent from the 77 K spectrum due to significant overlap of its doublet peaks with the Fe(II)-Al-LDH and green rust standards (Figure 2.4a). From spectra obtained below 77 K, however, it was possible to gain some insights. For example, the lack of well-defined Fe(III) sextets and Fe(II) octets in its 12 K spectrum (Figures 2.4c and 2.4d) clearly suggested that Fe(II)/Fe(III)-(oxyhydr)oxides, such as ferrihydrite, lepidocrocite, goethite, hematite, and magnetite/maghemite, that display distinct sextet features below 77 K (Murad and Cashion, 2004), and FeCO₃ (siderite) phase that exists as doublet at 77 K and as an octet below 35 K (Peretyazhko et al., 2012), were not precipitated. Furthermore, the derived 77 K Fe(III) doublet spectral parameters (not shown) unambiguously indicated non-precipitation of green rust (Kukkadapu et al., 2004), also evident from the Fe(III) peak positions (Figure 2.4a – GR is shown as black trace); 77 K parameters of the sample and standards are included in Appendix A. The absence of Fe(III)-oxides in the samples, which are typical air oxidation products of

sorbed Fe(II) (Peretyazhko et al., 2008), further indicated that the noted Fe(III) in the Mössbauer LDH sample was not an inadvertent oxidation product.

The Fe(III) in the sample is most likely due to precipitation of a hybrid Fe(II)-Fe(III)/Al(III)-LDH-like phase. The Fe(II) features, on the other hand, qualitatively match well with the Fe(II)-Al(III)-LDH standard (blue trace in Figure 2.4a). This match is in general agreement with the EXAFS data and interpretation. Changes between the sample and spectra, particularly the Fe(II) peak line widths that are apparent upon a closer inspection, suggest multiple Fe(II) environments. The broadness of the Fe(II) peaks is likely due to a distribution of LDHs with slightly different Fe(II)/Al(III) ratios as well as minor contributions from a hybrid Fe(II)-Al(III)/Fe(III)-LDH-like co-precipitate. Furthermore, from the decrease in the Fe(II)/Fe(III) ratio of the sample with reaction time (Figure 2.4e), it is clear that Fe(II) oxidation increases with reaction time. Finally, it is noteworthy that the oxidized product in this study is different than the products found in the Fe(II) and Fe(III)-rich N Au-2 clay system (Schaefer et al., 2011). This may be related to Fe location and its immediate environment in the clay. For example, it appears that the nature of the oxidized product in N Au-2 and N Au-1 nontronite differ in Fe/Al ratio, Fe content, and layer charge, an aspect that was not the focus of Schaefer et al. (2011) and Neumann et al. (2013). More importantly, the study emphasizes the advantage of using EXAFS and Mössbauer spectroscopy in tandem for identification of the Fe species in complex systems.

2.5 Discussion

2.5.1 Spectroscopic Studies

Sorbed Fe in the sorption samples have EXAFS edge shifts between those of Fe(II) and Fe(III), suggesting that Fe is present in multiple oxidation states in these samples. This is expected due to 1) the presence of Fe(III) in the pyrophyllite substrate used in the sorption reactions, 2) the potential for surface-sorption-induced electron-transfer oxidation from the clay surface (Géhin et al., 2007), and 3) the potential for electron transfer from sorbed Fe(II) to structural Fe(III) (Schaefer et al., 2011). Mössbauer spectra show an elevated presence of Fe(III) in the sorption samples. Evidence is presented through EXAFS and Mössbauer (Figures 2.4c and 2.4d and Figures A.2 and A.4) that our sample preparation, transfer, and spectroscopic analysis measures were successful in preventing accidental oxidation. Therefore, the excess Fe(III) observed is likely the result of $^{57}\text{Fe(II)}$ oxidation by the pyrophyllite lattice through surface-sorption-induced electron-transfer oxidation similar to the oxidation observed by Géhin et al. (2007) with $^{57}\text{Fe(II)}$ sorption to an Fe-free montmorillonite under strictly anoxic conditions and/or through interfacial electron transfer between sorbed Fe(II) and structural Fe(III) (Schaefer et al., 2011).

Fits of EXAFS data from Table 2.1 indicate the presence of a Fe(II)-Al(III)-LDH phase formed during these reactions. Growth in the second shell of the RSF in Figure 2.3 can be attributed to Fe/Al precipitation during sorption and is consistent with other studies examining Fe(II) sorption to Al-oxides and Fe-free clay at similar concentrations at pH 7.0-7.5 resulting in the formation of Fe(II)-Al(III)-LDH phases (Elzinga, 2012; Zhu and Elzinga, 2014). In k-space, the region of the k^3 -weighted χ function is known as a fingerprint region for LDH phases, exhibiting an oscillation

over this range of k (Scheinost and Sparks, 2000); however, green rust phases do not exhibit this feature (Suzuki et al., 2008; Thoraj et al., 2005). The spectra of high concentration Fe(II) sorption samples at longer reaction times contain features indicative of LDH phases. The bulk Fe-XAS data (shell-by-shell fits and χ functions) also demonstrate the predominance of LDH in the sorption samples at longer times. However, the EXAFS TT analyses and the ^{57}Fe Mössbauer results indicate the presence of at least two and possibly three Fe-bearing phases (pyrophyllite and one or two Fe sorption product). The broadness of the Mössbauer doublet peak in the sorption sample (Figure 2.4a) suggests multiple $^{57}\text{Fe(II)}$ environments. The $^{57}\text{Fe(II)}$ doublets present in the standards, although different from each other, coincide with the $^{57}\text{Fe(II)}$ present in the sorption products. Pure GR-Cl can be excluded as a product because $^{57}\text{Fe(III)}$ from a pure GR-Cl is absent, which is in agreement with the EXAFS k^3 -weighted χ functions. From a comparison of the ^{57}Fe Mössbauer standards and the Fe EXAFS data, the $^{57}\text{Fe(II)}$ signature here is proposed to result from a Fe(II)-Al(III)-LDH-like compound. The heterogeneity of the sorption sample and the presence of multiple $^{57}\text{Fe(II)}$ environments in the sorption sample could be explained by several mechanisms: 1) the increase in Fe(II):Al ratio of the Fe(II)-Al(III)-LDH phase over time, 2) the presence of an adsorbed Fe(II) phase alongside the Fe(II) incorporated into the LDH, and 3) the possibility of a hybrid Fe(II)-Al(III)/Fe(III)-LDH phase. LDH formation is controlled by Al release from the mineral substrate (Scheckel et al., 2000; Li et al., 2012). As Fe(II)-Al co-precipitation occurs, less Al is available for release from pyrophyllite, thus reducing the Al available for co-sorption with Fe(II).

Silicates are known to alter the structure and stability of LDH phases via substitution with interlayer anions, so their inclusion in the reactions could result in

the transformation of the LDH phase into a phyllosilicate with an octahedral sheet containing both Fe(II) and Al(III) (Ford et al., 2001; Scheckel and Sparks, 2001; Scheckel et al., 2000). The XAS data of the sorption system containing 0.8 mM Fe appear to demonstrate evolution of Fe(II)-Al(III)-LDH to a Fe(II)-Al(III)-phyllosilicate during aging. The 7 d sample from this system clearly contains the χ “beat” pattern at 7-8 Å⁻¹ indicating Fe(II)-Al(III)-LDH (Figure 2.3a). In contrast, the 28 d sample lacks this feature and more closely resembles the χ spectrum of the ferrous phyllosilicate standards (Figure 2.3a). An additional Fe-Si path was used in the fit of this sample to account for the increase in second-shell scattering evident in the RSF (Figure 2.3b), yielding the fit results consistent with Fe(II)-phyllosilicate (Table 2.1). Slow interlayer silication may also be occurring in the 3 mM Fe(II) sorption sample; however, the Fe:Si ratio of this system is much higher and may be limiting the observation of this process from the EXAFS spectra after the 28 d aging time considered here.

2.5.2 Environmental Implications

Previous studies have demonstrated Fe(II)-Al(III)-LDH phase formation from reactions of Al-oxides and phyllosilicates with Fe(II) in model geochemical systems (Elzinga, 2012; Zhu and Elzinga, 2014). We expand on the knowledge gained from those studies to show Fe(II)-Al(III)-LDH phase formation in the presence of Fe(III) and demonstrate the variability of Fe(II) phases that may form during sorption controlled by environmentally relevant factors, such as reaction time and phyllosilicate purity. The net Fe(II) oxidation observed through Mössbauer spectroscopy, despite the absence of O₂ in our system, and the potential formation of a hybrid Fe(II)-Al(III)/Fe(III)-LDH phase merits further attention and could suggest a new pathway

for LDH phases that has not been defined before. This study also examined the effects of impurities from one mineral. Further investigations of other Al-bearing minerals with higher Fe concentrations and a systematic study of aqueous Fe(III) concentrations on Fe(II) sorption should be conducted to determine the effects of higher concentrations on LDH phase formation and to better understand their potential to form in the natural environment. This work also demonstrates silica interlayer substitution at longer reaction times, which has been observed with the formation of other LDH phases (Ni, Zn, and Co) (Ford et al., 2001; Scheckel and Sparks, 2001; Scheckel et al., 2000). LDH phases form rapidly and extensively under conditions similar to those of riparian systems and are likely to occur in and impact Fe and trace metal geochemistry in such systems, having clear implications for the fate and speciation of Fe(II) in reducing geochemical environments. Determining the kinetics and thermodynamics of Fe/Al-LDH and similar phases will lead to a better understanding of metal cycling in suboxic and anoxic geochemical systems.

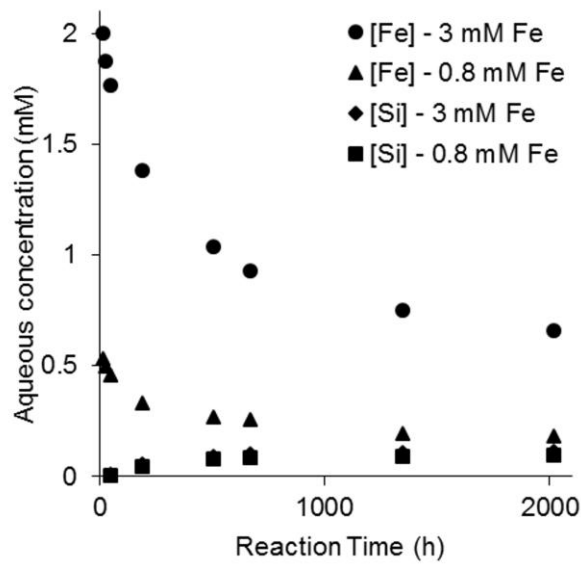


Figure 2.1: Kinetics of Fe(II) sorption to pyrophyllite containing structural Fe impurities by a 0.8 mM Fe(II) solution and a 3 mM Fe(II) solution at pH=7.5 expressed as aqueous concentration of Fe(II) and Si where the symbols ● and ▲ denote 0.8 mM Fe(II) and 3 mM Fe(II) concentrations, respectively, while the symbols ◆ and ■ denote Si concentrations during reactions of 0.8 mM Fe(II) or 3 mM Fe(II), respectively.

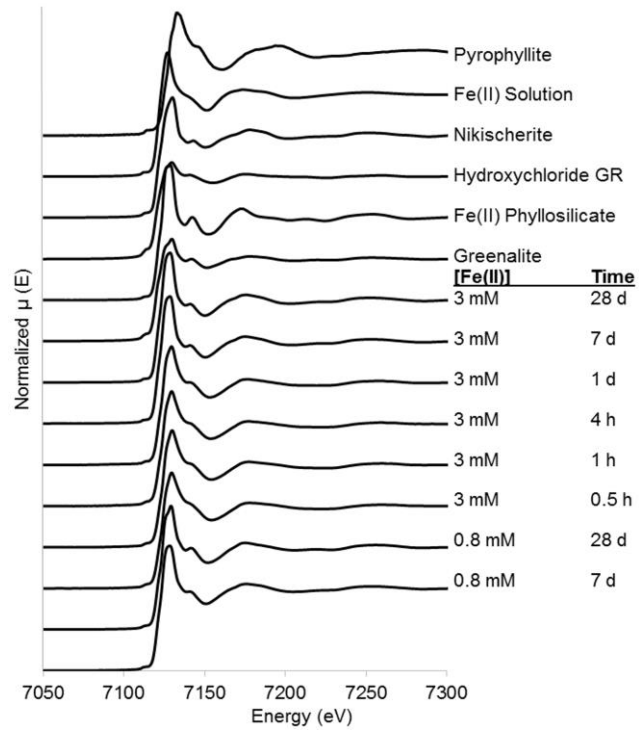


Figure 2.2: Fe K edge EXAFS spectra of Fe(II) sorption samples with pyrophyllite containing structural Fe impurities reacted at pH 7.5 under anoxic conditions and of reference Fe standards.

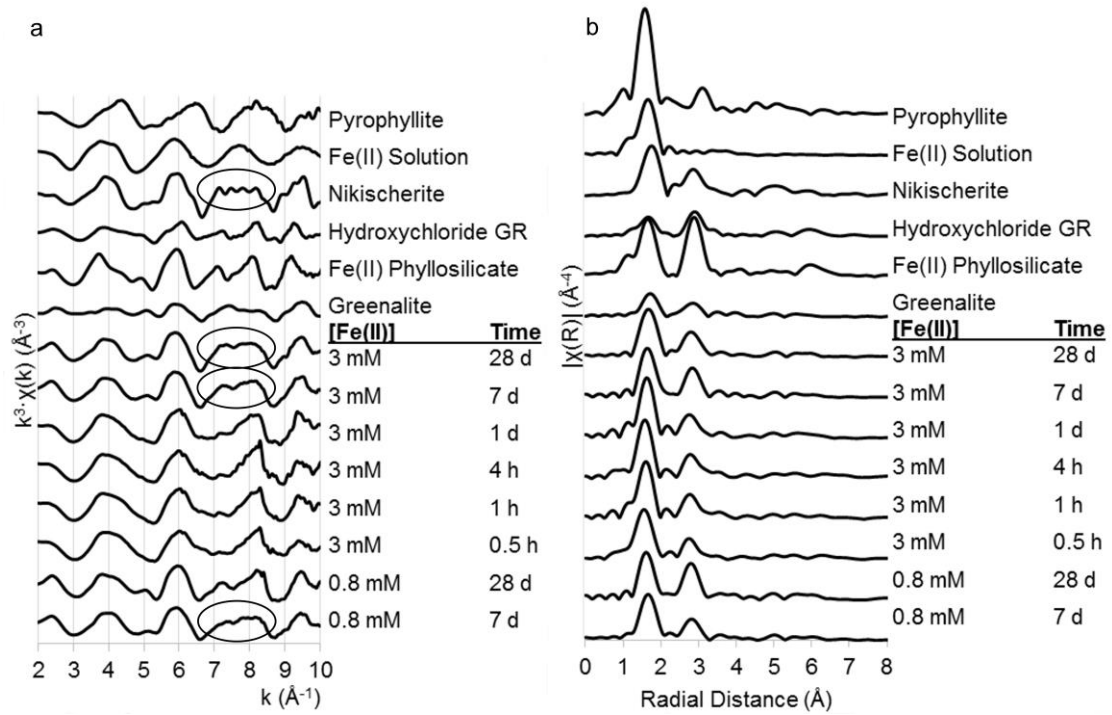


Figure 2.3: Fe K edge raw $k^3 \cdot \chi$ functions (a) and radial structure functions (RSF) (b) of Fe(II) sorption samples with pyrophyllite containing structural Fe impurities reacted at pH 7.5 under anoxic conditions and of reference Fe standards.

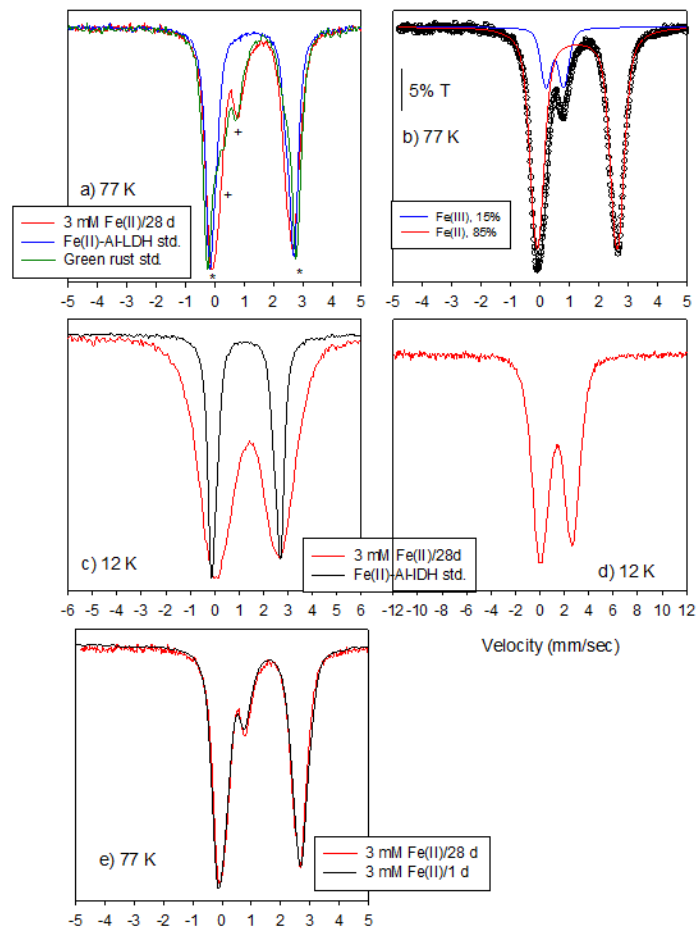


Figure 2.4: ^{57}Fe Mössbauer spectra of a) Fe(II)-pyrophyllite 28 d sorption sample and Fe(II)-Al(III)-LDH and hydroxylchloride green rust standards measured at $T = 77\text{ K}$; b) fits of 28 d sorption sample measured at $T = 77\text{ K}$; c and d) Fe(II)-pyrophyllite 28 d sorption sample and Fe(II)-Al(III)-LDH standard measured at $T = 12\text{ K}$; and e) Fe(II)-pyrophyllite 28 d and 1 d sorption samples measured at $T = 77\text{ K}$.

Table 2.1: Fe K-Edge EXAFS Fitting Results of Fe(II) Sorption and Reference Samples^a

Sorption Samples		Atomic Shell														ΔE (eV)	S_0^2	N_{ind}	N_{var}	χ^2	χ_v^2
		Fe-O			Fe-Fe			Fe-Al			Fe-Si										
[Fe(II)] (mM)	Time	R-factor	CN	R (Å)	σ^2 (Å ²)																
3	0.5 h	0.007	5.0	2.04	0.009	0.9	3.16	0.002							-	0.85	9.46	5	1072	240	
3	1 h	0.011	5.0	2.06	0.008	1.8	3.16	0.006							0.514	0.85	10.33	5	1300	243	
3	4 h	0.020	5.0	2.05	0.007	1.6	3.16	0.006							0.510	0.85	8.88	5	626	162	
3	1 d	0.018	5.0	2.08	0.007	2.0	3.17	0.007							0.045	0.85	9.46	5	1838	412	
3	7 d	0.010	6.0	2.11	0.009	3.8	3.15	0.009	1.8	3.15	0.009				0.030	0.85	9.75	5	4571	963	
3	28 d	0.009	6.3	2.11	0.009	4.0	3.14	0.010	2.0	3.14	0.010				0.192	0.85	10.77	5	5695	987	
0.8	7 d	0.006	5.8	2.10	0.009	1.5	3.14	0.004	0.7	3.14	0.004				0.044	0.85	9.31	5	2444	567	
0.8	28 d	0.002	5.8	2.07	0.010	3.1	3.14	0.007	1.4	3.14	0.008	1.7	3.35	0.008	0.432	0.85	9.60	5	535	116	
															1.239						
References																	Source				
			5.2	2.14	0.007	3.0	3.14	0.006	3.0	3.14	0.006					1.00	Zhu and Elzinga, 2014				
			5.2	2.14	0.006	6.0	3.26	0.006								1.00	Zhu and Elzinga, 2014				
			4.7	2.09	0.014	6.0	3.21	0.013								1.00	Zhu and Elzinga, 2014				
			5.3	2.12	0.009											1.00	Zhu and Elzinga, 2014				
			5.3	2.10	0.010	6.0	3.23	0.012				4.0	3.31	0.012		1.00	Zhu and Elzinga, 2014				

^aR-factor is the absolute misfit between the data and theory (as defined by Artemis), CN is coordination number, R is interatomic radial distance, σ^2 is Debye-Waller factor, ΔE is energy shift, S_0^2 is amplitude reduction factor, N_{ind} is the number of independent points, N_{var} is the number of variables, χ^2 is chi square, and χ_v^2 is reduced chi square.

REFERENCES

- Abdelmoula, M.; Trolard, F.; Bourrie, G.; Génin, J.M.R. Evidence for the Fe(II)-Fe(III) green rust “Fougerite” mineral occurrence in a hyromorphic soil and its transformation with time and depth. *Hyperfine Interact.*, **1998**, 112:235-238; DOI 10.1023/A:1010802508927.
- Brown, G.; Brindley, G.W. *Crystal structures of clay minerals and their X-ray identification*. Mineralogical Society: London, 1980.
- Charlet, L.; Manceau, A. Evidence for the neoformation of clays upon sorption of Co(II) and Ni(II) on silicates. *Geochim. Cosmochim. Acta*, **1994**, 58(11):2577-2582, DOI 10.1016/0016-7037(94)90034-5.
- Chen, C. Investigating organic matter-mineral interactions at a molecular scale: An integrated field and laboratory study. Ph.D. Dissertation, University of Delaware, Newark, DE, 2013.
- Christiansen, B.C.; Balic-Zunic, T.; Petit, P.O.; Frandsen, C.; Morup, S.; Geckeis, H.; Katerinopoulou, A.; Stipp, S.L.S. Composition and structure of an iron-bearing, layered double hydroxide (LDH) – Green rust sodium sulphate. *Geochim. Cosmochim. Acta*, **2009**, 73:3579-3592; DOI 10.1016/j.gca.2009.03.032.
- de Roy, A.; Forano, C.; Besse, J.P. Layered double hydroxides: Synthesis and post-synthesis modification, In *Layered Double Hydroxides: Present and Future*; Rives, V., Ed; Nova Science Publishers, Inc.: New York, 2001.
- Elzinga, E.J. Formation of layered Fe(II)-Al(III)-hydroxides during reaction of Fe(II) with aluminum oxide. *Environ. Sci. Technol.*, **2012**, 46:4894-4901; DOI 10.1021/es2044807.
- Essington, M.E. *Soil and water chemistry: An integrative approach*. CRC Press: New York, New York, 2004.
- Feder, F.; Trolard, F.; Klingelhöffer, G.; Bourrie, G. In situ Mössbauer spectroscopy: Evidence for green rust (fougerite) in a gleysol and its mineralogical transformations with time and depth. *Geochim. Cosmochim. Acta*, **2005**, 69:4463-4483; DOI 10.1016/j.gca.2005.03.042.

- Ford, R.G.; Scheinost, A.C.; Scheckel, K.G.; Sparks, D.L. The link between clay mineral weathering and the stabilization of Ni surface precipitates. *Environ. Sci. Technol.* **1999**, 33(18):3140-3144, DOI 10.1021/es990271d.
- Ford, R.G.; Scheinost, A.C.; Sparks, D.L. Frontiers in metal sorption/precipitation mechanisms on soil mineral surfaces. *Advances in Agronomy*, **2001**, 74:41-62; DOI 10.1016/S0065-2113(01)74030-8.
- Ford, R.G.; Sparks, D.L. The nature of Zn precipitates formed in the presence of pyrophyllite. *Environ. Sci. Tech.*, **2000**, 34:2479-2483; DOI 10.1021/es991330q.
- Gee, G.W.; Or, D. Particle-size analysis, In J. H. a. T. Dane, C., ed. *Methods of Soil Analysis, Part 4 Physical Methods*. Soil Science Society of America Book Series, Madison, Wisconsin, USA, 2002.
- Géhin, A.; Grenèche, J.-M.; Tournassat, C.; Brendlé, J.; Rancourt, D.G.; Charlet, L. Reversible surface-sorption-induced electron-transfer oxidation of Fe(II) at reactive sites on a synthetic clay mineral. *Geochim. Cosmochim. Acta*, **2007**, 71:863-876; DOI 10.1016/j.gca.2006.10.019.
- Génin, J.M.R.; Refait, P.; Bourrié, G.; Abdelmoula, M.; Trolard, F. Structure and stability of Fe(II)-Fe(III) green rust “fougerite” mineral and its potential for reducing pollutants in soil solutions. *Appl. Geochem.*, **2001**, 16: 559-570, DOI 10.1016/S0883-2927(00)00043-3.
- Hiemstra, T.; van Riemsdijk, W.H. 2007. Adsorption and surface oxidation of Fe(II) on metal (hydr)oxides. *Geochim. Cosmochim. Acta*, **2007**, 71:5913-5933; DOI 10.1016/j.gca.2007.09.030
- Huminicki, D.M.C.; Hawthorne, F.C. The crystal structure of nikischerite, Na₂Fe²⁺₆Al₃(SO₄)₂(OH)₁₈(H₂O)₁₂, a mineral of the shigaite group. *Can.Mineral.*, **2003**, 41:79-82, DOI 10.2113/gscanmin.41.1.79.
- Jackson, M.L. *Soil chemical analysis – Advanced course*. University of Wisconsin, Madison, WI, 1969.
- Jackson, M.L. *Soil chemical analysis - Advanced course*. 2nd ed. University of Wisconsin, Madison, WI, 1985.
- Jacquat, O.; Voegelin, A.; Villard, A.; Marcus, M.A.; Kretzschmar, R. Formation of Zn-rich phyllosilicates, Zn-layered double hydroxide and hydrozincite in contaminated calcareous soils. *Geochim. Cosmochim. Acta*, **2008**, 72(20):5034-5057; DOI 10.1016/j.gca.2007.09.030.

- Jaisi, D.P.; Liu, C.; Dong, H.; Blake, R.E.; Fein, J.F. Fe²⁺ sorption onto nontronite (Nau-2). *Geochim. Cosmochim. Acta*, **2008**, 72:5361-5371; DOI 10.1016/j.gca.2008.08.022.
- Jeon, B.H.; Dempsey, B.A.; Burgos, W.D. Kinetics and mechanisms for reactions of Fe(II) with iron(III) oxides. *Environ. Sci. Technol.*, **2003**, 37:3309-3315; DOI 10.1021/es025900p.
- Juillot, F.; Morin, G.; Ildefonse, P.; Trainor, T.P.; Benedetti, M.; Galois, L.; Calas, G.; Brown, G.E. Occurrence of Zn/Al hydrotalcite in smelter-impacted soils from northern France: Evidence from EXAFS spectroscopy and chemical extractions. *Am. Mineral.*, **2003**, 88:509-526; DOI 10.2138/am-2003-0405.
- Kelly, S.D.; Hesterberg, D.; Ravel, B. Analysis of soils and minerals using X-ray absorption spectroscopy. In *Methods of Soil Analysis, Part 5 – Mineralogical Methods*; Ulery, A.L.; Drees, L.R., Eds; Soil Science Society of America: Madison, WI, USA, 2008; pp 367-463.
- Kukkadapu, R.K.; Zachara, J.M.; Fredrickson, J.K.; Kennedy, D.W. Biotransformation of two-line silica-ferrihydrite by a dissimilatory Fe(III)-reducing bacterium: formation of carbonate green rust in the presence of phosphate. *Geochim. Cosmochim. Acta*, **2004**, 68(13):2799-2814, DOI 10.1016/j.gca.2003.12.024.
- Kunze, G.W.; Dixon, J.B. Pretreatment for mineralogical analysis. In *Methods of Soil Analysis. Part I Physical and Mineralogical Methods* (A. Klute, ed.), 2nd ed. pp. 91-100. American Society of Agronomy, Madison, WI, 1986.
- Li, W.; Livi, K.J.; Xu, W.; Siebecker, M.G.; Wang, Y.; Phillips, B.L.; Sparks, D.L. Formation of crystalline Zn-Al layered double hydroxide precipitates on γ -alumina: the role of mineral dissolution. *Environ. Sci. Technol.*, **2012**, 46(21):11670-11677, DOI 10.1021/es3018094.
- Livi, K.J.T.; Senesi, G.S.; Scheinost, A.C.; Sparks, D.L. Microscopic examination of nanosized mixed Ni-Al hydroxide surface precipitates on pyrophyllite. *Environ. Sci. Technol.*, **2009**, 43(5):1299-1304; DOI 10.1021/es8015606@proofing.
- McBride, M.B. *Environmental Chemistry of Soils*. Oxford University Press: New York, 1994.
- McNear, D.H. The plant soil interface: Nickel bioavailability and the mechanisms of plant hyperaccumulation. Ph.D. Dissertation, University of Delaware, Newark, DE, 2005.

- McNear, D.H.; Chaney, R.L.; Sparks, D.L. The effects of soil type and chemical treatment on nickel speciation in refinery enriched soils: A multi-technique investigation. *Geochim. Cosmochim. Acta*, **2007**, 71(9):2190–2208; DOI 10.1016/j.gca.2007.02.006.
- Merola, R.B.; Fournier, E.D.; McGuire, M.M. Spectroscopic investigations of Fe²⁺ complexation on nontronite clay. *Langmuir*, **2007**, 23:1223-1226; DOI 10.1021/la062467e.
- Murad, E.; Cashion, J. *Mössbauer spectroscopy of environmental materials and their industrial utilization*. Kluwer Academic Publishers, Norwell, MA, 2004.
- Nachtegaal, M.; Marcus, M.A.; Sonke, J.E.; Vangronsveld, J.; Livi, K.J.T.; van der Lelie, D.; Sparks, D.L. Effects of in-situ remediation on the speciation and bioavailability of zinc in a smelter contaminated soil. *Geochim. Cosmochim. Acta*, **2005**, 69:4649–4664; DOI 10.1016/j.gca.2005.05.019.
- Nano, G.V.; Strathmann, T.J. Ferrous iron sorption by hydrous metal oxides. *J. Colloid Interface Sci.*, **2006**, 297:443-454; DOI 10.1016/j.jcis.2005.11.030.
- O'Day, P. A.; Rehr, J. J.; Zabinsky, S. I.; Brown, G. E. Extended X-ray absorption fine structure (EXAFS) analysis of disorder and multiple-scattering in complex crystalline solids. *J. Am. Chem. Soc.*, **1994**, 116:2938–2949, DOI 10.1021/ja00086a026.
- Olszewski, W.; Szymanski, K.; Zaleski, P.; Zajac, D. A. X-ray absorption near edge structure and extended X-ray absorption fine structure analysis of Fe(II) aqueous and acetone solutions. *J. Phys. Chem. A*, **2011**, 115:13420–13424, DOI 10.1021/jp207587u.
- Parise, J. B.; Marshall, W. G.; Smith, R. I.; Lutz, H. D.; Moller, H. The nuclear and magnetic structure of “white rust” -- Fe-(OH_{0.86}D_{0.14})₂. *Am. Mineral.*, **2000**, 85:189–193, DOI 10.2138/am-2000-0118.
- Peretyazhko, T.; Zachara, J.M.; Heald, S.M.; Kukkadapu, R.K.; Liu, C.; Plymale, A.E.; Resch, C.T. Reduction of Tc(VII) by Fe(II) sorbed on Al (hydr)oxides. *Environ. Sci. Technol.*, **2008**, 42:5499-5506; DOI 10.1021/es8003156.
- Peretyazhko, T.; Zachara, J.M.; Kukkadapu, R.K.; Heald, S.M.; Kutnyakov, I.V.; Resch, C.T.; Arey, B.W.; Wang, C.M.; Kovarik, L.; Phillips, J.L.; Moore, D.A. Pertechnetate (TcO₄⁻) reduction by reactive ferrous iron forms in naturally anoxic, redox transition zone sediments from the Hanford Site, USA. *Geochim. Cosmochim. Acta*, **2012**, 92:48-66; DOI 10.1016/j.gca.2012.05.041; DOI 10.1016/j.gca.2012.05.041.

- Rancourt, D.G.; Ping, J.Y. Voigt-based methods for arbitrary-shape static hyperfine parameter distributions in Mössbauer spectroscopy. *Nucl. Inst. Meth. Phys. Res.*, **1991**, 58:85-97; DOI 10.1007/BF02401872.
- Ravel, B.; Newville, M. Athena, Artemis, Hephaestus: Data analysis for X-ray absorption spectroscopy using IFEFFIT. *J. Synchrotron Radiation*, **2005**, 12:537-541; DOI 10.1107/S0909049505012719.
- Refait, P.; Abdelmoula, M.; Trolard, F.; Génin, J.M.R.; Ehrhardt, J.J.; Bourrié G. Mössbauer and XAS study of green rust mineral; the partial substitution of Fe²⁺ by Mg²⁺. *Am. Mineral.*, **2001**, 86:731-739; DOI 10.2138/am-2001-5-613.
- Reichle, W.T. Synthesis of anionic clay-minerals (mixed metal-hydroxides, hydrotalcite). *Solid State Ionics*, **1986**, 22:135-141; DOI 10.1016/0167-2738(86)90067-6.
- Roberts, D.R.; Ford, R.G.; Sparks, D.L. Kinetics and mechanisms of Zn complexation on metal oxides using EXAFS spectroscopy. *J. Colloid Interface Sci.*, **2003**, 263:364-376; DOI 10.1016/S0021-9797(03)00281-9.
- Schaefer, M.V.; Gorski, C.A.; Scherer, M.M. Spectroscopic evidence for interfacial Fe(II)-Fe(III) electron transfer in a clay mineral. *Environ. Sci. Technol.*, **2011**, 45:540-545, DOI 10.1021/es102560m.
- Scheckel, K.G.; Scheinost, A.C.; Ford, R.G.; Sparks, D.L. Stability of layered Ni hydroxide surface precipitates: A dissolution kinetics study. *Geochim. Cosmochim. Acta*, **2000**, 64(16):2727-2735, DOI 10.1016/S0016-7037(00)00385-9.
- Scheckel, K.G.; Sparks, D.L. Kinetics of the formation and dissolution of Ni precipitates in a gibbsite/amorphous silica mixture. *J. Colloid Interface Sci.*, **2000**, 229(1):222-229, DOI 10.1006/jcis.2000.7001.
- Scheckel, K.G.; Sparks, D.L. Dissolution kinetics of nickel surface precipitates on clay mineral and oxide surfaces. *Soil Sci. Soc. Am. J.*, **2001**, 65(3):685-694, DOI 10.2136/sssaj2001.653685x.
- Scheidegger, A.M.; Lamble, G.M.; Sparks, D.L. Investigation of Ni sorption on pyrophyllite: An XAFS study. *Environ. Sci. Technol.*, **1996**, 30:548-554, DOI 10.1021/es950293+.
- Scheidegger, A.M.; Sparks, D.L. Kinetics of the formation and the dissolution of nickel surface precipitates on pyrophyllite. *Chem. Geol.* **1996**, 132:157-164, DOI 10.1016/S0009-2541(96)00051-4.

- Scheidegger, A.M.; Strawn, D.G.; Lamble, G.M.; Sparks, D.L. The kinetics of mixed Ni-Al hydroxide formation on clay and aluminum oxide minerals: a time-resolved XAFS study. *Geochim. Cosmochim. Acta*, **1998**, 62(13):2233-2245, DOI 10.1016/S0016-7037(98)00136-7.
- Scheinost, A.C.; Ford, R.G.; Sparks, D.L. The role of Al in the formation of secondary Ni precipitates on pyrophyllite, gibbsite, talc, and amorphous silica: A DRS study. *Geochim. Cosmochim. Acta*, **1999**, 63:3193-3203, DOI 10.1016/S0016-7037(99)00244-6.
- Scheinost, A.C.; Sparks, D.L. Formation of layered single- and double-metal hydroxides precipitates at the mineral/water interface: A multiple-scattering XAFS analysis. *J. Colloid Interface Sci.*, **2000**, 223:167-178, DOI 10.1006/jcis.1999.6638.
- Seiter, J.M.; Staats-Borda, K.E.; Ginder-Vogel, M.; Sparks, D.L. XANES spectroscopic analysis of phosphorus speciation in alum-amended poultry litter. *J. Environ. Qual.*, **2008**, 37:477-485, DOI 10.2134/jeq2007.0285.
- Shannon, R. D. Revised effective ionic radii and systematic studies of interatomic distances in halides and chalcogenides. *Acta Crystallogr.*, **1976**, A32:751-767, DOI 10.1107/S0567739476001551.
- Singh, B.; Grafe, M.. *Synchrotron-based techniques in soils and sediments*, Elsevier: Amsterdam, NL, 2010.
- Sparks, D.L. *Environmental soil chemistry*. 2nd ed. Academic Press, San Diego, CA, 2003.
- Suzuki, S.; Shinoda, K.; Sato, M.; Fujimoto, S.; Yamashita, M.; Konishi, H.; Doi, T.; Kaminura, T.; Inoue, K.; Waseda, Y. Changes in chemical state and local structure of green rust by addition of copper sulphate ions. *Corros. Sci.*, **2008**, 50:1761-1765, DOI 10.1016/j.corsci.2008.02.022.
- Thompson, H.A.; Parks, G.A.; Brown, G.E. Dynamic interactions of dissolution, surface adsorption, and precipitation in an aging cobalt(II)-clay-water system. *Geochim. Cosmochim. Acta*, **1999**, 63:1767-1779, DOI 10.1016/S0016-7037(99)00125-8.
- Thoral, S.; Rose, J.; Garnier, J.M.; Van Geen, A.; Refait, P.; Traverse, A.; Fonda, E.; Nahon, D.; Bottero, J.Y. XAS study of iron and arsenic speciation during Fe(II) oxidation in the presence of As(III). *Environ. Sci. Technol.*, **2005**, 39:9478-9485, DOI 10.1021/es047970x.

- Towle, S.N.; Bargar, J.R.; Brown, G.E.; Parks, G.A. Surface precipitation of Co(II)(aq) on Al₂O₃. *J. Colloid Interface Sci.*, **1997**, 187:62-82, DOI 10.1557/PROC-432-237.
- Trolard, F.; Génin, J.M.R.; Abdelmoula, M.; Bourrié, G.; Humbert, B.; Herbillon A. Identification of a green rust mineral in a reductomorphic soil by Mössbauer and Raman spectroscopies. *Geochim. Cosmochim. Acta*, **1997**, 61:1107-1111, DOI 10.1016/S0016-7037(96)00381-X.
- USEPA (U.S. Environmental Protection Agency). Method 3051A: Microwave Assisted Acid Digestion of Sediments, Sludges, Soils, and Oils. Washington, DC: USEPA, Office of Solid Waste, 2007.
- USEPA (U.S. Environmental Protection Agency). Method 6010C: Inductively Coupled Plasma-Atomic Emission Spectrometry. Washington, DC: USEPA, Office of Solid Waste, 2007.
- Voegelin, A.; Kretzschmar, R. Formation and dissolution of single and mixed Zn and Ni precipitates in soil: Evidence from column experiments and extended X-ray absorption fine structure spectroscopy. *Environ. Sci. Technol.*, **2005**, 39:5311-5318, DOI 10.1021/es0500097.
- Wasserman, S.R.; Allen, P.G.; Shuh, D.K.; Bucher, J.J.; Edelstein, N.M. EXAFS and principal component analysis: A new shell game. *J. Synchrotron Radiation*, **1999**, 6:284-286.
- Webb, S. M. 2005. SixPack: A graphical user interface for XAS analysis using IFEFFIT. *Phys. Scr.*, **2005**, T115:1011-1014, DOI 10.1238/Physica.Topical.115a01011.
- Whittig, L.D.; Allardice, W. R. X-ray diffraction techniques. In *Methods of Soil Analysis. Part I Physical and Mineralogical Methods*, 2nd ed.; A. Klute, Ed.; American Society of Agronomy, Madison, WI, 1986; pp. 331-362.
- Zhu, Y.; Elzinga, E.J. Formation of layered Fe(II)-hydroxides during Fe(II) sorption onto clay and metal-oxide substrates. *Environ. Sci. Technol.*, **2014**, 48:4937-4945, DOI 10.1021/es500579p.

Chapter 3

FORMATION OF A MIXED FE(II)-ZN-AL LAYERED HYDROXIDE: EFFECTS OF ZN CO-SORPTION ON FE(II) LAYERED HYDROXIDE FORMATION AND KINETICS

3.1 Abstract

Previous research demonstrated the formation of single divalent metal (Co-, Ni-, and Zn-Al) and mixed divalent metal (Ni-Zn-Al) layered double hydroxide (LDH) phases from reactions of the divalent metal with Al-bearing substrates and soils in both laboratory experiments and in the natural environment. Recently Fe(II)-Al-LDH phases have been found in laboratory batch reaction studies, and although they have yet to be found in the natural environment. Potential locations of Fe(II)-Al-LDH phases in nature include areas with suboxic and anoxic conditions. Because these areas can be environments of significant contaminant accumulation, it is important to understand the possible interactions and impacts of contaminant elements on LDH phase formation. One such contaminant, Zn, can also form as an LDH and has been found to form as a mixed divalent layered hydroxide phase. To understand how Zn impacts the formation of Fe(II)-Al-LDH phase formation and kinetics, 3 mM or 0.8 mM Fe(II) and 0.8 mM Zn were batch reacted with either 10 g/L pyrophyllite or 7.5 g/L γ -Al₂O₃ for up to three months under anoxic conditions. Aqueous samples were analyzed by inductively coupled plasma optical emission spectrometry (ICP-OES) and solid samples were analyzed with X-ray absorption spectroscopy (XAS). Shell-by-shell fits of Fe(II) and co-sorption samples with pyrophyllite show the formation of a

mixed divalent metal (Fe(II)-Zn-Al) layered hydroxide phase, while Fe(II) and Zn co-sorption samples with γ -Al₂O₃ produce Fe(II)-Al-LDH phases and Zn in inner-sphere complexation with the γ -Al₂O₃. This study demonstrates the formation of a mixed divalent metal layered hydroxide and further iterates the importance of sorbent reactivity on LDH phase formation.

3.2 Introduction

Reactions at the mineral-water interface can have a significant impact on metal sequestration in natural environments. Layered double hydroxides (LDH) are mineral phases that form from reactions of divalent metal ions (Ni, Zn, Co, and Fe(II)) with Al released due to mineral dissolution (Ford and Sparks, 2000; Roberts et al., 2003; Scheidegger et al., 1996; Scheidegger et al., 1998; Thompson, et al., 1999; Towle et al., 1997) and occur in natural and laboratory-contaminated soils (Jacquat et al., 2008; Juillot et al., 2003; McNear et al., 2007; Nachtegaal et al., 2005; Voegelin and Kretschmar 2005). The mineral phases formed are composed of brucite-like layers separated by interlayers; however, unlike brucite (Mg(OH)₂), LDHs have mixed-valence metal cations within the layers, yielding positively charged layers. These layers are separated by charge balancing interlayers composed of negatively charged anions (such as carbonate, nitrate, sulfate, chloride, and silicate) and water. As a result, these minerals are considered anionic clays since most clays contain cations, rather than anions, in their interlayers (de Roy et al., 2001). LDHs have the general chemical formula $[M^{II}_{1-x}M^{III}_x(OH)_2]_x+[A^{n-}]_{x/n}\cdot yH_2O$, where M^{II} is a divalent metal cation, M^{III} is a trivalent metal cation, and A is one of several possible interlayer anions (de Roy et al., 2001; Reichle, 1986). In environmentally relevant systems, Al is the most common trivalent metal cation.

Recently, it was determined by X-ray absorption spectroscopy (XAS) that Fe(II)-Al(III)-layered double hydroxide (LDH) phases form during reactions of γ -Al₂O₃ and Al-bearing clays with Fe(II) at near-neutral pH under anoxic conditions (Elzinga, 2012; Zhu and Elzinga, 2014; Starcher et al. 2016). It is currently unknown whether Fe(II)-Al(III)-LDH phases exist in the natural environment; however, other LDH phases (such as Al-bearing LDHs and green rusts) have been found in nature (Abdelmoula et al., 1998; Feder et al., 2005; Jacquat et al., 2008; Juillot et al., 2003; McNear et al., 2007; Nachtegaal et al., 2005; Trolard et al., 1997; Voegelin and Kretzschmar 2005).

The laboratory conditions under which Fe(II)-Al(III)-LDH phases form is representative of conditions in natural suboxic and anoxic environments, such as wetland soils. Such environments can frequently be areas of significant contaminant accumulation, so it is important to understand the possible interactions and impacts of contaminant elements on LDH phase formation. Zhu and Elzinga (2015) recently examined the impacts of As(III) and As(V) co-sorption on Fe(II)-Al(III)-LDH phase formation. They found that As(III) and Fe(II) react independently of one another and do not impact the other's sorption process; however, the presence of As(V) decreases Fe(II) sorption, limiting LDH formation at low concentrations and completely inhibiting its formation at higher concentrations.

Another soil contaminant, Zn, is also known to form LDH phases in laboratory and field environments (Ford and Sparks, 2000; Khaokaew et al., 2012; Li et al., 2012; Nachtegaal and Sparks, 2004; Paulhiac and Clause, 1993; Roberts et al., 2003; Trainor et al., 2000; Voegelin et al., 2005; Voegelin and Kretzschmar, 2005). Mixed divalent metal layered hydroxide phases (e.g. Ni-Zn-Al layered hydroxide) have been observed

in laboratory contamination column experiments in which soils were synthetically contaminated with Zn and Ni (Voegelin and Kretzschmar, 2005). Acidification of these soils resulted in the dissolution of Zn-bearing LDH phases before Ni-bearing LDH phases, suggesting that the rates of metal incorporation into the LDH determines the LDH structure. Therefore, LDH structure ultimately determines the rate of LDH dissolution in acidic conditions. Because Fe(II) ions are of similar size to the other divalent metal ions that form LDH phases, it is important to understand if and how these ions are incorporated into the LDH structure together. The objective of this study was to examine Fe(II) and Zn co-sorption to an Al-bearing oxide and phyllosilicate to determine the effects of Zn on sorption products and kinetics, and ultimately determine if formation of a mixed divalent metal (Fe(II)-Zn-Al-LDH) phase will form from these reactions. By understanding how Zn may interact with Fe-sorption, we can better understand natural environments in which Fe(II)-Al(III)-LDH phases may occur.

3.3 Materials and Methods

3.3.1 Mineral Characterization

This study was conducted using pyrophyllite and γ -Al₂O₃. The pyrophyllite was previously characterized in Starcher et al., 2016. The 5-nm γ -Al₂O₃ (product # 1328Q1) was reported to have a purity of 99.9% and a surface area of 300 m²/g by the manufacturer (SkySpring Nanomaterials).

3.3.2 Maintaining an Anoxic Atmosphere

Reactions were conducted using the experimental setup reported in Starcher et al. (2016). A Coy glovebox containing a 96% N₂ – 4% H₂ atmosphere and a

palladium catalyst for trace O₂ removal was used to maintain an anoxic environment. O₂ levels were monitored using an O₂-H₂ meter to ensure an atmospheric O₂ concentration of <1 ppm, and a dehumidifier was used to reduce humidity produced by the catalyst. DI water for the batch reactions was prepared by simultaneously boiling and N₂ purging the water, followed by 2 d of cooling in the glovebox to outgas remaining O₂.

3.3.3 Macroscopic Sorption Experiments

Reaction kinetics of Fe(II) and Zn co-sorption onto pyrophyllite and γ -Al₂O₃ were examined using a batch reaction method following the method used by Starcher et al. (2016) for a reaction time of up to 12 weeks. Solid concentrations of either 10 g/L pyrophyllite or 7.5 g/L γ -Al₂O₃ were prepared in polypropylene tubes inside the glovebox and hydrated for either 1 d or 3 d, respectively, while open to the glovebox atmosphere (Elzinga, 2012; Scheidegger et al., 1996). Background electrolytes consisted of 0.1 M NaCl and 50 mM 4-(2-hydroxyethyl)-piperazine-1-ethanesulfonic acid (HEPES) buffer to maintain a pH of 7.5. The pH was adjusted to 7.5 using 1 M and 0.1 M HCl. Fe(II) and Zn(II) stock solutions (1.0 M and 0.1 M, respectively) were prepared by dissolving either FeCl₂·H₂O or ZnCl₂ salts in anoxic 0.1 M HCl and filtering the solute through a 0.22 μ m nitrocellulose filter membrane. Appropriate aliquots of the Fe(II) and Zn(II) stock solutions were added slowly to the batch reaction vessel under vigorous mixing to achieve final Fe(II) (0.8 mM or 3 mM) and Zn(II) (0.8 mM) concentrations. After the initial addition of metal solutions, the batch reaction vessels were placed on rotators to ensure mixing throughout the entire experiment. The pH and initial Fe(II) and Zn concentrations were selected for direct comparison with other studies using similar reaction conditions (Elzinga, 2012; Ford

and Sparks, 2000; Li et al., 2012; Scheidegger et al., 1996; Starcher et al., 2016; Zhu and Elzinga, 2014; Zhu and Elzinga, 2015). The pH of the batch reaction was measured at each sampling point, and it was found to deviate from the initial pH value by <0.4 pH units over the entire reaction period. Macroscopic kinetic samples were removed from the batch reaction vessel in 10-mL increments and were syringe-filtered with a 0.22 μm nitrocellulose filter.

Samples were prepared for elemental analysis by inductively coupled plasma optical emission spectrometry (ICP-OES) by adding the appropriate aliquot of anoxic 1 M HCl to achieve a 5% HCl background to prevent precipitation (USEPA, 2007b). Blanks and Fe, Zn, and Si standards were prepared with a 5% HCl background. The University of Delaware Soil Testing Laboratory used the USEPA Method 6010C (USEPA, 2007b) to measure elemental concentrations with ICP-OES.

3.3.4 Speciation of Sorption Samples and Standards

3.3.4.1 Preparation of Sorption Samples

Batch reactions for XAS analysis were prepared using identical solid concentration, background electrolytes, hydration time, pH, and metal concentrations as the previously mentioned macroscopic kinetics experiment; however, XAS samples were reacted in 50-mL polypropylene tubes with a 30 mL total sample volume. Samples were centrifuged outside the glovebox for 5 min at 10,000 g and returned to the glovebox for 24 h before brief air-drying inside the glovebox to create a wet paste. Each wet paste was sealed into lucite sample holders with Kapton[®] tape.

3.3.4.2 Preparation of Standards

A 1:1:1 Fe(II)/Zn(II)/Al(III) mixed divalent metal LDH standard was prepared by coprecipitation inside the glovebox under anaerobic conditions, following a method similar to that of Li et al. (2004). Briefly, a metal solution (10 mM Fe(II), Zn(II), and Al(III)) was prepared by adding the appropriate aliquots of 1 M Fe(II), 0.1 M Zn(II), and 50 mM Al(III) stock solutions. Stock solutions were prepared from anoxic deionized water and FeCl₂, ZnCl₂, and AlCl₃, respectively, and had a 0.1 M HCl background. To the metal solution, 1 M NaOH was added dropwise under vigorous stirring until the pH reached 8.0. A maximum pH of 8.0 was selected to ensure that the solution was above the pH at which the pure metal hydroxide phase forms for each metal (at 10⁻² M, pH of Fe(II) = 7.5, Zn(II) = 6.5, and Al(III) = 3.9) but was below the pH at which Al and Zn hydroxides re-dissolve (pH of Al hydroxide = 9.0-12.0 and Zn hydroxide = 14.0) (Cavani et al., 1991). The suspension was then aged for 4 h inside the glovebox and centrifuged for 5 minutes at 10,000 g to separate the solid phase (Li et al., 2004). The solid was then washed with anoxic deionized water and centrifuged for 5 minutes at 10,000 g, and the resulting standard was air-dried inside the glovebox. The supernatant was acidified with a 5% HCl background and analyzed by the University of Delaware Soil Testing Laboratory with ICP-OES to determine elemental concentrations of Fe, Zn, and Al (USEPA, 2007b). The air-dried standards were microwave-digested by the University of Delaware Soil Testing Laboratory according to procedures in USEPA Method 3051 (USEPA, 2007a).

Other Fe and Zn standards used in this study include those used in previously published studies: nikischerite (NaFe^{II}₆Al₃(SO₄)₂(OH)₁₈(H₂O)₁₂), an Fe(II)-Al(III)-LDH; 10 mM Fe^{II} solution; “white rust” (Fe^{II}(OH)₂) (Elzinga, 2012); magnetite (Fe^{III}₂Fe^{II}O₄); 2-line ferrihydrite (5Fe^{III}₂O₃·9H₂O); hydroxylchloride green rust; Fe(II)-

phyllosilicate (Zhu and Elzigna, 2014); goethite (α -FeO(OH)); hematite (Fe₂O₃); lepidocrocite (γ -FeO(OH)); pyrite (FeS₂); vivianite (Fe(PO₄)₂•nH₂O); siderite (FeCO₃) (Chen, 2013); natural pyrophyllite with Fe(III) impurities; and greenalite ((Fe^{II}, Fe^{III})₂₋₃Si₂O₅(OH)₄) (Starcher et al., 2016); Zn/Al-LDH (Li et al., 2012); Zn-(OH)₂ (Roberts et al., 2003); aqueous Zn solution (Nachtegaal and Sparks, 2004); Zn-kerolite; (Zn₅(CO₃)₂(OH)₆); ZnO; franklinite (ZnFe₂O₄); and willemite (Zn₂SiO₄) (Khaokaew et al., 2012).

3.3.4.3 Bulk Extended X-Ray Absorption Fine Structure Spectroscopy (EXAFS)

Bulk-XAS analysis was performed at the National Synchrotron Light Source (NSLS) at beamline X11-A and at Stanford Synchrotron Radiation Lightsource (SSRL) at beamline 4-1. Samples were individually sealed in five ziplock bags for transport to the beamline, which has been shown to be effective at maintaining sample oxidation state (Elzinga, 2012; Starcher et al., 2016). For Fe, the Si(III) monochromator was calibrated with an Fe foil to record Fe *K* edge spectra at an E₀ of 7112 eV. For Zn, Si(III) monochromator calibration was performed using a Zn foil, and Zn *K* edge spectra were recorded at an E₀ of 9659 eV. Both Stern-Heald Lytle and passivated implanted planar silicon (PIPS) detectors were used to collect the fluorescence data. Elastic scattering was reduced by placing a Mn or Cu filter between the detector and sample for Fe and Zn analyses, respectively. When collecting data at NSLS beamline X11-A, 50% detuning was used to reduce harmonics. Samples were removed from the ziplock bags just prior to analysis, and no visual signs of oxidation were observed before or after XAS analysis. A minimum of three scans were collected for each sample to improve signal-to-noise ratio.

After bulk-EXAFS $\mu(E)$ spectra were averaged, background subtracted, and normalized, the $\chi(k)$ functions were k^3 -weighted using Athena (Demeter 0.9.16) (Ravel and Newville, 2005). Forward and backward Fourier transforms of the k^3 -weighted χ functions were performed in Athena (Demeter 0.9.16) using Hanning windows with a dk of 0.5 and a dR of 0.2, respectively.

Wavelet transform (WT) analysis was used to visually determine differences for Fe and Zn first metal shell (second overall shell) coordination environments in RSFs. WT analysis was performed with the WT calculation in Igor Pro 6.37 and the Morlet mother wavelet function (Funke et al., 2005). The Morlet parameters used on the non-phase shift corrected k^3 -weighted χ spectra were $\eta = 5.5$ and $\sigma = 1$ to optimize resolution in r - and k -space. The range in r -space over which the transform was applied was 2.4 - 3.2 Å.

Shell-by-shell fits of Fe(II)-Zn co-sorption samples and standards were performed in Artemis (Demeter 0.9.16) (Ravel and Newville, 2005). RSF data were transformed for fitting over a k -range of 3.0 to 10.5. Theoretical back-scattering paths were determined by Feff 6.0 calculations using an augmented lizardite crystal structure in which Fe, Zn, and Al were substituted for Mg in the octahedra. The amplitude reduction factor (S_0^2) was 0.85 for all fits (O'Day et al., 1994). Data were fitted with Fe-O for the first shell, and Fe-Fe, Fe-Al, Fe-Zn, and/or Fe-Si for the second shell. The Debye-Waller factors (σ^2) and the radial distance (R) were restricted for all elements in the second shell according to the isotropic expansion-contraction fitting model used, and the second shell CN was restricted to ~ 6 , consistent with octahedral coordination in the LDH structure (Kelly et al., 2008). However, when Si was included in the fits an additional CN of 2 was allowed for an

Fe/Zn-Si path due to the presence of Si in the local coordination environment of the central atom through interlayer silication (Charlet and Manceau, 1994).

3.4 Results

3.4.1 Sorption Kinetics

Figure 3.1a shows relative Fe and Zn removed from the Fe(II) (3mM and 0.8 mM) and Zn (0.8 mM) solutions during co-sorption reactions with pyrophyllite compared to the results for sorption of Fe(II) with pyrophyllite from a previous study (Starcher et al., 2016). Fe data were corrected for Fe that was released into solution during dissolution of pyrophyllite that occurred during the pyrophyllite hydration period of 24 h, which was approximately 1×10^{-6} M Fe. These results demonstrate an initial fast reaction step for all systems followed by a slower step, which is typical of metal(loid) sorption onto mineral surfaces (Elzinga, 2012; Ford and Sparks, 2000; Roberts et al., 2003; Scheidegger et al., 1996; Scheidegger et al., 1998; Thompson, et al., 1999; Towle et al., 1997). In both pyrophyllite co-sorption reactions, >90% of Zn is removed from both Zn solutions during the first 24 h, and >97% of Zn is removed by the end of the 12 wk reaction time, at which point the Zn removal appears to have approached an equilibrium. For the co-sorption reaction containing 3 mM Fe, 32% of Fe is removed during the first 24 h and 77% of Fe by the end of the 12 wk reaction time. A lower relative Fe removal was observed in the co-sorption reaction containing 0.8 mM Fe where 7% of Fe was removed in the first 24 h and 71% of Fe was removed by the end of the reaction time. Fe removal does not appear to have reached an equilibrium by the end of the reaction time in either co-sorption reaction. When

compared to the pyrophyllite sorption systems containing only Fe(II), the Fe removal in the respective co-sorption systems is less than those systems not containing Zn.

Relative Fe and Zn removal from the Fe(II) (3mM) and Zn (0.8 mM) solutions during the co-sorption reaction with γ -Al₂O₃ is shown in Figure 3.1b. Also shown is Fe removal from an Fe(II) (3 mM) only sorption reaction with γ -Al₂O₃. These results exhibit the same bimodal kinetics as observed in reactions with pyrophyllite above and as seen in previous studies (Elzinga, 2012; Ford and Sparks, 2000; Roberts et al., 2003; Scheidegger et al., 1996; Scheidegger et al., 1998; Thompson, et al., 1999; Towle et al., 1997). In the reaction containing Zn, >99% of Zn is removed from solution during the first 24 h; soon after the Zn removal appears to have approached an equilibrium. For the co-sorption reaction, 79% of the Fe is removed during the first 24 h and 93% by the end of the 12 wk reaction time. Iron removal appears to have reached an equilibrium by the end of the reaction time. Like the reactions with pyrophyllite, sorption kinetics of the Fe(II)-only reaction with γ -Al₂O₃ exhibits a greater percentage of Fe removed from the system than the reaction containing both Fe(II) and Zn; however, the difference between Fe removal in the γ -Al₂O₃ systems is much less than the difference in Fe removal in the pyrophyllite systems. The difference between Fe removal during Fe sorption and Fe-Zn co-sorption for all systems appears to decrease with time; however, longer reaction times would be required to confirm this trend.

Figure 3.2 shows simultaneous Si dissolution from the pyrophyllite in the Fe(II)-Zn co-sorption systems and in the Fe(II) only system previously reported. Silicon data were corrected for the approximately 1×10^{-4} M Si that was released into solution during dissolution of pyrophyllite that occurred during the pyrophyllite

hydration period of 24 h, as reported in the previous study (Starcher et al., 2016). The observed concentration agrees well with the Si dissolution observed by Scheidegger et al. (1996) for the same pyrophyllite. Silicon release is greatest in the systems containing the highest total metal concentrations. When comparing the co-sorption systems to the Fe(II) only systems, Si release is greater in systems that also contain Zn. The increased release of Si from pyrophyllite in the systems with higher total Fe(II) and Zn concentrations agrees with results of previous work showing that pyrophyllite dissolution and Si release is enhanced by these metal sorption processes (Scheidegger et al., 1996). With increased reaction time, Si concentrations in solution begins to decrease, indicating Si sorption. This is consistent with previous studies by Ford et al. (2001), Scheckel and Sparks (2001), and Scheckel et al. (2000).

3.4.2 Standards Characterization

A 1:1:1 Fe(II)-Zn(II)-Al(III) mixed divalent metal layered hydroxide standard was prepared by coprecipitation inside the glovebox under anaerobic conditions (Li et al., 2004). From ICP-OES analysis for total elemental concentrations, the concentrations of Fe, Zn, and Al remaining in solution were determined to be 0.075, 0.022, and 0.101 ppm, respectively. Concentrations of Fe, Zn, and Al in solution that precipitated into the solid LDH phases were calculated to be 558.4, 653.8, and 269.7 ppm, respectively, resulting in >99% inclusion of all elements into the precipitate phase. This agrees well with the acid digestion data, which also resulted in a 1.2, 1.2, and 1.3 mol/kg (~1:1:1) Fe(II)-Zn(II)-Al(III) layered hydroxide standard. The resulting Fe(II)-Zn(II)-Al(III) layered hydroxide standard has a M^{II}/M^{III} ratio of ~2, which is consistent with preferred M^{II}/M^{III} ratios of LDH phases (Bravo-Suárez et al., 2004; Cavani et al., 1991; Khan and O'Hare, 2002; Takagi et al., 1999).

Powder XRD data are presented in Figure 3.3. The XRD sample showed visible signs of oxidation during data collection; when the sample was removed from the glovebox it was blue-green and shortly after beginning XRD data collection the sample became yellowed with oxidation. This sample, unlike the XAS sample, was not protected from oxidation during data collection with Kapton® tape. The XRD data was fit with zaccagnaite (Zn-Al-LDH) and fougérite (Fe(II)-Fe(III)-LDH).

The Fe(II)-Zn-Al layered hydroxide was characterized with Fe and Zn XAS. Fe and Zn K edge k^3 -weighted χ functions and radial structure functions (RSF) are given in Figure 3.4 and Figure 3.6, respectively. This standard has the diagnostic LDH oscillation pattern in the χ spectra at 7-8 Å⁻¹ of both Zn and Fe, suggesting that each of these elements has contributions from Al backscattering and is precipitated as an LDH (Scheinost and Sparks, 2000). The RSF has the first Fe coordination shell (O ligands in the first shell surrounding Fe) at ~1.6 Å (uncorrected for phase shift). Through shell-by-shell fitting (Table 3.1) the Fe-O shell was fitted with 5.5 O atoms at a radial distance of 2.12 Å. This arrangement is consistent with O atoms in octahedral coordination with the central Fe(II) atom (Elzinga, 2012; Huminicki and Hawthorne, 2003; Olszewski et al., 2011; Parise et al.; 2000; Shannon 1976). The second shell was fitted with Fe, Al, and Zn atoms at a distance of 3.15 Å. The Fe-Al path was included due to the presence of the diagnostic “beat” pattern, and the Fe-Zn path was included in this fit because it improved the R-factor of the fit by greater than 20% (Malinowski, 1978). The first Zn coordination shell (O ligands in the first shell surrounding Fe) are at ~1.6 Å (uncorrected for phase shift) in the RSF. Through shell-by-shell fitting (Table 3.2) the Zn-O shell was fitted with 5.5 O atoms at a radial distance of 2.12 Å. This arrangement is consistent with O atoms in octahedral

coordination with the central Zn atom (Waychunas et al., 2002). The second shell was fitted with Zn, Al, and Fe atoms at a distance of 3.15 Å. The Zn-Al path was included due to the presence of the diagnostic “beat” pattern, and the Zn-Fe path was included in this fit because it improved the R-factor of the fit by greater than 20% (Malinowski, 1978). The M^{II}/M^{III} ratio from the shell-by-shell fits for the Fe and Zn k edges are both 2.2, which is consistent with the ratios determined from both the mineral acid digestion data and the reaction solution analysis.

3.4.3 XAS Data

3.4.3.1 Fe EXAFS

Fe K edge k^3 -weighted χ functions and radial structure functions (RSF) of Fe(II)-Zn co-sorption samples with pyrophyllite containing structural Fe impurities or γ - Al_2O_3 reacted at pH 7.5 under anoxic conditions are given in Figure 3.4. Figure 3.3 also shows data for reference Fe standards nikischerite, Fe(II)-phyllosilicate, and Fe(II)-Zn(II)-Al(III) layered hydroxide. When comparing the 7-8 Å⁻¹ fingerprint regions of the k^3 -weighted χ functions for samples and standards in Figure 3.4a, the sorption samples appear most similar to nikischerite, Fe(II)-Zn-Al layered hydroxide, and Fe(II)-phyllosilicate, which is consistent with results previously found for sorption of Fe(II) to clays and Al-oxides under similar conditions (Elzinga, 2012; Starcher et al., 2016; Zhu and Elzinga, 2014).

RSFs of co-sorption samples are shown in Figure 3.4b. Through shell-by-shell fitting (Table 3.1) the Fe-O shell was fitted with 5.5-6.0 O atoms at radial distances of 2.08-2.12 Å. This arrangement is consistent with O atoms in octahedral coordination with the central Fe(II) atom (Elzinga, 2012; Huminicki and Hawthorne, 2003;

Olszewski et al., 2011; Parise et al.; 2000; Shannon 1976). A growth in the second shell was observed in the pyrophyllite co-sorption samples, suggesting increased backscattering from heavier elements with time. This is consistent with the macroscopic data showing increased Fe removal from solution in the pyrophyllite systems over time; the system had not yet reached equilibrium at the end of the reaction period. On the other hand, there is no growth observed in the second shell of the γ -Al₂O₃ samples taken at longer times suggesting that there was no increase in backscattering from heavier elements with reaction time. This agrees well with the macroscopic data; the reaction reached equilibrium within a week of reaction time. The second shells of pyrophyllite and γ -Al₂O₃ co-sorption samples were fitted with Fe, Al, and Zn or Fe and Al atoms, respectively, at a distance of 3.14-3.17 Å, consistent with the structure of LDHs found in previous works (Elzinga, 2012; Starcher et al., 2016; Zhu and Elzinga, 2014; Zhu and Elzinga, 2015). Zn was removed from Fe XAS fits of the γ -Al₂O₃ sorption samples due to the mixed structure of Zn (discussion below). The LDH fingerprint is present in both of the γ -Al₂O₃ systems and in the 7 d pyrophyllite co-sorption samples (circled regions in Figure 3.4a). The spectra for the 7 d co-sorption pyrophyllite systems appear strikingly similar to the chi spectra for Fe(II) sorption pyrophyllite studied previously (Starcher et al., 2016). The fingerprint oscillation is missing in the 28 d pyrophyllite co-sorption samples, although present in the 7 d samples, consistent with the previous study which found interlayer silication with increased reaction time (Starcher et al., 2016). From the shell-by-shell fits, the co-sorption samples have M^{II}/M^{III} ratios ranging from 3.2-3.8. These ratios fall into the range of preferred M^{II}/M^{III} for LDH phase formation of 2-4 (Bravo-Suárez et al., 2004; Cavani et al., 1991; Khan and O'Hare, 2002; Takagi et al., 1999).

WT plots of Fe EXAFS data with optimization in r- and k-space for the first metal coordination shell (second overall coordination shell) for central Fe(II) of the co-sorption samples and standards Fe(OH)₂, nikischerite, and the Fe(II)-Zn-Al layered hydroxide standard are presented in Figure 3.5. The Al and Fe atoms in the first metal coordination shell of central Fe(II) are resolved through two k maxima at R = 2.5 Å in the Fe(II)-Al-LDH (nikischerite) and Fe(II)-Zn-Al layered hydroxide WT plots (Figure 3.5b,c). In these figures, the lowest k maximum represents a light second shell neighbor, in this case Al, while the higher k maximum represents a heavy second shell neighbor, in this case Fe (Funke et al., 2005). Fe(II)-Zn co-sorption samples also have WT plots in which Al and Fe are resolved in the second shell (Figure 3.5d-i). The β-Fe(OH)₂ first metal coordination shell WT plot shows only one k maximum of 8-9 Å⁻¹ at R = 2.5 Å (Figure 3.5a) as expected due to the presence only of Fe(II) as the metal cation in the mineral structure (Zhu and Elzinga, 2014).

3.4.3.2 Zn EXAFS

Zinc K edge k³-weighted χ functions and radial structure functions (RSF) of Fe(II)-Zn co-sorption samples with pyrophyllite containing structural Fe impurities or γ -Al₂O₃ reacted at pH 7.5 under anoxic conditions are given in Figure 3.6. Figure 3.6 also shows data for reference Zn standards: Zn-Al-LDH, Zn-kerolite, and Fe(II)-Zn(II)-Al(III) layered hydroxide. When comparing the 7-8 Å⁻¹ regions of the k³-weighted χ functions, the fingerprint region for LDH phases, for samples and standards in Figure 3.6a, the pyrophyllite co-sorption samples appear most similar to Zn-Al-LDH, Zn-kerolite, and Fe(II)-Zn-Al layered hydroxide, which is consistent with results previously found for sorption of Zn to clays and Al-oxides under similar conditions (Ford and Sparks, 2000; Li et al., 2012; Nachtegaal and Sparks, 2004;

Roberts et al., 2003). The LDH fingerprint feature is present in all of the pyrophyllite co-sorption samples (circled regions in Figure 3.6a). Co-sorption samples with γ - Al_2O_3 , however, do not exhibit this feature. Instead, they show a splitting feature near 4 \AA^{-1} indicative of backscattering from lighter atoms (such as Al) beyond the second shell as in Zn-Al-Al multiple scattering paths (Roberts et al., 2003; Yamaguchi et al., 2002).

RSFs of Zn co-sorption samples are shown in Figure 3.6b. Through shell-by-shell fitting (Table 3.2) the Zn-O shell for pyrophyllite co-sorption samples was fitted with 6.5 O atoms at a radial distance of 2.01-2.07 \AA . The second shell in the pyrophyllite co-sorption samples experienced no growth with time, which is consistent with the macroscopic Zn data due to Zn sorption in these systems reaching equilibrium by the first EXAFS sampling point. The second shell was fitted with Zn, Al, and Fe atoms at a distance of 3.11-3.14 \AA , consistent with the structure of LDH phases found previously (Ford and Sparks, 2000).

The Zn-O shell of γ - Al_2O_3 co-sorption samples was fitted with 5.1 O atoms at 1.98 to 2.01 \AA . This radial distance is consistent with other studies that have shown Zn in mixed tetrahedral-octahedral coordination during sorption to Al oxides (Li et al., 2012; Roberts et al., 2003; Trainor et al., 2000). No growth is observed in the second shell of the γ - Al_2O_3 samples taken at longer times which agrees well with the macroscopic data as the reaction had reached equilibrium within a week of reaction time. The second shell was fitted with Zn and Al atoms at a distance of 3.09 to 3.11 \AA . The LDH fingerprint oscillation at $7\text{-}8 \text{ \AA}^{-1}$ is missing in the γ - Al_2O_3 co-sorption samples. This is expected due to the presence of a mixed tetrahedral-octahedral coordination for the Zn-O shell, and it has been observed in other studies of Zn

sorption to Al oxides (Li et al., 2012; Roberts et al., 2003; Trainor et al., 2000). A Zn-Fe path was excluded from the fit because of: 1) the presence of a mixed tetrahedral-octahedral structure; and 2) its inclusion did not improve the fit by 20% (Malinowski, 1978).

WT plots of Zn EXAFS data with optimization in r- and k-space for the first metal coordination shell (second overall coordination shell) for central Zn of the co-sorption samples and standards Zn(OH)₂, Zn-Al-LDH, and the Fe(II)-Zn-Al layered hydroxide standard are presented in Figure 3.7. The Al and Zn atoms in the first metal coordination shell of central Zn are resolved through two k maxima at R = 2.5 Å in the Zn-Al-LDH and Fe(II)-Zn-Al layered hydroxide WT plots (Figure 3.7b,c). In these figures, the lowest k maximum represents Al, the lighter second shell neighbor, and the higher k maximum represents Zn, the heavy second shell neighbor (Funke et al., 2005). Fe(II)-Zn co-sorption samples also have WT plots in which Al and Zn are resolved in the second shell (Figure 3.6d-i). The Zn(OH)₂ first metal coordination shell WT plot also shows two k maxima at R = 2.5 Å (Figure 3.7a) which is surprising due to the presence of only Zn as the metal cation in the octahedral oxide structure. The presence of the second k maximum at 8-9 Å⁻¹ is expected due to Zn backscattering; however, the lower k maximum is unexpected. Previous work has attributed the presence of two maxima in single metal hydroxides to: 1) Si contamination during sample preparation; and 2) contamination from salts (Siebecker, 2013; Zhu and Elzinga, 2014).

3.5 Discussion

3.5.1 Macroscopic Study

A comparison of Figures 3.1 and 3.1b demonstrates more rapid Fe sorption by γ -Al₂O₃ than pyrophyllite in the 3 mM Fe – 0.8 mM Zn co-sorption reactions: 32% Fe was sorbed during the first 24 h of reaction time with pyrophyllite while 79% was sorbed during the reaction with γ -Al₂O₃. A similar trend was observed by others with reactions of metals with Al-bearing substrates (Ford et al., 1999; Ford et al., 2001; Johnson and Glasser, 2003; Li et al., 2012; Peltier et al., 2010; Roberts et al., 2003; Scheckel et al., 2000; Scheidegger et al., 1998; Scheinost and Sparks, 2000). In a study by Zhu and Elzinga (2014), clay suspensions exhibited slower Fe(II) sorption kinetics than γ -Al₂O₃ suspensions, and ultimately Fe(II)-Al(III)-LDH phases were observed after longer reaction times in the clay suspensions than those with γ -Al₂O₃. Slower dissolution of Al from the clays relative to γ -Al₂O₃ results in slower kinetics of LDH phase formation, and this slower dissolution by clays has also been shown to limit formation of phyllosilicates due to slower Si release (Li et al., 2012; Scheidegger et al., 1998; Zhu and Elzinga, 2014). The types of mineral sorbents used in metal sorption reactions are significant factors to consider, as their dissolution ultimately controls the Al and Si available for LDH phase formation and stabilization.

3.5.2 Spectroscopic Study

The spectroscopic study demonstrates the formation of Fe(II)-Zn-Al layered hydroxide through Fe(II) and Zn co-sorption to pyrophyllite. Sorption of either Fe(II) or Zn exclusively to this pyrophyllite has shown to form Fe(II)- and Zn-Al-LDH phases in other studies (Ford and Sparks, 2000; Starcher et al., 2016). EXAFS spectra (Figures 3.4a and 3.6a) and WT plots (Figures 3.5 and 3.7) for the co-sorption samples

are similar to that of both the Fe(II)- and the Zn-Al-LDH phases as well as the Fe(II)-Zn-Al layered hydroxide phase. The χ spectra of all LDH phases are similar due to Al backscattering causing destructive interference at 7-8 Å⁻¹, and the WT plots are not sensitive enough to the first metal shell to discriminate between the two high Z (i.e. Fe and Zn) elements, contributing to the maximum for the heavier atoms. Inclusion of the co-sorbed element to the original element's fits following the Al path significantly improved (>20% decrease in R-factor) the fits found in Tables 3.1 and 3.2 (Malinowski, 1978). Voegelin and Kretzschmar (2005) have also demonstrated through XAS the formation of mixed divalent metal layered hydroxides (i.e. Ni(II)-Zn(II)-Al(III) layered hydroxide) in column experiments. In these systems, the mixed divalent metals had similar retention rates as the single divalent metal systems; however, acidification of the precipitates resulted in complete dissolution of the Zn-Al and Ni-Zn-Al-LDH phases formed whereas the Ni-Al-LDH remained largely intact upon acidification. Their study suggested that the individual rates at which the divalent metal forms an LDH precipitate affects the rate at which these phases dissolve upon acidification.

In the Fe EXAFS spectra of the pyrophyllite co-sorption samples it is clear that an LDH phase has formed at the 7 d sample times due to the presence of the “beat” pattern at 7-8 Å⁻¹ (Figure 3.4a) and the Fe-Fe/Al bond distances (Table 3.1). At the 28 d sample time, however, the diagnostic “beat” pattern indicative of LDH phase formation is missing. In previous work with Fe(II), Starcher et al. (2016) found the incorporation of Si into the interlayer of low Fe(II) concentration sorption samples at 28 d of reaction time; although it was not observed in the high Fe(II) concentration samples, likely due to interference from relative contributions of Fe and Si to the

EXAFS spectra. In the co-sorption systems, however, there is enhanced mineral dissolution and increased release of Si compared to those systems without Zn (Figure 3.2), suggesting that Zn is enhancing the pyrophyllite dissolution. Li et al. (2012) and Scheidegger et al. (1998) observed enhanced mineral dissolution during metal sorption which was found to be a key factor in the formation of LDH phases. The increased aqueous Si concentrations in these systems will allow for silication of the LDH interlayer, which has been previously observed in M^{II} sorption to clays and soils (Ford et al., 1999; Ford et al., 2001; Scheckel and Sparks, 2001; Scheckel et al., 2000; Scheinost et al., 1999; Starcher et al., 2016). The change in the pyrophyllite co-sorption Fe χ spectra at 7-8 \AA^{-1} in Figure 3.4a suggests silicate substitution in the interlayer after longer reaction times.

A mixed divalent metal layered hydroxide phase formed in the presence of pyrophyllite during co-sorption reactions; LDH phase formation was expected in this system as was found in other studies (Ford and Sparks, 2000; Scheidegger et al., 1996; Starcher et al., 2016). Due to the solubility of $\gamma\text{-Al}_2\text{O}_3$ and previous studies demonstrating rapid formation of LDH phases with this similar $\gamma\text{-Al}_2\text{O}_3$ substrates, we would expect both Fe(II)- and Zn-Al-LDH phase formation in this system (Elzinga, 2012; Li et al., 2012; Trainor et al. 2000). However, the formation of Fe(II)-Al-LDH and Zn in inner-sphere complexation was found in the $\gamma\text{-Al}_2\text{O}_3$ co-sorption system studied here. In the case of Fe for the $\gamma\text{-Al}_2\text{O}_3$ systems, the formation of Fe(II)-Al-LDH phases is still observed, as clearly demonstrated through the: 1) LDH diagnostic at 7-8 \AA^{-1} (Figure 3.4a), which was also observed in Fe(II) sorption to $\gamma\text{-Al}_2\text{O}_3$ by Elzinga (2012); 2) the two k maxima present in the WT plots in Figures 3.5f and 3.5i; and 3) the Fe-O and Fe-Fe/Al bond distances indicative of octahedral coordination and

LDH phase formation (Table 3.1). Bond distances from Zn-O paths (Table 3.2) show a mix of tetrahedral and octahedral coordination consistent with previous findings of inner-sphere complexation (Li et al., 2012; Roberts et al., 2003). In previous work on Zn-Al-LDH formation and Zn sorption to Al oxides, it was determined that the reactivity of the surface sites on the substrate, not only the total surface area, was a key factor controlling the Zn sorption (Roberts et al., 2003). This is an important consideration when comparing co-sorption between the two substrates used in this study. Roberts et al. (2003) found rapid bimodal sorption of Zn on a high surface area gibbsite, and the mechanism of Zn uptake was attributed to inner-sphere complexation that did not change with aging time. This configuration would allow Zn to be in either tetrahedral or octahedral coordination and is due to having: 1) a zero value for crystal field stabilization energy; and 2) an intermediate radius-ratio for either coordination geometry (Waychunas et al., 2002). Alternatively, Roberts et al. (2003) found formation of Zn-Al-LDH from the slower sorption of Zn on a low surface area gibbsite. The difference in their results is attributed to the influence of pH on the sorbent phase functional group and metal ion hydrolysis (Kinniburgh and Jackson, 1981).

WT plots of standards and sorption samples can clearly resolve light (in these reactions Al) and heavy (in this case either Fe or Zn) contributions to the first metal shell and overcome the issue of Fe and Zn destructive interference masking of the Al backscattering wave (Manceau, 1990; Scheinost et al., 1999). Although the usefulness of WT by the Morlet function has been demonstrated in this and other studies to examine LDH phase formation (Funke et al., 2005; Siebecker, 2013; Zhu and Elzinga, 2014), in this study it fails to clearly resolve second and third shells in *r*- and *k*-space

(data not shown). FEFF-Morlet mother wavelet has been used to overcome this problem in other studies by demonstrating the presence of both heavy and light metals in the third metal shell of an LDH structure (Funke et al., 2007). LDH phases contain both three M^{II} and M^{III} in the first metal shell, six M^{II} in the second metal shell, and both three M^{II} and M^{III} in the third metal shell. Using this approach could discriminate between the presence of Fe(II)-Zn-Al layered hydroxides and Fe(II)- or Zn-Al-LDH phases in the systems studied here. This could be achieved by determining if the second metal shell is solely a single metal (either Fe or Zn) or if both Fe and Zn contribute.

3.5.3 Environmental Implications

This study demonstrates the formation of a mixed divalent metal layered hydroxide at conditions that are representative of those found in reducing natural environments (i.e. anoxic, circumneutral pH, environmentally relevant metal concentrations). At longer reaction times, these phases began conversion to a phyllosilicate through incorporation of Si released from the pyrophyllite structure into their interlayer. Such sorbents as Al-bearing oxides and phyllosilicates are ubiquitous in the environment and can release not only Al critical to the formation of LDH phases but also Si which has been shown to increase their stability (Li et al., 2012; Ford et al., 1999; Ford et al., 2001; Scheckel and Sparks, 2001; Scheckel et al., 2000; Scheidegger et al., 1998; Scheinost et al., 1999; Starcher et al., 2016; Zhu and Elzinga, 2014). The formation of Fe(II)-Al-LDH and Zn in inner-sphere complexation with γ - Al_2O_3 further iterates the importance of sorbent reactivity on LDH phase formation which has been demonstrated in other work (Li et al., 2012; Roberts et al., 2003). To better understand the importance of mixed divalent metal layered hydroxides in laboratory

studies and natural systems and their abilities to affect the fate of contaminants in the natural environment, future research should examine the stability and dissolution of these phases as affected by changes in external conditions such as the impacts of: 1) sample aging; 2) acidification; and 3) changes in oxidation-reduction chemistry.

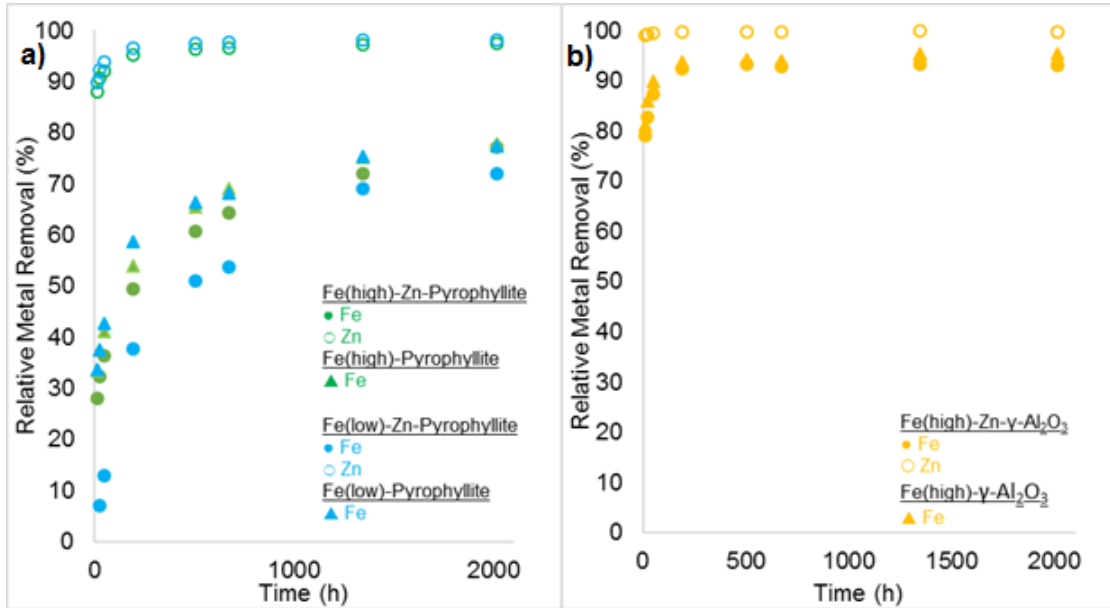


Figure 3.1: Comparison of Fe(II) and Zn co-sorption kinetics (% relative removal) with Fe(II) sorption only to a) natural pyrophyllite containing Fe(III) impurities and b) γ - Al_2O_3 . Pyrophyllite co-sorption systems contained either high (3 mM) or low (0.8 mM) Fe concentrations and 0.8 mM Zn, while γ - Al_2O_3 co-sorption systems contain 3 mM Fe(II) and 0.8 mM Zn. Fe(II)-pyrophyllite sorption data was previously reported in Starcher et al. (2016).

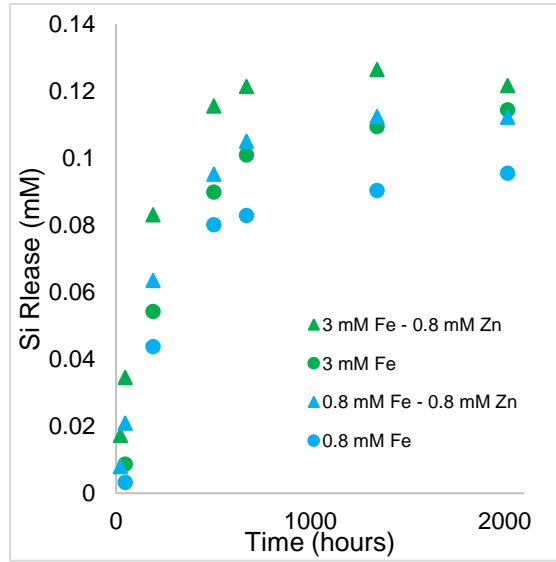


Figure 3.2: Si release during Fe(II)-Zn co-sorption and Fe(II) sorption reaction with pyrophyllite. Data from Fe(II) sorption to pyrophyllite was previously reported in Starcher et al. (2016).

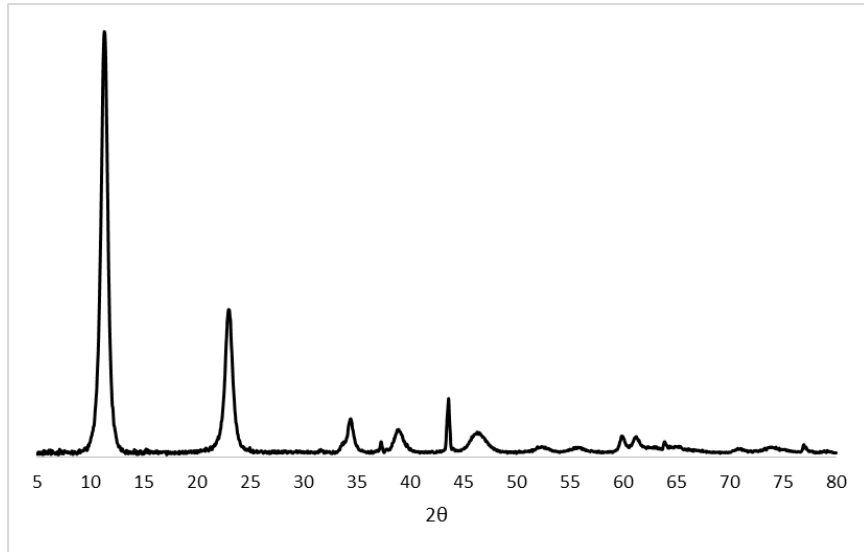


Figure 3.3: Powder XRD data of Fe(II)-Zn-Al layered hydroxide standard

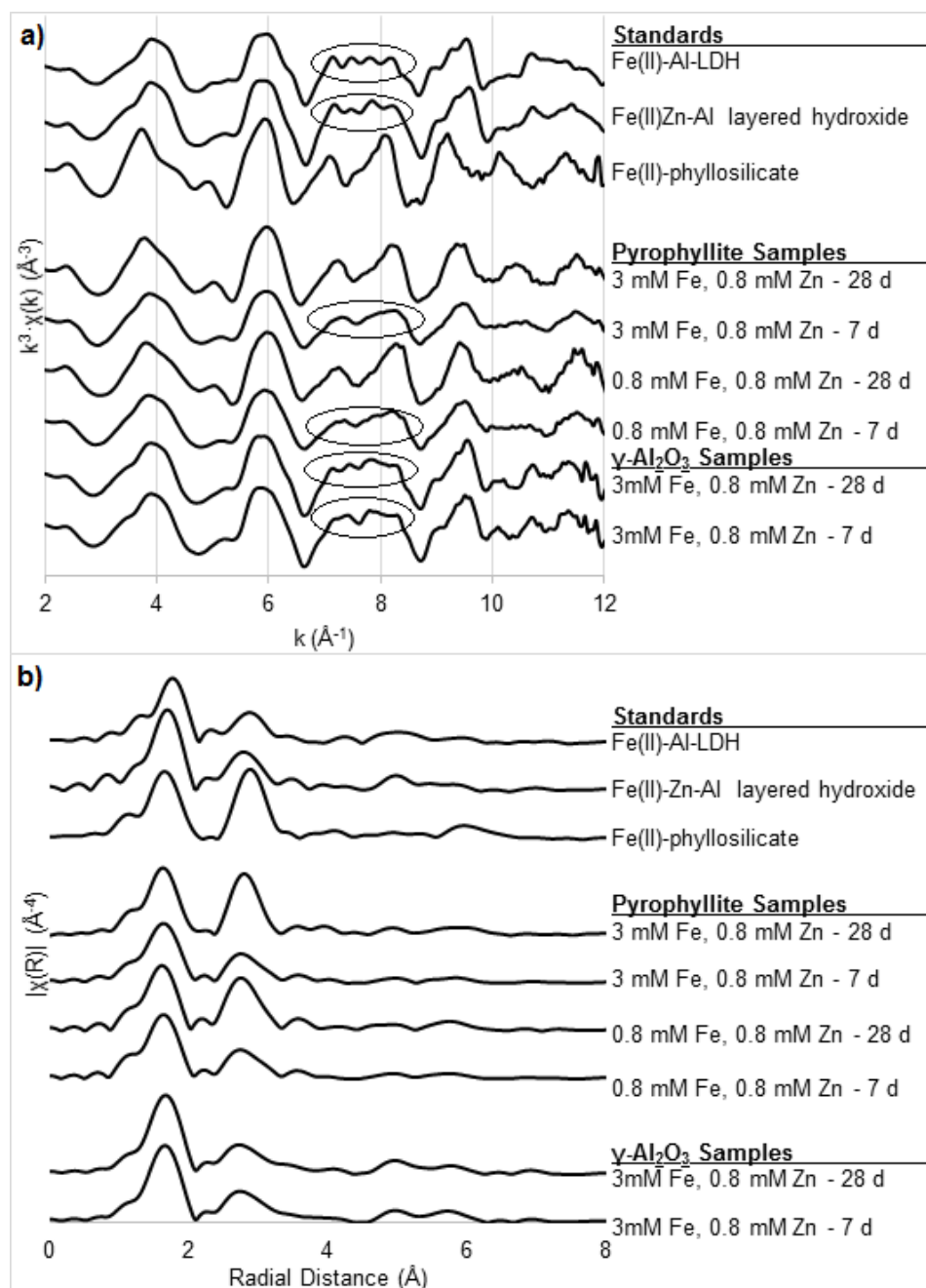


Figure 3.4: Fe K edge raw $k^3 \cdot \chi$ functions (a) and radial structure functions (RSF) (b) of Fe(II)-Zn co-sorption samples with either pyrophyllite or γ -Al₂O₃ reacted at pH 7.5 under anoxic conditions and of reference Fe standards. Diagnostic LDH "beat" pattern is circled in 3.4a.

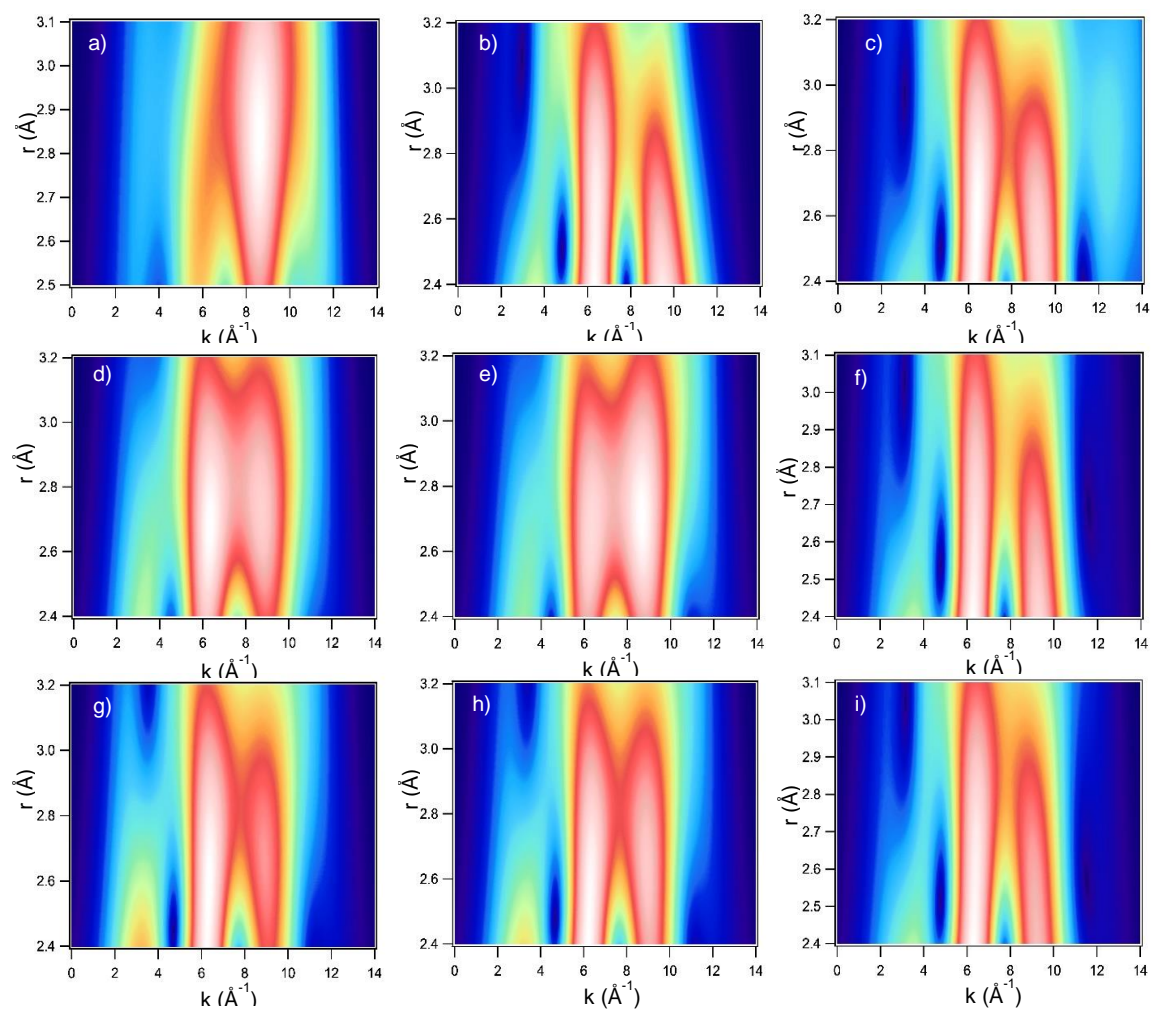


Figure 3.5: Wavelet transform (WT) analyses of Fe EXAFS data with $\eta=5.5$ and $\sigma=1$ of the first metal shell for Fe references, a) $\text{Fe}(\text{OH})_2$, b) nikischerite, and c) Fe/Zn/Al-LDH, and Fe/Zn co-sorption samples, d) high Fe/Zn-pyrophyllite at 28 d, e) low Fe/Zn-pyrophyllite at 28 d, f) Fe/Zn- γ - Al_2O_3 at 28 d, g) high Fe/Zn-pyrophyllite at 7 d, h) low Fe/Zn-pyrophyllite at 7 d, and i) Fe/Zn- γ - Al_2O_3 at 7 d.

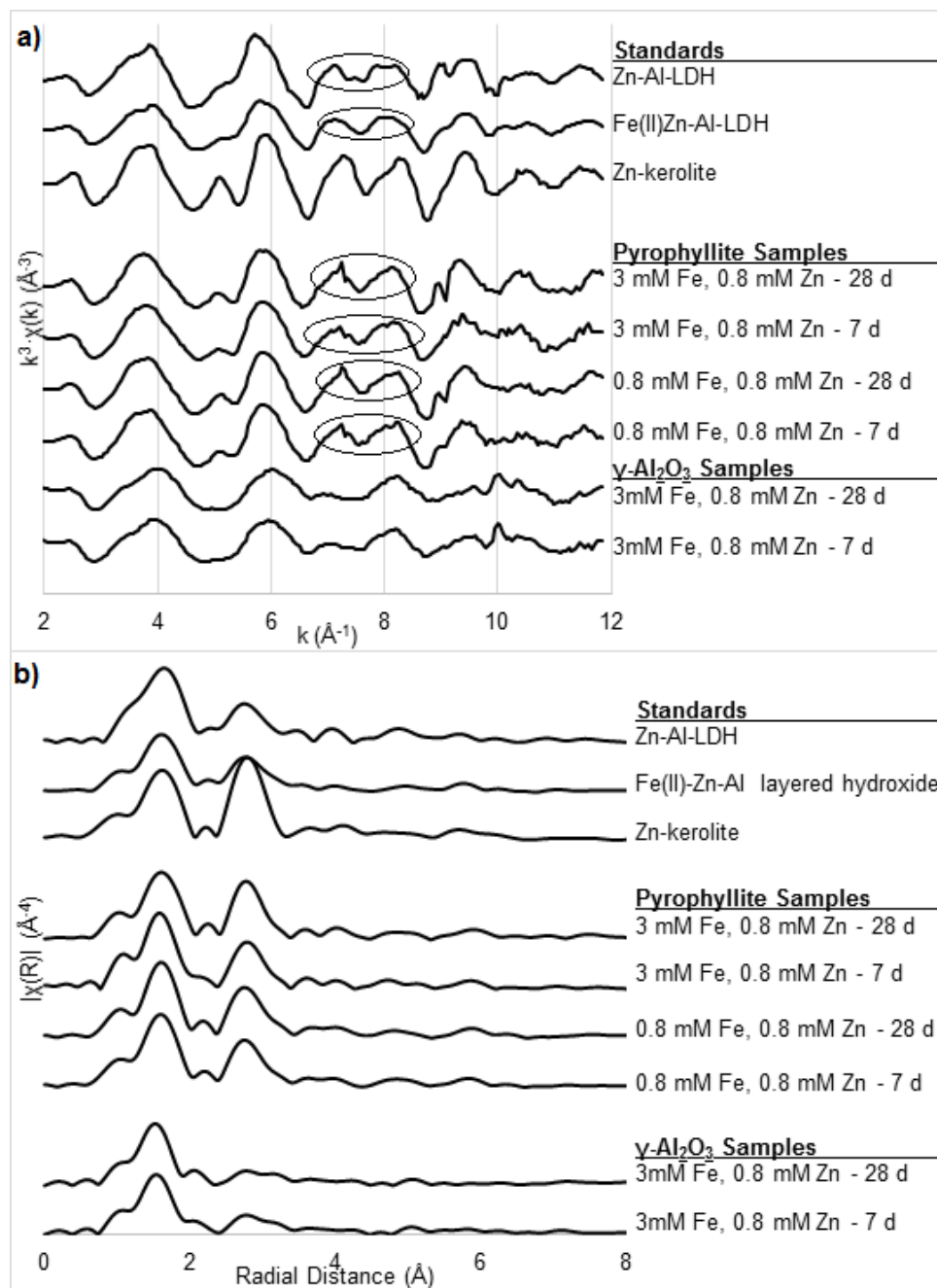


Figure 3.6: Zn K edge raw $k^3 \cdot \chi(k)$ functions (a) and radial structure functions (RSF) (b) of Fe(II)-Zn co-sorption samples with either pyrophyllite or $\gamma\text{-Al}_2\text{O}_3$ reacted at pH 7.5 under anoxic conditions and of reference Zn standards. Diagnostic LDH “beat” pattern is circled in 3.6a.

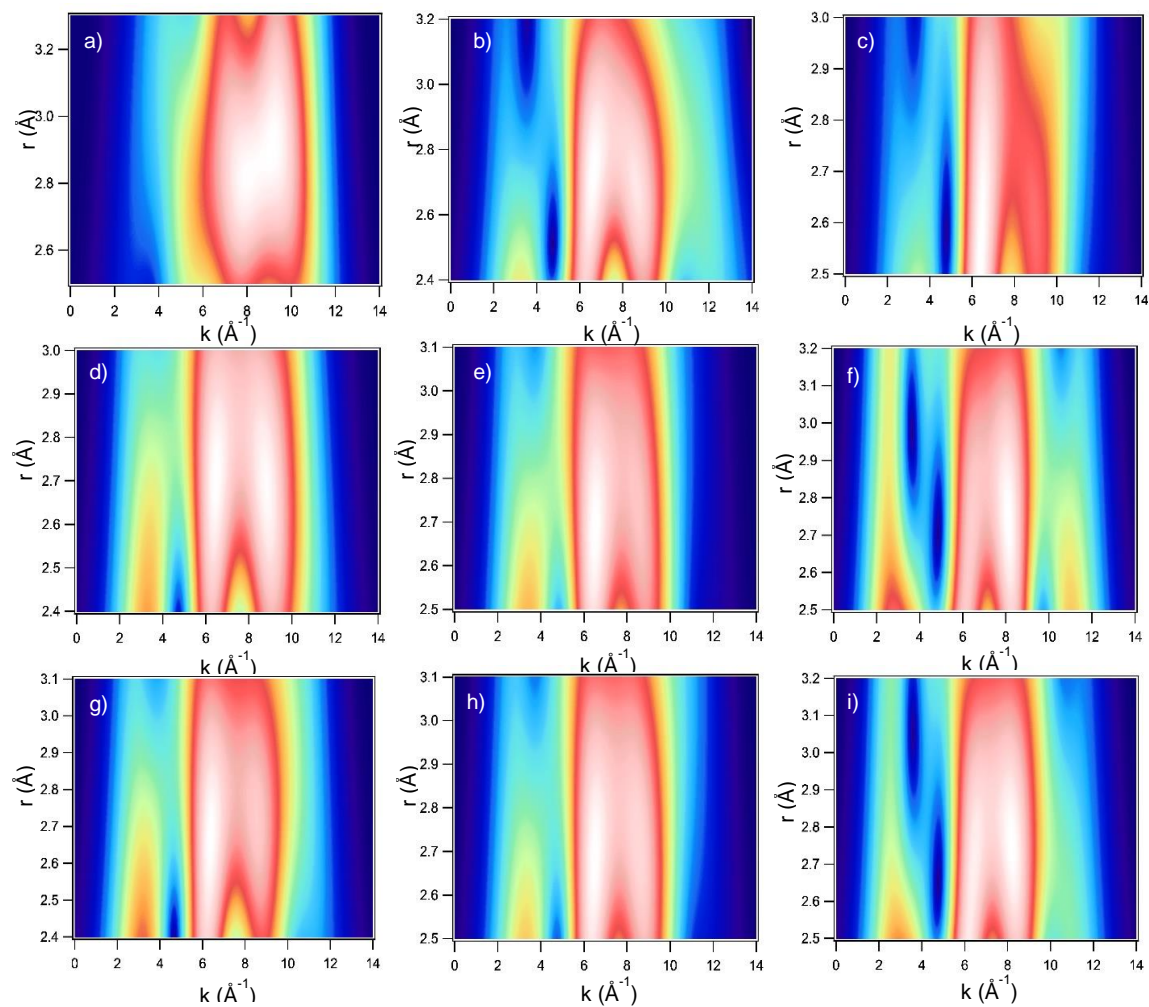


Figure 3.7: Wavelet transform (WT) analyses of Zn EXAFS data with $\eta=5.5$ and $\sigma=1$ of the first metal shell for Zn references, a) $\text{Zn}(\text{OH})_2$, b) Zn/Al -LDH, and c) $\text{Fe}/\text{Zn}/\text{Al}$ -LDH, and Fe/Zn co-sorption samples, d) high Fe/Zn-pyrophyllite at 28 d, e) low Fe/Zn-pyrophyllite at 28 d, f) $\text{Fe}/\text{Zn}-\gamma\text{-Al}_2\text{O}_3$ at 28 d, g) high Fe/Zn-pyrophyllite at 7 d, h) low Fe/Zn-pyrophyllite at 7 d, and i) $\text{Fe}/\text{Zn}-\gamma\text{-Al}_2\text{O}_3$ at 7 d.

Table 3.1: Fe K-edge EXAFS fitting results of Fe(II)/Zn co-sorption and reference samples^a

Sorption Time (d)	R-factor	Atomic Shell															ΔE (eV)	S_0^2	N_{ind}	N_{var}
		Fe-O			Fe-Fe			Fe-Al			Fe-Zn			Fe-Si						
		CN	R (Å)	σ^2 (Å ²)	CN	R (Å)	σ^2 (Å ²)	CN	R (Å)	σ^2 (Å ²)	CN	R (Å)	σ^2 (Å ²)	CN	R (Å)	σ^2 (Å ²)				
<u>Fe(II)-Zn-γ-Al₂O₃</u>																				
7	0.012	5.5	2.12	0.006	3.0	3.14	0.007	1.5	3.14	0.007							1.206	0.85	9.31	5
28	0.011	5.5	2.12	0.006	3.2	3.15	0.007	1.6	3.15	0.007							1.441	0.85	9.31	5
<u>Fe(II)-Zn-pyrophyllite high Fe(II)</u>																				
7	0.010	6.0	2.12	0.008	2.9	3.17	0.010	1.2	3.17	0.010	1.7	3.17	0.010				1.267	0.85	9.31	5
28																	-			
	0.002	6.0	2.10	0.009	3.2	3.16	0.009	1.4	3.16	0.009	1.9	3.16	0.009	2.0	3.37	0.009	0.143	0.85	9.31	5
<u>Fe(II)-Zn-pyrophyllite low Fe(II)</u>																				
7	0.004	5.6	2.10	0.009	1.9	3.15	0.010	1.2	3.15	0.010	2.0	3.15	0.010				0.503	0.85	9.75	5
28																	-			
	0.004	5.5	2.08	0.009	3.0	3.15	0.009	1.4	3.15	0.009	2.0	3.15	0.009	2.0	3.36	0.009	0.239	0.85	9.31	5
<u>References</u>																				
Fe(II)-Zn-Al-LDH	0.009	5.5	2.12	0.005	2.1	3.15	0.008	2.0	3.15	0.008	2.3	3.15	0.008				1.126	0.85	9.31	5
Nikischerite ^b		5.2	2.14	0.007	3.0	3.14	0.006	3.0	3.14	0.006										1.00
Fe(OH) ₂ ^b		5.2	2.14	0.006	6.0	3.26	0.006													1.00
Green rust (chloride) ^b		4.7	2.09	0.014	6.0	3.21	0.013													1.00
Aqueous Fe(II) ^b		5.3	2.12	0.009																1.00
Fe(II) phyllosilicate ^b		5.3	2.10	0.010	6.0	3.23	0.012							4.0	3.31	0.012				1.00

^a*R-factor* is the absolute misfit between the data and theory (as defined by Artemis), *CN* is coordination number, *R* is interatomic radial distance, σ^2 is Debye-Waller factor, ΔE is energy shift, S_0^2 is amplitude reduction factor, N_{ind} is the number of independent points, and N_{var} is the number of variables.

^bStandards were previously fit in Zhu and Elzinga (2014)

Table 3.2: Zn K-edge EXAFS fitting results of Fe(II)/Zn co-sorption and reference samples^a

Sorption Time (d)	R-factor	Atomic Shell															ΔE (eV)	S_o^2	N_{ind}	N_{var}
		Zn-O			Zn-Zn			Zn-Al			Zn-Fe			Zn-Si						
		CN	R (Å)	σ^2 (Å ²)	CN	R (Å)	σ^2 (Å ²)	CN	R (Å)	σ^2 (Å ²)	CN	R (Å)	σ^2 (Å ²)	CN	R (Å)	σ^2 (Å ²)				
Fe(II)-Zn- γ -Al ₂ O ₃																				
7	0.014	5.1	2.01	0.010	2.7	3.11	0.010	1.5	3.11	0.010							-0.23	0.85	9.75	5
28	0.015	5.1	1.98	0.010	2.9	3.09	0.012	1.7	3.09	0.012							2.019	0.85	9.75	5
Fe(II)-Zn-pyrophyllite high Fe(II)																				
7	0.019	6.5	2.06	0.010	3.4	3.13	0.009	1.3	3.13	0.009	1.2	3.13	0.009				2.098	0.85	9.31	5
28	0.005	6.5	2.01	0.010	3.5	3.14	0.009	1.4	3.14	0.009	1.6	3.14	0.009	2.0	3.35	0.009	2.634	0.85	9.31	5
Fe(II)-Zn-pyrophyllite low Fe(II)																				
7	0.014	6.5	2.07	0.009	3.4	3.12	0.009	1.4	3.12	0.009	1.4	3.12	0.009				2.094	0.85	9.31	5
28	0.008	6.5	2.07	0.009	3.6	3.11	0.010	1.4	3.11	0.010	1.4	3.11	0.010	2.0	3.33	0.010	2.172	0.85	9.31	5
References																				
Fe(II)-Zn-Al-LDH	0.009	5.5	2.12	0.005	2.1	3.15	0.008	2.0	3.15	0.008	2.3	3.15	0.008				1.126	0.85	9.31	5
ZnAl-LDH ^b	0.015	6.2	2.08	0.008	3.9	3.10	0.008	2.7	3.07	0.009							1.77	0.935		
Zn(OH) ₂ ^c		4	1.99		2.2	3.29														
Aqueous Zn ^d		6.0	2.07	0.009													-0.45	0.85		

^a*R-factor* is the absolute misfit between the data and theory (as defined by Artemis), *CN* is coordination number, *R* is interatomic radial distance, σ^2 is Debye-Waller factor, ΔE is energy shift, S_o^2 is amplitude reduction factor, N_{ind} is the number of independent points, and N_{var} is the number of variables

Standards were previously fit in ^bLi et al. (2012), ^cRoberts et al. (2003), and ^dNachegaal and Sparks (2004)

REFERENCES

- Abdelmoula, M.; Trolard, F.; Bourrie, G.; Génin, J.M.R. Evidence for the Fe(II)-Fe(III) green rust “Fougerite” mineral occurrence in a hydromorphic soil and its transformation with time and depth. *Hyperfine Interact.*, **1998**, 112:235-238; DOI 10.1023/A:1010802508927.
- Bravo-Suárez, J.J.; Páez-Mozo, E.A.; Oyama, S.T. Microtextural properties of layered double hydroxides: a theoretical and structural model. *Micropor. Mesopor. Mat.*, **2004**, 67:1-17; DOI 10.1016/j.micromeso.2003.10.003.
- Cavani, F.; Trifirò, F.; Vaccari, A. Hydrotalcite-type anionic clays: preparation, properties and applications. *Catal. Today*, **1991**, 11:173-301; DOI 10.1016/0920-5861(91)80068-K.
- Charlet, L.; Manceau, A. Evidence for the neoformation of clays upon sorption of Co(II) and Ni(II) on silicates. *Geochim. Cosmochim. Acta*, **1994**, 58(11):2577-2582, DOI 10.1016/0016-7037(94)90034-5.
- Chen, C. Investigating organic matter-mineral interactions at a molecular scale: An integrated field and laboratory study. Ph.D. Dissertation, University of Delaware, Newark, DE, 2013.
- de Roy, A.; Forano, C.; Besse, J.P. Layered double hydroxides: Synthesis and post-synthesis modification, In *Layered Double Hydroxides: Present and Future*, Rives, V., Ed. Nova Science Publishers, Inc.: New York, 2001.
- Elzinga, E.J. Formation of layered Fe(II)-Al(III)-hydroxides during reaction of Fe(II) with aluminum oxide. *Environ. Sci. Technol.*, **2012**, 46:4894-4901; DOI 10.1021/es2044807.
- Feder, F.; Trolard, F.; Klingelhöffer, G.; Bourrie, G. In situ Mössbauer spectroscopy: Evidence for green rust (fougerite) in a gleysol and its mineralogical transformations with time and depth. *Geochim. Cosmochim. Acta*, **2005**, 69:4463-4483; DOI 10.1016/j.gca.2005.03.042.
- Ford, R.G.; Scheinost, A.C.; Scheckel, K.G.; Sparks, D.L. The link between clay mineral weathering and the stabilization of Ni surface precipitates. *Environ. Sci. Technol.* **1999**, 33(18):3140-3144, DOI 10.1021/es990271d.

- Ford, R.G.; Sparks, D.L. The nature of Zn precipitates formed in the presence of pyrophyllite. *Environ. Sci. Technol.*, **2000**, 34:2479-2483; DOI 10.1021/es991330q.
- Ford, R.G.; Scheinost, A.C.; Sparks, D.L. Frontiers in metal sorption/precipitation mechanisms on soil mineral surfaces. *Adv. Agron.*, **2001**, 74:41-62; DOI 10.1016/S0065-2113(01)74030-8.
- Funke, H.; Scheinost, A.C.; Chukalina, M. Wavelet analysis of extended X-ray absorption fine structure data. *Phys. Rev. B*, 2005, 71:094110; DOI 10.1103/PhysRevB.71.094110.
- Funke, H.; Chukalina, M.; Scheinost, A.C. A new FEFF-based wavelet for EXAFS data analysis. *J. Synchrotron Radiation*, **2007**, 14(5):426-432; DOI 10.1107/S0909049507031901.
- Huminicki, D.M.C.; Hawthorne, F.C. The crystal structure of nikischerite, Na₂NaFe²⁺₆Al₃(SO₄)₂(OH)₁₈(H₂O)₁₂, a mineral of the shigaite group. *Can. Mineral.*, **2003**, 41:79-82, DOI 10.2113/gscanmin.41.1.79.
- Jacquat, O.; Voegelin, A.; Villard, A.; Marcus, M.A.; Kretzschmar, R. Formation of Zn-rich phyllosilicates, Zn-layered double hydroxide and hydrozincite in contaminated calcareous soils. *Geochim. Cosmochim. Acta*, **2008**, 72(20):5034-5057; DOI 10.1016/j.gca.2007.09.030.
- Johnson, C.A.; Glasser, F.P. Hydrotalcite-like minerals (M₂Al(OH)₆(CO₃)_{0.5}.XH₂O where M)Mg, Zn, Co, Ni) in the environment: synthesis, characterization and thermodynamic stability. *Clay Clay Miner.*, **2003**, 51:1-8; DOI 10.1346/CCMN.2003.510101.
- Juillot, F.; Morin, G.; Ildefonse, P.; Trainor, T.P.; Benedetti, M.; Galoisy, L.; Calas, G.; Brown, G.E. Occurrence of Zn/Al hydrotalcite in smelter-impacted soils from northern France: Evidence from EXAFS spectroscopy and chemical extractions. *Am. Mineral.*, **2003**, 88:509-526; DOI 10.2138/am-2003-0405.
- Khan, A.I.; O'Hare, D. Intercalation chemistry of layered double hydroxides: recent developments and applications. *J. Mater. Chem.*, **2002**, 12:3191-3198; DOI 10.1039/b204076j.
- Khaokaew, S.; Landrot, G.; Chaney, R.L.; Pandya, K.; Sparks, D.L. Speciation and release kinetics of zinc in contaminated paddy soils. *Environ. Sci. Technol.*, **2012**, 46:3957-3963; DOI 10.1021/es103971y.

- Kelly, S.D.; Hesterberg, D.; Ravel, B. Analysis of soils and minerals using X-ray absorption spectroscopy. In *Methods of Soil Analysis, Part 5 – Mineralogical Methods*; Ulery, A.L.; Drees, L.R., Eds; Soil Science Society of America: Madison, WI, USA, 2008; pp 367-463.
- Kinniburgh, D.G.; Jackson, M.L. Cation adsorption by hydrous metal oxides and clay, In *Adsorption of Inorganics at Solid-Liquid Interfaces*; Anderson, M.A.; Rubin, A.J., Eds; Ann Arbor Science: Ann Arbor, MI, 1981.
- Li, F.; Liu, J; Evans, D.G.; Duan, X. Stoichiometric synthesis of pure MFe_2O_4 ($M = Mg, Co, \text{ and } Ni$) spinel ferrites from tailored layered double hydroxide (hydrotalcite-like) precursors. *Chem. Mater.*, **2004**, 16:1597-1602; DOI 10.1021/cm035248c.
- Li, W.; Livi, K.J.; Xu, W.; Siebecker, M.G.; Wang, Y.; Phillips, B.L.; Sparks, D.L. Formation of crystalline Zn-Al layered double hydroxide precipitates on γ -alumina: the role of mineral dissolution. *Environ. Sci. Technol.*, **2012**, 46(21):11670-11677, DOI 10.1021/es3018094.
- Malinowski, E.R. Theory of error for target factor analysis with applications to mass spectrometry and nuclear magnetic resonance spectrometry. *Anal. Chim. Acta*, **1978**, 103:339-354; DOI 10.1016/S0003-2670(00)00088-X.
- Manceau, A. Distribution of cations among the octahedra of phyllosilicates: Insight from EXAFS. *Can. Mineral.*, **1990**, 28:321-328; DOI 10.1007/BF00200132.
- McNear, D.H.; Chaney, R.L.; Sparks, D.L. The effects of soil type and chemical treatment on nickel speciation in refinery enriched soils: A multi-technique investigation. *Geochim. Cosmochim. Acta*, **2007**, 71(9):2190–2208; DOI 10.1016/j.gca.2007.02.006.
- Nachtegaal, M.; Marcus, M.A.; Sonke, J.E.; Vangronsveld, J.; Livi, K.J.T.; van der Lelie, D.; Sparks, D.L. Effects of in-situ remediation on the speciation and bioavailability of zinc in a smelter contaminated soil. *Geochim. Cosmochim. Acta*, **2005**, 69:4649–4664; DOI 10.1016/j.gca.2005.05.019.
- Nachtegaal, M.; Sparks, D.L. Effect of iron oxide coatings on zinc sorption mechanisms at the clay-mineral/water interface. *J. Colloid Interface Sci.*, **2004**, 276:13-23; DOI 10.1016/j.jcis.2004.03.031.
- O'Day, P. A.; Rehr, J. J.; Zabinsky, S. I.; Brown, G. E. Extended X-ray absorption fine structure (EXAFS) analysis of disorder and multiple-scattering in complex crystalline solids. *J. Am. Chem. Soc.*, **1994**, 116:2938–2949, DOI 10.1021/ja00086a026.

- Olszewski, W.; Szymanski, K.; Zaleski, P.; Zajac, D. A. X-ray absorption near edge structure and extended X-ray absorption fine structure analysis of Fe(II) aqueous and acetone solutions. *J. Phys. Chem. A*, **2011**, 115:13420–13424, DOI 10.1021/jp207587u.
- Parise, J. B.; Marshall, W. G.; Smith, R. I.; Lutz, H. D.; Moller, H. The nuclear and magnetic structure of “white rust” -- Fe-(OH_{0.86}D_{0.14})₂. *Am. Mineral.*, **2000**, 85:189–193, DOI 10.2138/am-2000-0118.
- Paulhiac, J.L.; Clause, O. Surface coprecipitation of Co(II), Ni(II), or Zn(II) with Al(III) ions during impregnation of gamma-alumina at neutral pH. *J. Am. Chem. Soc.*, **1993**, 115(24):111602-11603; DOI 10.1021/ja00077a071.
- Peltier, E.; van der Lelie, D.; Sparks, D.L. Formation and stability of Ni-Al hydroxide phases in soils. *Environ. Sci. Technol.*, **2010**, 44:302-308; DOI 10.1021/es902332b.
- Ravel, B.; Newville, M. Athena, Artemis, Hephaestus: Data analysis for X-ray absorption spectroscopy using IFEFFIT. *J. Synchrotron Radiation*, **2005**, 12:537-541; DOI 10.1107/S0909049505012719.
- Reichle, W.T. Synthesis of anionic clay-minerals (mixed metal-hydroxides, hydrotalcite). *Solid State Ionics*, **1986**, 22:135-141; DOI 10.1016/0167-2738(86)90067-6.
- Roberts, D.R.; Ford, R.G.; Sparks, D.L. Kinetics and mechanisms of Zn complexation on metal oxides using EXAFS spectroscopy. *J. Colloid Interface Sci.*, **2003**, 263:364-376; DOI 10.1016/S0021-9797(03)00281-9.
- Scheckel, K.G.; Scheinost, A.C.; Ford, R.G.; Sparks, D.L. Stability of layered Ni hydroxide surface precipitates: A dissolution kinetics study. *Geochim. Cosmochim. Acta*, **2000**, 64(16):2727–2735, DOI 10.1016/S0016-7037(00)00385-9.
- Scheckel, K.G.; Sparks, D.L. Dissolution kinetics of nickel surface precipitates on clay mineral and oxide surfaces. *Soil Sci. Soc. Am. J.*, **2001**, 65(3):685–694, DOI 10.2136/sssaj2001.653685x.
- Scheidegger, A.M.; Lamble, G.M.; Sparks, D.L. Investigation of Ni sorption on pyrophyllite: An XAFS study. *Environ. Sci. Technol.*, **1996**, 30:548-554, DOI 10.1021/es950293+.

- Scheidegger, A.M.; Strawn, D.G.; Lamble, G.M.; Sparks, D.L. The kinetics of mixed Ni-Al hydroxide formation on clay and aluminum oxide minerals: a time-resolved XAFS study. *Geochim. Cosmochim. Acta*, **1998**, 62(13):2233-2245, DOI 10.1016/S0016-7037(98)00136-7.
- Scheinost, A.C.; Ford, R.G.; Sparks, D.L. The role of Al in the formation of secondary Ni precipitates on pyrophyllite, gibbsite, talc, and amorphous silica: A DRS study. *Geochim. Cosmochim. Acta*, **1999**, 63:3193-3203, DOI 10.1016/S0016-7037(99)00244-6.
- Scheinost, A.C.; Sparks, D.L. Formation of layered single- and double-metal hydroxides precipitates at the mineral/water interface: A multiple-scattering XAFS analysis. *J. Colloid Interface Sci.*, **2000**, 223:167-178, DOI 10.1006/jcis.1999.6638.
- Shannon, R. D. Revised effective ionic radii and systematic studies of interatomic distances in halides and chalcogenides. *Acta Crystallogr.*, **1976**, A32:751-767, DOI 10.1107/S0567739476001551.
- Siebecker, M.G. Environmental speciation, chemistry, stability and kinetics of nickel in soils, mineral systems and plants. Ph.D. Dissertation, University of Delaware, Newark, DE, 2013.
- Starcher, A.N.; Elzinga, E.J.; Kukkadapu, R.K.; Sparks, D.L. Evidence for the formation of Fe-layered hydroxides using spectroscopic techniques. 251st American Chemical Society National Meeting and Exposition, San Diego, CA, March 13-17, **2016**, poster presentation.
- Takagi, K.; Saito, N.; Shichi, T.; Sawaki, Y. Intercalation of aliphatic carboxylates in hydrotalcite interlayers: Selective photochemical hydrogen abstraction by benzophenonecarboxylate. *Chem. Lett.*, **1999**, 4:275-276, DOI 10.1246/cl.1999.275.
- Thompson, H.A.; Parks, G.A.; Brown, G.E. Dynamic interactions of dissolution, surface adsorption, and precipitation in an aging cobalt(II)-clay-water system. *Geochim. Cosmochim. Acta*, **1999**, 63:1767-1779, DOI 10.1016/S0016-7037(99)00125-8.
- Towle, S.N.; Bargar, J.R.; Brown, G.E.; Parks, G.A. Surface precipitation of Co(II)(aq) on Al₂O₃. *J. Colloid Interface Sci.*, **1997**, 187:62-82, DOI 10.1557/PROC-432-237.

- Trainor, T.P.; Brown, G.E.; Parks, G.A. Adsorption and precipitation of aqueous Zn(II) on alumina powders. *J. Colloid Interface Sci.*, **2000**, 231:359-372; DOI 10.1006/jcis.2000.7111.
- Trolard, F.; Génin, J.M.R.; Abdelmoula, M.; Bourrié, G.; Humbert, B.; Herbillon A. Identification of a green rust mineral in a reductomorphic soil by Mössbauer and Raman spectroscopies. *Geochim. Cosmochim. Acta*, **1997**, 61:1107-1111, DOI 10.1016/S0016-7037(96)00381-X.
- USEPA (U.S. Environmental Protection Agency). Method 3051A: Microwave Assisted Acid Digestion of Sediments, Sludges, Soils, and Oils. Washington, DC: USEPA, Office of Solid Waste, 2007.
- USEPA (U.S. Environmental Protection Agency). Method 6010C: Inductively Coupled Plasma-Atomic Emission Spectrometry. Washington, DC: USEPA, Office of Solid Waste, 2007.
- Voegelin, A.; Kretzschmar, R. Formation and dissolution of single and mixed Zn and Ni precipitates in soil: Evidence from column experiments and extended X-ray absorption fine structure spectroscopy. *Environ. Sci. Technol.*, **2005**, 39:5311-5318, DOI 10.1021/es0500097.
- Voegelin, A.; Pfister, S.; Scheinost, A.C.; Marcus, M.A.; Kretzschmar, R. Changes in zinc speciation in field soil after contamination with zinc oxide. *Environ. Sci. Technol.*, **2005**, 9(17):6616-23; DOI 10.1021/es047962g.
- Waychunas, G.A.; Fuller, C.C.; Davis, J.A. Surface complexation and precipitate geometry for aqueous Zn(II) sorption on ferrihydrite I: X-ray absorption extended fine structure spectroscopy analysis. *Geochim. Cosmochim. Acta.*, **2002**, 66:1119-1137; DOI 10.1016/S0016-7037(01)00853-5.
- Yamaguchi, N.; Scheinost, A.C.; Sparks, D.L. Influence of gibbsite surface area and citrate on Ni sorption mechanisms at pH 7.5. *Clay Clay Miner.*, **2002**, 50:784-790; DOI 10.1346/000986002762090182.
- Zhu, Y.; Elzinga, E.J. Formation of layered Fe(II)-hydroxides during Fe(II) sorption onto clay and metal-oxide substrates. *Environ. Sci. Technol.*, **2014**, 48:4937-4945, DOI 10.1021/es500579p.
- Zhu, Y.; Elzinga, E.J. Macroscopic and spectroscopic assessment of the cosorption of Fe(II) with As(III) and As(V) on Al-oxide. *Environ. Sci. Technol.*, **2015**, 49:13369-13377; DOI 10.1021/acs.est.5b04525.

Chapter 4

INHIBITION OF FE(II)-AL-LAYERED DOUBLE HYDROXIDE PHASE FORMATION FROM REDUCTIVE DISSOLUTION OF TWO SOIL SOLUTIONS: EFFECTS OF ENVIRONMENTAL VARIABLES

4.1 Abstract

Fe(II)-Al-layered double hydroxide (LDH) phases have formed in laboratory conditions similar to those found in anoxic geochemical environments such as wetland soils; however, it is unknown if these phases exist in the natural environment, and limited data exist on solid phase speciation of Fe(II) in anoxic environments. The potential for Fe(II)-Al-LDH phase formation from the reductive dissolution of soil Fe(II)-oxides was examined. Soil solutions of 50 g/L <2 mm size fraction of soil from the Great Cypress Swamp in Delaware (GCS) and the Stroud Water Research Center (SWRC) in Pennsylvania were induced into reductive dissolution inside a glovebox with inert conditions (4% H₂ – 96% N₂ atmosphere) for 21 days or more. During this time, 1 kDa MWCO dialysis tubes with 7.5 g/L γ -Al₂O₃ were submerged in the soils solution. Following the reactions, the γ -Al₂O₃ sorption samples were analyzed with X-ray diffraction (XRD), X-ray fluorescence spectrometry (XRF), X-ray absorption spectroscopy (XAS), and by acid digestion. The GCS- γ -Al₂O₃ sorption samples had insufficient Fe sorption to produce usable XAS data. The low concentration of Fe released to the soil solution during reductive dissolution and low soil solution pH were not ideal conditions for LDH phase formation, as seen in other LDH work. Fe(II)-Al-LDH phases were not observed in the EXAFS spectra of SWRC- γ -Al₂O₃ sorption

samples; instead, a mononuclear surface species with multiple coordination environments is the most likely sorption product formed. Other elements that complex Fe and Al or that inhibit the dissolution of γ -Al₂O₃ were also included in the sorption products, as observed by acid digestion and XRF. Because EXAFS is a bulk technique, an average of all species of the element of interest (in this case Fe) is taken. Although a mononuclear surface species is likely the dominant sorption form, other Fe phases may have formed with the complexing elements in this system, such as carbonates, P, S, Si, and OM. Further systematic research is required to better understand the conditions in the natural environment that are ideal for Fe(II)-Al-LDH phase formation.

4.2 Introduction

Recently, Fe(II)-Al-LDH phases have formed in laboratory conditions similar to those found in anoxic geochemical environments such as wetland soils (i.e. circumneutral pH, environmentally relevant Fe(II) concentrations, Al-bearing mineral undergoing dissolution) (Elzinga, 2012; Starcher et al., 2016; Zhu and Elzinga, 2014; Zhu and Elzinga, 2015). However, it is unknown if these phases exist in the natural environment. Limited data exist on solid phase speciation of Fe(II) in anoxic environments. Species of known importance in such environments have been observed from ferrihydrite (Fe(OH)₃) microbial reduction model reactions and include green rust ($\{Fe^{II}_{(6-x)}Fe^{III}_x(OH)_{12}\}^{x+}\{(A^{2-})_{x/2}\cdot yH_2O\}^{x-}$), ferrihydrite (Fe(OH)₃), siderite (FeCO₃), magnetite (Fe^{II}Fe^{III}₂O₄), and vivianite (Fe(PO₄)₂·nH₂O) (Abdelmoula et al., 1998; Cooper et al., 2000; Feder et al., 2005; Fredrickson et al., 1998; Hansel et al., 2003; Inskeep and Bloom, 1986; Lovley et al., 1987; Lovley and Phillips, 1988;

Mortimer and Coleman, 1997; Roden and Lovley, 1993; Trolard et al., 1997; Zachara et al. 2002).

Naturally-occurring conditions in wetland soils have significant influence on the redox chemistry of Fe. As a result of the reductive dissolution that occurs under anaerobic conditions, Fe(II) is released into the soil solution (Kirk, 2004). This transformation of Fe oxidation state results in increased concentrations of soluble Fe(II) in the system (Kirk, 2004), followed by adsorption and precipitation of the Fe with increased time under anoxic conditions (Ponnamperuma, 1972). It is important to understand solid phase distribution of Fe(II) in wetlands because Fe cycling influences the speciation of other important elements, including sulfur, nitrogen, carbon, phosphorus, and metal(loid)s and because wetlands act as an intermediate between terrestrial and aquatic systems (Kirk, 2004; Stumm and Sulzberger, 1992). Dissolution of Fe(III)-minerals, which can serve as sinks for metal(loid)s, could affect the mobility of the metal(loid)s in these systems.

Other forms of layered double hydroxides beside Fe(II)-Al-LDH have been confirmed in nature. These phases can occur from reactions of aqueous divalent metals such as Ni, Zn, and Co with Al-bearing substrates in natural soils, often as a result of metal contamination (Khaokaew et al., 2012; McNear et al., 2007; Nachtegaal et al., 2005; Roberts et al., 1999). Green rusts are LDH phases of mixed Fe oxidation states that have been observed in reduced soils that undergo periodic changes in redox conditions and are considered to be important Fe(II) phases in the environment (Abdelmoula et al., 1998; Christiansen et al., 2009; Feder et al., 2005; Refait et al., 2001; Trolard et al., 1997). Other Fe layered hydroxides phases have not yet been reported, but if present in nature they could play important roles in

biogeochemical cycling due to their potentially high reactivity towards redox-sensitive toxic elements (e.g. Cr(VI) and As(V)) and divalent metals (e.g. Ni(II) and Zn(II)).

The objective of this study was to determine if Fe(II)-Al-LDH phases can form in natural soils using two soils with different physicochemical properties. Upon reductive dissolution of the soils, the Fe(II) in solution was reacted with γ -Al₂O₃, which was then examined with X-ray absorption spectroscopy (XAS). One limitation of previous attempts to characterize Fe in soils is the ubiquitous nature of Fe in soils. Because XAS provides the average speciation of the element of interest, signals from dominant Fe-bearing species in the sample overpower any signals from those species present to a lesser extent. This study has overcome this limitation through the methodologies described below; however, the formation of Fe(II)-Al-LDH phases was not observed. This study highlights potentially limiting factors to Fe(II)-Al-LDH formation that were previously unrecognized and provides future directions for research including systematic laboratory studies to investigate the limits of environmental conditions on LDH formation. Understanding these factors in detail will better enable successful searches for these phases in the natural environment in the future.

4.3 Materials and Methods

4.3.1 Site Selection and Sampling Procedures

4.3.1.1 Great Cypress Swamp

The Great Cypress Swamp in Frankford, DE, (hereafter referred to as GCS) was selected based on the following criteria: 1) the sampling area was an undisturbed forest/wetland in recordable history and 2) soils in the sampling area remain inundated

throughout the year. GCS is one of the largest areas of contiguous forest present in the Delmarva Peninsula and is a land holding of Delaware Wild Lands, Inc. Details of the sample site locations are given in Table B.1. Two sites were selected in an undisturbed area that was known to remain be semi-permanently or seasonally flooded (as defined by Reddy and DeLaune, 2008) according to the land manager, and five cores were taken from each site. The geologic and hydrologic properties of a nearby area in the GCS has previously been described by Andres and Howard (2000) and Andres and Howard (2002).

Sample preservation methods were designed to follow United States Environmental Protection Agency (USEPA)-suggested methods to prohibit inadvertent oxidation (Wilkin, 2006), but were optimized for the sampling site. Soil cores were taken using a PN150 JMC Environmentalist's Sub-Soil Probe equipped with 1"-diameter inserts to a 4'-depth. The 1"-diameter plastic inserts were utilized to minimize oxidation between soil sampling and bagging. Prior to sampling, the inserts were purged with N₂ gas and capped in the laboratory, and inserts were uncapped just prior to sampling. To further minimize oxidation, soil cores in inserts were immediately cut into 12"-sections, bagged in gallon vacuum-seal Ziploc® freezer bags with two AnaeroPouch™ System Pouch-Keep O₂ scrubbers and one AnaeroPack™ System Pack-Anaero O₂ scrubber, and then vacuum-sealed using the Ziploc® brand vacuum freezer system to remove any air. Cores were immediately placed on ice for preservation and were transported to the laboratory to be placed inside the glovebox. Samples were air-dried in a H₂-N₂ atmosphere inside the glovebox. The gleyed and oxidized portions of the soil cores from each site were separately sieved to pass a 2-mm sieve and composited by combining approximately equal volumes of soil.

4.3.1.2 Stroud Water Research Center

The second sampling site was located at the Stroud Water Research Center in Avondale, PA (hereafter referred to as SWRC). Previous studies have examined soils from this area in detail (Chen, 2013; Newbold, 1997; Walter and Merritts, 2008). This soil was selected because 1) it has a near-neutral pH required for LDH phase formation and 2) it is located along a stream with the potential to become inundated upon flooding. SWRC has been a study site frequently used by the Christina River Basin Critical Zone Observatory. Approximately 23% of the total watershed is covered with forests while 74% has been historically used for agricultural purposes (Newbold, 1997).

Samples for this site were taken from the relatively undisturbed, forested area along White Clay Creek. Soils were field-tested for pH using a 1:1 volume ratio to selectively find soils with higher pH values (~6). Soil samples were taken from three areas in the site at to a depth of 5 in. No additional measures were used to maintain oxidation state for the SWRC soils as these soils were not saturated upon retrieval. The air-dried soil was sieved to pass a 2-mm sieve and composited by combining approximately equal volumes of soil.

4.3.2 Soil Characterization

4.3.2.1 Standard Methods

Soil color was determined using a Munsell soil color chart. Particle size of each composite sample was determined using a Beckman Coulter LS13 320 laser diffraction particle size analyzer. Soil texture was determined from percent size fraction calculated by particle size analysis using the United States Department of Agriculture soil particle classification system (Brady and Weil, 2009).

To determine total elemental concentrations, the untreated composite soil samples were microwave digested in a CEM Mars 5 microwave digestion oven and analyzed by inductively coupled plasma optical emission spectroscopy (ICP-OES) with a Thermo Elemental Intrepid II XSP Duo View by the University of Delaware Soil Testing Laboratory according to procedures in USEPA Methods 3051 and 6010C (USEPA, 2007a; USEPA, 2007b). Soil total C and total N were determined by dry combustion using an Elementar VarioMax CN Analyzer (Elementar Americas) at the University of Delaware Soil Testing Laboratory (Bremner, 1996; Nelson and Sommers, 1996).

Mehlich 3 extraction was used to determine exchangeable nutrient concentrations as this method has been shown to best determine these concentrations for soils of the Mid-Atlantic region (Gartley et al. 2002; Sims 1989). Samples were extracted using Mehlich 3 soil test extractant for elemental analysis of plant available nutrients (P, K, Ca, Mg, Mn, Zn, Cu, F, B, S, and Al) by ICP-OES at the University of Delaware Soil Testing Laboratory (Mehlich, 1984; Wolf and Beegle, 2011).

4.3.2.2 Chemical Treatments to Determine Principal Forms of Soil Fe

Soil total “free” iron oxides were determined using the citrate-bicarbonate-dithionite method (Na-DCB) (Jackson et al., 1986; Loeppert and Inskeep, 1996; Mehra and Jackson, 1960). Soil “active” or “amorphous” iron oxides were determined using the acid ammonium oxalate in darkness or Tamm’s reagent method (Schwertmann, 1964; McKeague and Day, 1966; Loeppert and Inskeep, 1996). Details of these procedures are given in Appendix C.

4.3.2.3 X-Ray Diffraction Analysis

The composite soils from each site were characterized with X-ray diffraction (XRD). To increase particle dispersion and improve diffractogram quality, soluble salts, carbonates, organic matter, and free iron oxides were removed from the samples prior to XRD analysis (Kunze and Dixon, 1986). K^+ - and Mg^{2+} -saturated samples were analyzed with XRD at 298 K and after heating to 823 K (Jackson, 1969; Whittig and Allardice, 1986). Details of saturation procedures are given in Appendix C. Diffraction patterns were obtained with a Philips X'Pert PW3040 powder diffractometer using randomly oriented powder mounts and Cu $K\alpha$ radiation (Whittig and Allardice, 1986). Scans were made from 5° to 70° 2θ , with a counting time of 3 seconds, and a step size of 0.02° 2θ . The generator current and voltage were at 44 mA and 40 kV, respectively. Data were background-subtracted, smoothed, and fitted using Philips X'Pert High Score.

4.3.3 Determination of LDH Phase Formation from Reductive Dissolution of Soil Fe Species

4.3.3.1 Sorption Experiment

A Coy glovebox containing a 96% N_2 – 4% H_2 atmosphere and a Pd catalyst for trace O_2 removal was used to maintain an anoxic environment. O_2 levels were monitored using an O_2 - H_2 meter to ensure an atmospheric O_2 concentration of <1 ppm, and a dehumidifier was used to reduce humidity produced by the catalyst. DI water for the batch reactions was prepared by simultaneously boiling and N_2 purging the water, followed by 2 d of cooling in the glovebox to outgas remaining O_2 .

To determine if Fe layered hydroxide phases could form from the release of aqueous Fe(II) during reductive dissolution of Fe(III)-(hydr)oxides in a wetland soil,

dialysis tubes with γ -Al₂O₃ solutions were submerged in suspensions of GCS composite and SWRC composite soils in an inert atmosphere for up to 28 d.

For the dialysis tubes, 30 mL of 7.5 g/L γ -Al₂O₃ solutions with a background of 0.1 M NaCl and 50 mM 4-(2-hydroxyethyl)-piperazine-1-ethanesulfonic acid (HEPES) buffer were prepared and adjusted to a pH of 7.5. The γ -Al₂O₃ was hydrated for 24 h prior to being placed into dialysis tubes. Spectra/Por® 7 Standard RC dialysis membrane tubes of molecular weight cutoff (MWCO) 1 kDa were used to permit diffusion of Fe(II) ions, but limit diffusion of organic matter (Connell, 2005; Leenheer and Croué, 2003; Louie et al., 2015; Piccolo, 2001). The presence of heavy metals and sulfides in these dialysis tubes is limited due to pretreatment by the manufacturer. Dialysis tubing was prepared according to manufacturer instructions prior to use, which included 30 min of submersion in anoxic DI water to remove 0.05% sodium azide preservative used for tubing pretreatment and storage. Dialysis tubes were then filled with 7.5 g/L γ -Al₂O₃ solution and clamped.

To prepare the GCS soil solutions, 1-L solutions of 50 g/L of the <2 mm composite soils in anoxic water were prepared in 2-L beakers. A 10 mM glucose background was provided initially to enhance microbial reduction of Fe(III) (Yu and Rinklebe, 2013). Soil solutions were moderately stirred with magnetic stir bars on a stir plate. To each of the soil solution beakers were added four dialysis tubes with 30 mL of pH-adjusted 7.5 g/L γ -Al₂O₃ solution. The soil solution pH was monitored throughout the reaction, and soil solution samples for elemental analysis by ICP-OES at the University of Delaware Soil Testing Laboratory were taken at various time intervals throughout the reaction period (USEPA, 2007b). After 28 d of reaction time, the γ -Al₂O₃ solutions were removed from the dialysis tubing and centrifuged for 10

min at 10,000 g outside the glovebox. The solid residues were immediately returned to the glovebox and prepared for X-ray absorption spectroscopy (XAS) analysis by briefly air-drying in the glovebox. The wet pastes were individually sealed into lucite sample holders using Kapton® tape. Samples for X-ray fluorescence spectrometry (XRF) and XRD were air-dried completely in the glovebox. Because the monitored pH and Fe concentrations were deemed insufficient for LDH phase formation based on previous studies, the reactions using GCS soils were terminated after these samples were taken.

Soil solutions from SWRC were prepared in the same manner as the GCS solutions. The solutions were reacted for 21 d, at which time the pH rose from 5.6 to approximately 6.9. The dialysis tubes were removed, and the solids within were prepared for XAS, XRF, and XRD analyses as described above. After reacting for 56 d, the soil solution reached a pH of 7.4. A second set of dialysis tubing with 7.5 g/L γ - Al_2O_3 solution was placed in the soil solution after reductive dissolution had begun with an initial soil solution pH of 7.4. Samples were collected after 28 d of reaction time and prepared for XAS analysis as described above.

Due to the decline of Fe concentration found in the SWRC soil solution after 16 d of reaction time, a second set of reductive dissolution experiments were prepared to reduce back-reactions of Fe with the soil substrate. Soil solutions from SWRC were prepared in the same manner as previously described; however, the soil was removed from the soil solution before the dialysis tubes containing 7.5 g/L γ - Al_2O_3 solution were added. Once the soil solution reached pH 7.0 and 7.5, it was centrifuged outside the glovebox at 10,000 g for 5 min to separate the solid phase. The solution was immediately returned to the glovebox, and dialysis tubes with 7.5 g/L γ - Al_2O_3 solution

were added and reacted for 28 d. After the 28 d reaction time the solid samples were prepared for XAS analysis as previously described.

4.3.3.2 **X-Ray Fluorescence**

X-ray fluorescence (XRF) spectrometry data was collected for the SWRC (with soil, pH 5.6), GCS1, and GCS2 γ -Al₂O₃ sorption samples using the Rigaku Supermini200, a wavelength spectrometer with a 200 keV Pt X-ray source. Standards for calibration were the Montana NIST soils 2011 and 2010a (National Institute of Standards and Technology).

4.3.3.3 **Bulk Extended X-Ray Absorption Fine Structure Spectroscopy (EXAFS)**

Bulk-XAS analysis was performed at the National Synchrotron Light Source (NSLS) at beamline X11-A, at Stanford Synchrotron Radiation Lightsource (SSRL) at beamline 4-1, and at the Canadian Light Source (CLS) at the HXMA beamline. For transport to the beamlines, samples were individually sealed into two ziplock bags and placed into an airtight AnaeroPack™ box with two AnaeroPouch™ O₂ scrubbers to prevent sample oxidation. The Si(III) monochromator was calibrated with an Fe foil to record Fe *K* edge spectra at an E₀ of 7112 eV. Stern-Heald Lytle, passivated implanted planar silicon (PIPS) detectors, and 13-element Ge detectors were used to collect the fluorescence data. Elastic scattering was reduced by placing a Mn filter between the detector and sample for Fe analysis. When collecting data at NSLS beamline X11-A, 50% detuning was used to reduce harmonics. Samples were removed from the ziplock bags just prior to analysis, and no visual signs of oxidation were observed before or after XAS analysis. A minimum of three scans were collected for each sample to improve signal-to-noise ratio.

After bulk-EXAFS $\mu(E)$ spectra were averaged, background subtracted, and normalized, and the $\chi(k)$ functions were k^3 -weighted using Athena (Demeter 0.9.16) (Ravel and Newville, 2005). Forward and backward Fourier transforms of the k^3 -weighted χ functions were performed in Athena (Demeter 0.9.16) using Hanning windows with a dk of 0.5 and a dR of 0.2, respectively. Shell-by-shell fits of γ -Al₂O₃ sorption samples were performed in Artemis (Demeter 0.9.16) (Ravel and Newville, 2005). Theoretical back-scattering paths determined by Feff 6.0 calculations using an augmented lizardite crystal structure in which Fe and Al were substituted for Mg in the octahedra. The amplitude reduction factor (S_0^2) was 0.85 for all fits, and data were fitted with Fe-O for the first shell (O'Day et al., 1994).

Fe XAS standards examined in this study are those used in previously published studies: nikischerite (NaFe^{II}₆Al₃(SO₄)₂(OH)₁₈(H₂O)₁₂), an Fe(II)-Al(III)-LDH; 10 mM Fe^{II} solution; “white rust” (Fe^{II}(OH)₂) (Elzinga, 2012); magnetite (Fe^{III}₂Fe^{II}O₄); 2-line ferrihydrite (5Fe^{III}₂O₃·9H₂O); hydroxychloride green rust; Fe(II)-phyllosilicate (Zhu and Elzinga, 2014); goethite (α -FeO(OH)); hematite (Fe₂O₃); lepidocrocite (γ -FeO(OH)); Fe(II) sulfide (FeS); pyrite (FeS₂); vivianite (Fe(PO₄)₂·nH₂O); Fe(III)-OM; and siderite (FeCO₃) (Chen, 2013).

4.4 Results

4.4.1 Soil Characterization

Site descriptions are given in Appendix C and in Table B.1. Physicochemical properties of the composite soils are given in Table 4.1. At the soil depths where reduced conditions were present, the GCS soils were found to have a sandy texture, which agrees well with previous descriptions of the soil series and area (Andres and

Howard, 2000; Andres and Howard, 2002; USDA Soil Survey Staff, 2014). The soil texture at SWRC was also sandy; however, it had clay and silt particle sizes several orders of magnitude larger than those found in the GCS soils (Table 4.1). Total elemental concentrations were also significantly higher (at least one order of magnitude) for the SWRC soil than for the GCS soils. Mehlich 3 extraction data are presented in Table 4.2. Concentrations of plant available elements are also typically higher for the SWRC soil than the GCS soils. Plant available Fe is highest for SWRC, followed by the GCS anoxic soils, and finally the GCS oxic soil. GCS1 and GCS 2 Ca concentrations are higher for the Mehlich 3 extraction than total elemental concentration by acid digestion. This discrepancy could be due to sample heterogeneity or to the concentration approaching instrument detection limits and should be investigated further. DCB chemical extraction elemental concentrations for the SWRC soil are presented Table 4.3 and show relatively high concentrations of Al, Ca, Fe, Mn, and P released upon extraction of “free” Fe-oxides, such as goethite, hematite, and ferrihydrite (Parfitt and Childs, 1988). Concentrations of As, B, and Ca are higher for the DCB extraction than the total elemental concentration by acid digestions. This discrepancy could be due to sample heterogeneity or to the concentration approaching instrument detection limits and should be investigated further.

4.4.2 Chemical Extractions for Fe

Chemical extraction data are presented in Figure 4.1. Of the 484 mg Fe per kg soil present in the composite soil for GCS1 from microwave digestion, 60 mg kg⁻¹ (12% of total Fe) and 36 mg kg⁻¹ (7% of total Fe) are present as DCB and Tamm’s reagent extractable Fe, respectively. For the composite soil for GCS2, there was 1014

mg Fe per kg soil from microwave digestion, 47 ppm (5% of total Fe) and 30 ppm (3% of total Fe) of which are present as DCB and Tamm's reagent extractable Fe, respectively. For the composite oxic GCS2 soil, of the 719 mg Fe per kg soil, 166 ppm (23% of total Fe) and 68 ppm (9% of total Fe) are present as DCB and Tamm's reagent extractable Fe, respectively. Of the 22,994 mg Fe per kg soil present in the composite SWRC soil, 14,123 ppm (61% of total Fe) and 4,001 ppm (17% of total Fe) are present as DCB and Tamm's reagent extractable Fe, respectively. DCB and Tamm's reagent extractable Fe represent total "free" Fe oxides and amorphous Fe oxides, respectively.

Maximum potential Fe concentrations in 50 g/L soil solution during reductive dissolution reactions were calculated based on data from Tamm's and DCB extractions and are presented in Table 4.4. Molar concentrations of maximum Fe concentrations were one magnitude of order higher for the DCB extractable Fe than for the Tamm's extractable Fe for both the GCS2 oxic and SWRC soils; GCS1 and GCS2 soils had maximum potential concentrations that were similar to each other across sites and extractions.

4.4.3 XRD Data

XRD data from the GCS soil sand/silt and clay fractions are presented in Figure 4.2. Primary components of the sand/silt fraction for both GCS sites were determined to be quartz. The K⁺- and Mg²⁺-saturated clay fractions at 298 K for both sites contain peaks for quartz, kaolinite, and magnetite. In the samples that had been heated to 823 K, peaks at 12 and 25 2 θ representing kaolinite disappeared, confirming the presence of kaolinite in these soils (Sparks, 2003).

Figure 4.3 shows SWRC soil sand/silt and clay fractions XRD data. Primary components from the sand/silt fraction are quartz and apatite. The K^+ - and Mg^{2+} -saturated clay fractions at 298 K contain quartz, kaolinite, and magnetite. K^+ - and Mg^{2+} -saturated clay fraction samples that been heated to 823 K no longer contained peaks at 12 and 25 2θ , confirming the presence of kaolinite in these samples (Sparks, 2003).

XRD data of the γ - Al_2O_3 sorption samples from SWRC (not shown) indicates the presence of γ - Al_2O_3 , which was expected as this is the mineral sorbent present in this system. No other phase of long-range order in these samples was detected through this technique.

4.4.4 Soil Dissolution Data

Table 4.5 shows soil solution Fe concentrations and pH for reactions with γ - Al_2O_3 solutions at the initial reaction time and final sampling point. Fe concentration are highest in the SWRC soil solution when the soil pH during the reaction was below 7.4, especially during the sorption reaction occurring between pH 5.6 and 6.9. Soil solution Fe concentrations during reductive dissolution reactions with γ - Al_2O_3 are presented in Figure 4.4. GCS soils reached a maximum of 0.1 ppm Fe ($1.8 \mu M$ Fe) by the end of the 21 d reaction time because most of the microbially reducible Fe had been reduced and leached from the soil. The SWRC soil had a much higher concentration of Fe entering solution, with a maximum of 142 ppm Fe ($2.5 mM$ Fe) at 16 d of reaction time. This concentration declined upon continued reaction and reached a concentration of 3.4 ppm ($0.06 mM$ Fe) by completion of the second iteration of γ - Al_2O_3 sorption where it appeared to reached equilibrium. During this time, the SWRC soil solution pH quickly dropped from approximately 5.5 to

approximately 5.0 and then steadily increased to approximately 7.5 where it appeared to reach equilibrium (Figure 4.5). Total elemental concentrations of the soil solutions at the start of the γ -Al₂O₃ sorption reactions are provided in Table 4.6. Elemental concentrations of γ -Al₂O₃ sorption samples from acid digestion are given in Table 4.7. The most considerable concentrations present include Fe, Mn, P, and S. These data are consistent with the soil solution elemental concentrations released from reductive dissolution as observed in Table 4.6.

4.4.5 XRF Data

XRF data are presented in Table 4.8, and are primarily qualitative due to ongoing calibrations with this relatively new instrument. Greater than 94% of all γ -Al₂O₃ sorption samples exist as Al, consistent with the sorbent phase used in this study. GCS1 and GCS2 γ -Al₂O₃ sorption samples contain considerable amounts of S, Si, and La, with lesser amounts of Fe, Cl, and K. The SWRC γ -Al₂O₃ sorption sample also shows high concentrations of Si, Fe, P, and S with lesser amounts of Ca, Cl, Cr, and K. These data are consistent with the concentrations found from acid digestion of the γ -Al₂O₃ sorption samples (Table 4.7). The presence of La in the GCS1 and GCS2 γ -Al₂O₃ sorption samples was unexpected and not considered for measure by other techniques. La is used as a growth promoter in livestock and can be released through excretion (Von Tucher and Schmidhalter, 2005), and the nearby area's agricultural history could explain its presence in this soil. The presence and effects of La merit further study.

4.4.6 XAS Data

XAS analysis was performed at the Fe K edge (7112 eV) for the GCS and SWRC sorption samples. Sorption samples from the GCS soils did not have high enough concentrations to collect fluorescence data. X-ray absorption near-edge structure (XANES) spectroscopic data are shown in Figure 4.6 for the SWRC sorption samples. The pre-edge feature indicates the presence of Fe(III) while the white line of the sample is indicative of a predominantly Fe(II) oxidation state (~ 7121 eV), suggesting a mixed Fe(II)/Fe(III) oxidation state in all sorption samples. The Fe K edge k^3 -weighted χ functions and radial structure functions (RSF) of γ -Al₂O₃ sorption during soil reductive dissolution of the SWRC soil are presented in Figure 4.7. The k^3 -weighted χ functions of SWRC- γ -Al₂O₃ sorption samples do not exhibit the diagnostic region oscillations at $7-8 \text{ \AA}^{-1}$ indicative of LDH phases (excluding green rusts) (Figure 4.7a) (Elzinga, 2012; Scheinost and Sparks, 2000; Starcher et al., 2016; Suzuki et al., 2008; Thoraj et al., 2005; Zhu and Elzinga, 2014; Zhu and Elzinga, 2015). RSFs of sorption samples are shown in Figure 4.7b. The first coordination shell of sorption samples is present at $\sim 1.6 \text{ \AA}$ (uncorrected for phase shift), which represent O ligands surround Fe. The first shell was fitted with a Fe-O bond distance of 2.01 to 2.08 \AA and coordination number of 4.8 to 6.2 (Table 4.9). No second shell is observed in these samples. Scattering contributions for second shell neighbors and beyond are limited for the sorption samples, thus limiting the sample identification beyond the Fe-O shell by Fe EXAFS.

4.4.7 Visual Examination of Sorption Samples

When SWRC reacted γ -Al₂O₃ sorption samples were collected from dialysis tubing, they were primarily orange-colored with some blue-green mottling throughout

(not shown); however, samples from GCS reacted γ -Al₂O₃ sorption were a light orange. Figure 4.8 shows three γ -Al₂O₃ sorption samples that were analyzed with EXAFS following centrifugation and prior to air-drying. The SWRC reacted γ -Al₂O₃ sorption sample is much darker in color than the two GCS reacted γ -Al₂O₃ sorption samples, and all samples show the presence of a dark phase (indicated by arrows in Figure 4.8).

4.5 Discussion

LDH phase formation was not observed from reductive dissolution of either soil system. Reducing conditions upon sampling of the GCS soils may have caused the soil Fe concentrations to be too low (Tables 4.1, 4.5, and 4.6) for LDH formation within the dialysis tubing. These soils have already experienced natural reductive dissolution and even though some Fe-oxides were available for reductive dissolution (Figure 4.1 and Table 4.4), the maximum potential concentrations that could be available in the soil solution (Table 4.4) were likely insufficient for LDH phase formation (Li et al., 2012). Furthermore, the soils were acidic upon sampling following natural reductive dissolution (Table 4.1), and remained acidic after further incubation in the laboratory (Table 4.5). Fe(II)-Al-LDH phases typically form in pH ≥ 7.0 , and other LDH phases do not form in soils below pH 6.5 (Elzinga, 2012; Peltier et al., 2010; Shi et al., 2012; Starcher et al., 2016; Zhu and Elzinga, 2014; Zhu and Elzinga, 2015). A combination of low Fe concentration and solution acidity were likely the causes of low Fe sorption observed in this system.

The formation of Fe(II)-Al-LDH phases was also not observed in the EXAFS data presented in Figure 4.7 and Table 4.9. The lack of backscattering from second-shell neighbors and higher has limited the ability of this study to determine the exact

nature of Fe sorption. A comparison of the χ functions and RSFs of the sorption samples and standards suggest that these phases are most similar to Fe(III)-OM and aqueous Fe(II). The lack of second-shell neighbors suggests the formation of a mononuclear surface species with multiple coordination environments. XRF and acid digestion data (Tables 4.7 and 4.8) of the γ -Al₂O₃ sorption samples from reductive dissolution of SWRC soils show Fe, S, and P sorbed to the γ -Al₂O₃ substrate. The elements that are co-sorbed to γ -Al₂O₃ could be inhibiting Fe(II)-Al-LDH formation by complexing Fe or Al, or restricting the dissolution of γ -Al₂O₃. Because bulk-XAS uses an average of the species for the element of interest, it is possible that other sorption phases are present in lesser quantities. Due to the presence of a number of sorbed elements and the limitations present in the EXAFS data, several possible sorption products for Fe in this system are discussed below.

In the SWRC soil reductive dissolution and γ -Al₂O₃ sorption system, the increase and subsequent decrease in aqueous Fe concentration of the soil solution (Figure 4.4) coincides with an increase in solution pH (Figure 4.5). Increased Fe concentrations under soil flooding conditions often result from the reductive dissolution of Fe(III)-(hydr)oxides through biotic processes. Microbial communities deplete O₂ during respiration of organic carbon and resort to alternative electron acceptors, such as nitrate, Mn(IV)-(hydr)oxides, Fe(III)-(hydr)oxides, and sulfate (Borch et al., 2010; Gambrell, 1994; Kirk, 2004; Ponnampereuma, 1972). Microbial respiration can also result in a moderated soil pH to circumneutral values, as also observed in this study, due to consumption of protons and production of dissolved carbonates (Kirk, 2004; Ponnampereuma, 1972). The soil solution can become oversaturated with respect to dissolved Fe(II) and carbonate and the phosphates and

sulfides also released during Fe(III)-(hydr) reductive dissolution, leading to the precipitation of Fe-carbonate, -phosphate, and -sulfide phases (Jensen, et al., 2002; Ponnampereuma, 1972; Wolthers et al., 2005). The precipitation of these phases could explain the decrease in aqueous Fe concentrations of the SWRC soil solution at longer reaction times (Figure 4.4). Furthermore, green rust, ferrihydrite, siderite, magnetite, and vivianite have been observed as products of microbial reduction (Abdelmoula et al., 1998; Cooper et al., 2000; Feder et al., 2005; Fredrickson et al., 1998; Hansel et al., 2003; Inskeep and Bloom, 1986; Lovley et al., 1987; Lovley and Phillips, 1988; Mortimer and Coleman, 1997; Roden and Lovley, 1993; Trolard et al., 1997; Zachara et al. 2002). Other studies have also observed the increased Fe concentrations shortly after soil inundation that ultimately decrease over time due to Fe(II) sorption to solid phases (Gambrell, 1994; Kirk, 2004; Mitsch and Gosselink, 2000; Ponnampereuma, 1972). Fe(II)-Al-LDH phases have been shown to form at $\text{pH} \geq 7.0$ from sorption reactions to Al-oxides and clays (Elzinga, 2012; Starcher et al., 2016; Zhu and Elzinga, 2014); however, at the reaction time at which this pH is observed in this study the Fe concentrations of the system have dropped significantly. Further research should be conducted to determine the minimum Fe(II) concentrations required at $\text{pH} \geq 7.0$ for LDH phase formation.

High concentrations of C and TOC were observed in the SWRC soil and soil solution, respectively (Tables 4.1 and 4.6). Previous research has shown that LDH phase formation has been slowed or inhibited by the presence of OM by competing for Al or slowing substrate dissolution (Nachtegaal, and Sparks, 2003; Peltier et al., 2010; Shi et al., 2012). Other work has demonstrated strong complexation of Fe and Al with OM (Benke et al., 1999; Kaiser and Guggenberger, 2003; Kaiser and Zech, 2000).

OM may be: 1) competing with Fe for Al that would otherwise be incorporated into the LDH structure; 2) complexing the Fe and prohibiting LDH precipitate formation; or 3) may be preventing the dissolution of Al-bearing substrates in the soil (Benke et al., 1999; Kaiser and Guggenberger, 2003; Kaiser and Zech, 2000; Nachtegaal, and Sparks, 2003; Peltier et al., 2010; Shi et al., 2012). Dialysis tubing with a low MWCO (1 kDa) was used to limit effects of OM on Fe sorption to γ -Al₂O₃. Humic acids typically have larger molecular weights (2-5 kDa) while fulvic acids typically have lower molecular weights (0.5-2 kDa), suggesting that fulvic acids could have inhibited LDH formation (Connell, 2005; Leenheer and Croué, 2003; Louie et al., 2015; Piccolo, 2001). Siderite (FeCO₃) has been observed from the oversaturation of the soil solution with dissolved Fe(II) and CO₃ following microbial reduction (Jensen et al., 2002; Mortimer and Coleman, 1997). This is another possible C phase that could be forming in these systems.

Another Fe sorption phase that could be present in this system is green rust. Formation of these phases has been observed in the presence of mixed Fe(III) and Fe(II) oxidation states in anoxic soils and laboratory reactions (Abdelmoula et al., 1998; Christiansen et al., 2009; Feder et al., 2005; Refait et al., 2001; Suzuki et al., 2008; Trolard et al., 1997). Fe(III) presence in the sorption samples is indicated by the pre-edge feature of the XANES spectra (Figure 4.6) even though the white lines of the spectra a relatively low (~7121 eV) suggesting a mixed Fe(II)/Fe(III) oxidation state within the sorption samples. Fe concentrations at the early stages of the reaction were at their highest (Figure 4.4). These phases are also blue-green in color, which could explain the presence of the blue-green mottling observed in the γ -Al₂O₃ sorption

samples (not shown). Previous work has shown the potential for mixed Fe(II)-Al(III)/Fe(III)-LDH formation (Starcher et al., 2016).

Fe-phosphates are known to form in conditions similar to those found in the system studied here. Vivianite can form in reducing soil conditions with high concentrations of aqueous Fe(II) and P, and they have been observed as a result of reductive dissolution of Fe(III)-oxides by dissimilatory iron-reducing bacteria (DIRB) in systems with adequate phosphate concentrations (Berner, 1981; Borch and Fendorf, 2007; Nriagu, 1972; Nriagu and Dell, 1974; O'Loughlin et al., 2013; Roden and Edmonds, 1997). Vivianite in soils turns blue upon oxidation, which suggests that vivianite may be the blue/green mottling observed on γ -Al₂O₃ sorption samples (not pictured) and may be the dark phases observed in SWRC soil solution γ -Al₂O₃ sorption samples in Figure 4.8. XRD of the γ -Al₂O₃ sorption samples from SWRC (not shown) does not indicate the presence of vivianite; however, the presence of vivianite is typically difficult to observe in bulk mineral samples (Rothe et al., 2014). Furthermore, vivianite formation is inhibited in sulfidic soils (Nriagu, 1972; Nriagu and Dell, 1974; Roden and Edmonds, 1997), and significant S sorption was observed in the γ -Al₂O₃ XRF and acid digestion data (Tables 4.6, 4.7, and 4.8). This could also suggest the precipitation of FeS, which has been observed in sulfur-rich systems (Wolthers et al., 2005).

Also present in high concentrations in both the soil solution at reaction start (Table 4.6) and in the γ -Al₂O₃ sorption samples from both sites after reaction (Table 4.8) is Si. It is possible at higher pH that Fe(II) sorption to Si is occurring. A previous study by Zhu and Elzinga (2014) examined Fe(II) sorption to clays and amorphous SiO₂ at range of pH from 6.5 to 8.0. Fe(II) sorption was considerably lower (<20%) at

pH \leq 7.0 for both systems; however, sorption for the clay was $>50\%$ and for the SiO₂ was $>90\%$ at pH \geq 7.5. Their studies resulted in the formation of Fe(II)-Al-LDH at high pH in the clay system and a poorly crystalline Fe(II)-phyllosilicate in the SiO₂ system. In the systems studied here, Fe(II) could be complexing with Si, especially in those with higher pH.

The inhibitive effect of P in the SWRC soils on Fe(II)-Al-LDH phase formation is also not surprising due to the similarities in reactivity between phosphate and arsenate (Cui and Weng, 2013; Neupane et al., 2014; Violante and Pigna, 2002). In a previous study by Zhu and Elzinga (2015) assessing co-sorption between Fe(II) and As on γ -Al₂O₃, they found that As(III) sorbs independently of Fe(II), which formed Fe(II)-Al-LDH. However, low concentration of As(V) slowed Fe(II)-Al-LDH formation while higher concentrations prevented their formation altogether. The inhibition of Fe(II)-Al-LDH formation in the high As(V) concentration systems is thought to be a result of: 1) interaction of As(V) with Fe(II)-Al-LDH crystal growth; 2) As(V) inner-sphere complexation with the Al-oxide blocking Al release; or 3) competitive formation of As(V)-Al(III) phases. Secondary Fe(II)-As(V) formation was not observed by EXAFS in the study by Zhu and Elzinga (2015); however, their results suggest that the most likely Fe(II) phase present is a mononuclear surface species with multiple coordination environments. Similarities are observed between the Fe EXAFS sorption samples observed in their study and the SWRC γ -Al₂O₃ sorption samples in this study (Figure 4.7). The most likely Fe sorption product they found was a mononuclear surface species; however, they suspected that multiple coordination environments were present due to the lack of backscattering contributions from second shell neighbors and beyond (Zhu and Elzinga, 2015). It is

hypothesized that a similar reaction could have prevented LDH formation in this study. Further work is required to elucidate the Fe phase formed in this study, although these results clearly demonstrate the inhibition of Fe(II)-Al-LDH phase formation.

4.6 Environmental Implications and Future Directions

This study did not result in the formation of a Fe(II)-Al-LDH phase from reductive dissolution of soils with different physicochemical properties; however, it did raise a series of questions to be examined further through systematic investigations and experiments on the environmental factors that can inhibit the formation of these phases. In this study, low Fe concentrations in solution, lower pH, and high concentrations of carbonates, P, S, Si, and OM are potential inhibitors of LDH phase formation. LDH phases are known to form in soils with circumneutral pH and sufficiently high concentrations of the divalent metal (McNear et al., 2007) and are typically more favorable phases over pure divalent metal hydroxide formation in phases that contain soluble aluminum (Allada et al., 2006; Peltier et al., 2006). However, sufficient thermodynamic data does not exist for comparisons of Fe(II)-Al-LDH phases with Fe(II) (oxy-hydr)oxides and should be examined in the future. OM has also been shown to inhibit LDH phase formation (Nachtegaal, and Sparks, 2003; Peltier et al., 2010; Shi et al., 2012).

In a recent study by Zhu and Elzinga (2015), high concentrations of As(V) were found to prevent Fe(II)-Al-LDH phase formation. The potential inhibition of Fe(II)-Al-LDH phases by phosphate due to its similar reactivity to arsenate as well as the potential for vivianite formation in the presence of phosphates (Berner, 1981; Borch and Fendorf, 2007; Cui and Weng, 2013; Neupane et al., 2014; Nriagu, 1972;

Nriagu and Dell, 1974; O'Loughlin et al., 2013; Roden and Edmonds, 1997; Violante and Pigna, 2002) make the examination of increasing phosphate concentrations on Fe(II)-Al-LDH formation an important study. Understanding how these phases change with time in environmental systems is also critical as these phases may become more stable with aging due to Ostwald ripening and interlayer silication (Peltier et al., 2006). Oxidation-reduction cycling is common in areas of flooding and periodic inundation, and Fe(II) is sensitive to oxidation. Understanding the redox effects on LDH stability and formation and potential links to green rust formation is also an important consideration (Starcher et al., 2016).

Future investigations should look for soils with the following qualities: 1) circumneutral pH; 2) low concentrations of organic matter; 3) low concentrations of potentially inhibitive elements, such as As and P; and 4) sufficient Fe concentrations in forms that can undergo biotic reductive dissolution. Fully understanding Fe(II)-bearing mineral phases that may form in anoxic environments such as wetland soils is important due to the prevalence and reactivity of Fe phases in these environments.

Table 4.1: Physicochemical properties of composite soil samples from the Great Cypress Swamp in Frankford, DE, (GCS1 and GCS2) and Stroud Water Research Center in Avondale, PA (SWRC).

Sample	pH	pH _b ^a	Total Concentration (mg/kg)																
			Al	As	B	Ca	Cd	Cr	Cu	Fe	K	Mg	Mn	Na	Ni	P	Pb	S	Zn
GCS1	4.7	7.85	2735	0.1	0.6	14	0.03	2.5	0.9	484	83.3	80.4	5.3	31	2.1	11	2.5	32	2.2
GCS2	3.9	7.91	4663	0.2	1.1	20	0.01	4.5	2.1	1014	212	117	12.0	13	2.8	16	3.5	25	3.1
SWRC	5.4	7.7	8253	4.9	2.2	2588	0.36	45	30	22994	2250	5181	663	46	28	659	31	504	98
Sample	Soil Color		Particle Size			Texture	Total C (%)	Total N (%)											
			% Clay	% Silt	% Sand														
GCS1	10YR7/1	Light gray	0.01	0.04	99.95	Sand	0.14	0.12											
GCS2	10YR6/2	Light brownish gray	B.D.	0.06	99.94	Sand	0.12	0.07											
SWRC	10YR5/2	Grayish brown	4	2	94	Sand	4.05	0.32											

^apH_b is buffer pH.

Table 4.2: Mehlich 3 chemical extraction concentrations for composite soils taken from the Great Cypress Swamp, Frankford, DE, (GCS1, GCS2) and Stroud Water Research Center in Avondale, PA (SWRC).

Sample	Mehlich 3 Extractable Elements (mg/kg)									
	P	K	Ca	Mg	Mn	Zn	Cu	B	S	Al
GCS1	8.0	14.8	44.23	12.6	0.51	0.25	0.12	0.21	20.0	746
GCS2	4.3	11.5	31.27	12.8	0.28	0.27	0.53	0.08	16.1	536
SWRC	16.0	105.1	1199.2	213.4	29.21	5.41	2.12	0.48	17.7	838

Table 4.3: DCB chemical extraction concentrations for composite soil from Stroud Water Research Center in Avondale, PA (SWRC).

Sample	Elemental Concentrations (mg/kg)												
	Al	As	B	Ca	Cr	Cu	Fe	K	Mg	Mn	P	Pb	Zn
SWRC	1966	10.8	4.2	2888	10.3	0.9	14123	429.0	405.0	657.5	485.2	5.1	21.9

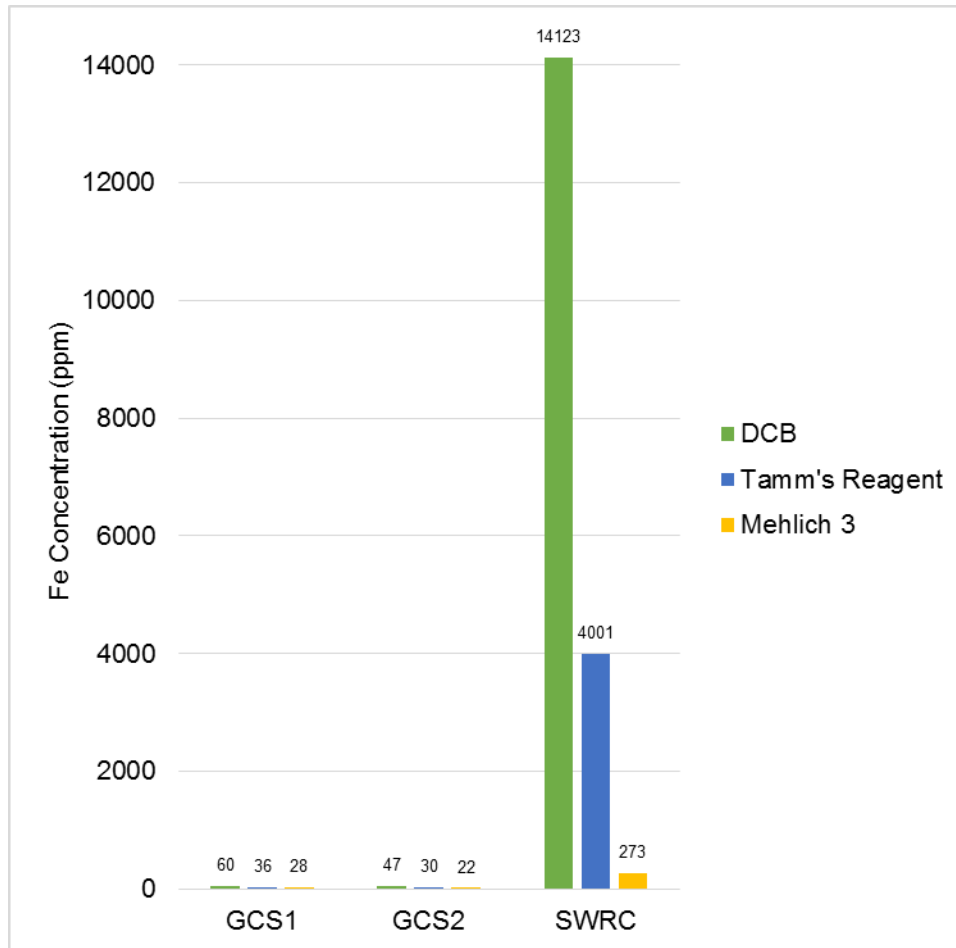


Figure 4.1: Soil Fe concentrations from DCB, Tamm's reagent (acid ammonium oxalate), and Mehlich 3 chemical extraction for composite soils taken from the Great Cypress Swamp, Frankford, DE, (GCS1, GCS2) and Stroud Water Research Center in Avondale, PA (SWRC).

Table 4.4: Maximum soil solution [Fe] at 50 g/L from reductive dissolution estimated from DCB and Tamm's extractions for soils from the Great Cypress Swamp, Frankford, DE, (GCS1, GCS2) and Stroud Water Research Center in Avondale, PA (SWRC).

	Maximum [Fe] calculated from Tamm's extractable Fe	Maximum [Fe] calculated from DCB extractable Fe
	(ppm)	(ppm)
GCS1	1.81	3.00
GCS2	1.50	2.34
SWRC	200.05	707.16

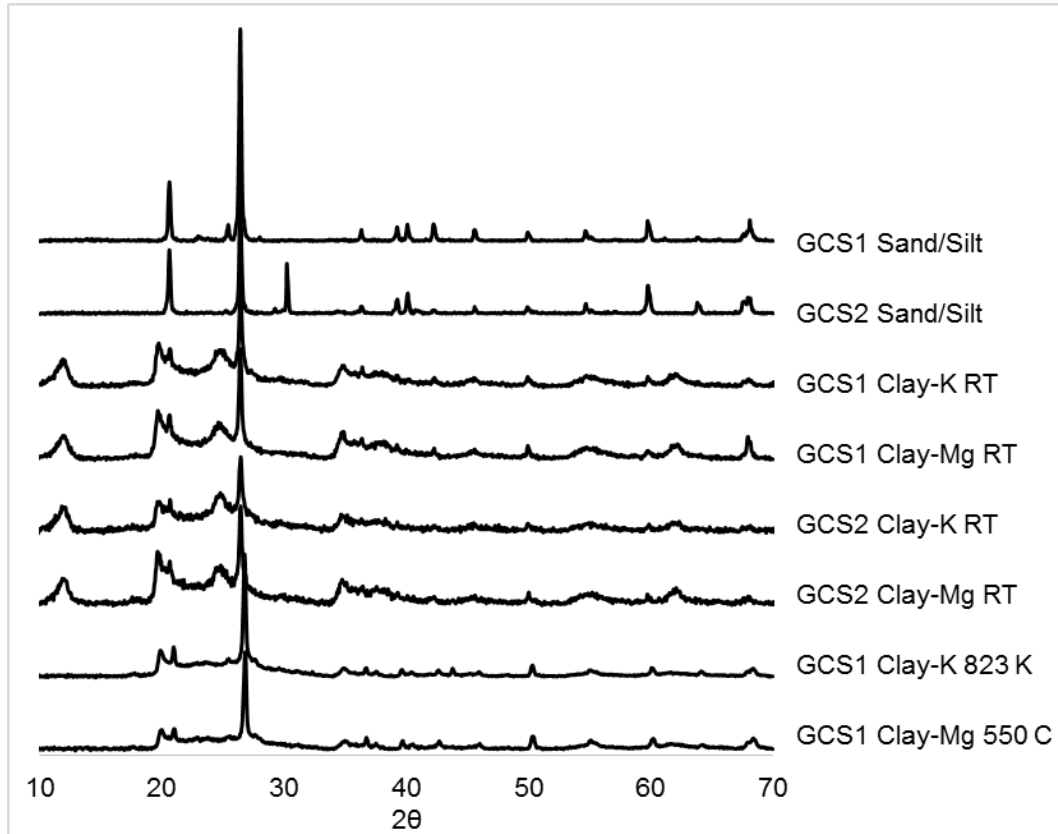


Figure 4.2: Powder XRD data of Great Cypress Swamp Sites 1 (GCS1) and 2 (GCS2) sand/silt and K^+ - and Mg^{2+} -clay fractions at 298 K (RT) and 823 K.

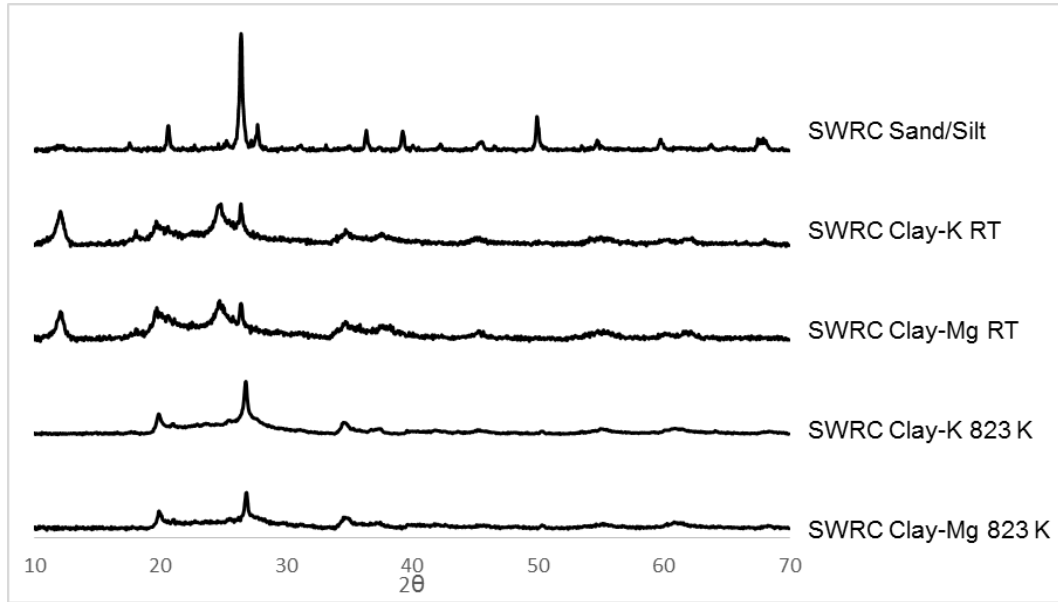


Figure 4.3: Powder XRD data of Stroud Water Research Center soil sand/silt and K^+ - and Mg^{2+} -clay fractions at 298 K (RT) and 823 K.

Table 4.5: Soil solution Fe concentrations and pH for reactions with $\gamma\text{-Al}_2\text{O}_3$ solutions at the initial reaction time and final sampling point.

Soil Solution	Initial		Final	
	pH	[Fe] (ppm)	pH	[Fe] (ppm)
GCS1	4.8	0.1	4.0	0.7
GCS2	4.5	0.1	3.9	0.4
SWRC, with soil pH 5.6	5.6	32.7	6.9	101.4
SWRC, with soil pH 7.4	7.4	7.1	7.5	4.3
SWRC, without soil pH 7.0	7.0	36.9	7.2	35.8
SWRC, without soil pH 7.5	7.5	4.3	7.5	4.4

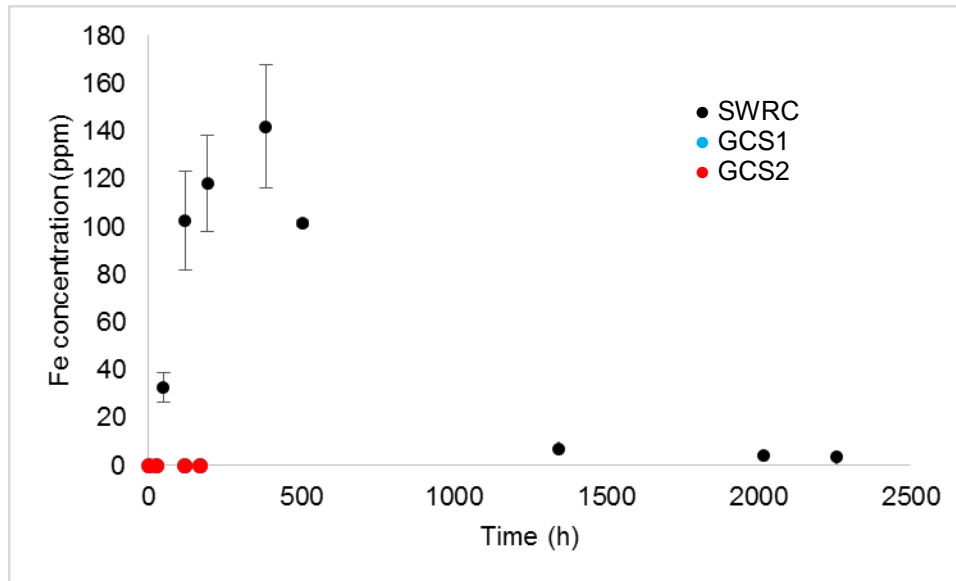


Figure 4.4: Fe concentration in soil solution during reductive dissolution of soils from the Great Cypress Swamp, Frankford, DE, (GCS1, GCS2) and Stroud Water Research Center in Avondale, PA (SWRC).

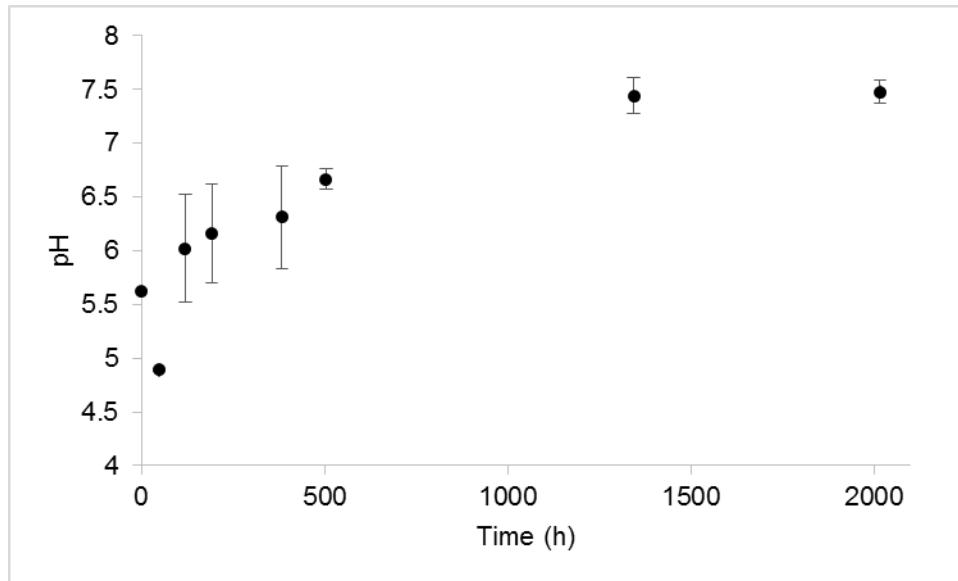


Figure 4.5: Change in soil solution pH during reductive dissolution of soil from the Stroud Water Research Center in Avondale, PA (SWRC).

Table 4.6: Great Cypress Swamp (GCS1, GCS2) and Stroud Water Research Center (SWRC) soil solution elemental concentrations at reaction start.

Sample	Elemental Concentrations (ppm)																
	Al	B	Ca	Cu	Fe	K	Mg	Mn	Na	P	S	Si	Zn	TIC	TC	TOC	TNb
GCS 1	2.3	0.002	4.42	ND	0.13	6.04	0.03	ND	1.30	0.066	0.36	0.31	0.013	ND	380.8	380.8	0.66
GCS 2	ND	0.002	0.04	ND	0.06	0.65	0.03	ND	0.28	0.004	0.23	0.13	0.004	0.04	408.3	408.3	0.69
SWRC, without soil pH 7.0	0.04	0.099	49.92	0.05	84.90	7.96	12.27	10.64	60.8	0.17	0.47	11.92	0.043	0.05	295.9	295.8	4.39
SWRC, without soil pH 7.5	0.05	0.034	29.05	0.01	17.16	8.40	8.90	4.54	65.9	0.32	0.80	15.67	0.013	0.07	217.2	217.2	4.41

ND is not detected

Table 4.7: Elemental concentrations of γ -Al₂O₃ sorption samples after reaction with reductive dissolution soil solutions from acid digestion.

	Total Concentration (mg/kg)																
	Al	As	B	Ca	Cd	Cr	Cu	Fe	K	Mg	Mn	Na	Ni	P	Pb	S	Zn
GCS1	266707	187	6.8	8.4	1.8	51.8	9.3	225	57.0	19.8	2.5	757	26.9	38.5	221	3427	115
GCS2	250716	172	6.4	21.3	2.3	49.8	8.7	214	87.5	17.8	2.3	1022	68.9	39.1	209	3841	223
SWRC, with soil pH 5.6	305140	72.5	20.6	58.3	3.5	84.5	16.0	1632	26.8	38.5	30.3	663	137	608	185	1221	197
SWRC, without soil pH 7.0	212087	139	184	774	0.7	35.7	1.9	3750	110	95.9	242	482	429.8	185	154	1084	75.2
SWRC, without soil pH 7.5	184074	136	55.1	912	1.8	33.5	2.0	1968	94.3	122	243	843	42.7	646	144	771	88.0

Table 4.8: Elemental concentrations of γ -Al₂O₃ sorption samples after reaction with reductive dissolution soil solutions from XRF.

	Elemental Concentrations (mass %)												
	Al	Si	P	S	Cl	K	Ca	Cr	Fe	Zn	Zr	La	
GCS1	94.71	2.59	ND	0.91	0.64	0.12	0.01	ND	0.07	0.01	0.01	0.92	
GCS2	94.35	2.65	ND	1.08	0.76	0.15	ND	ND	0.11	0.04	0.02	0.85	
SWRC	96.69	1.75	0.28	0.41	0.06	0.18	0.11	0.10	0.42	ND	ND	ND	

ND is not detected

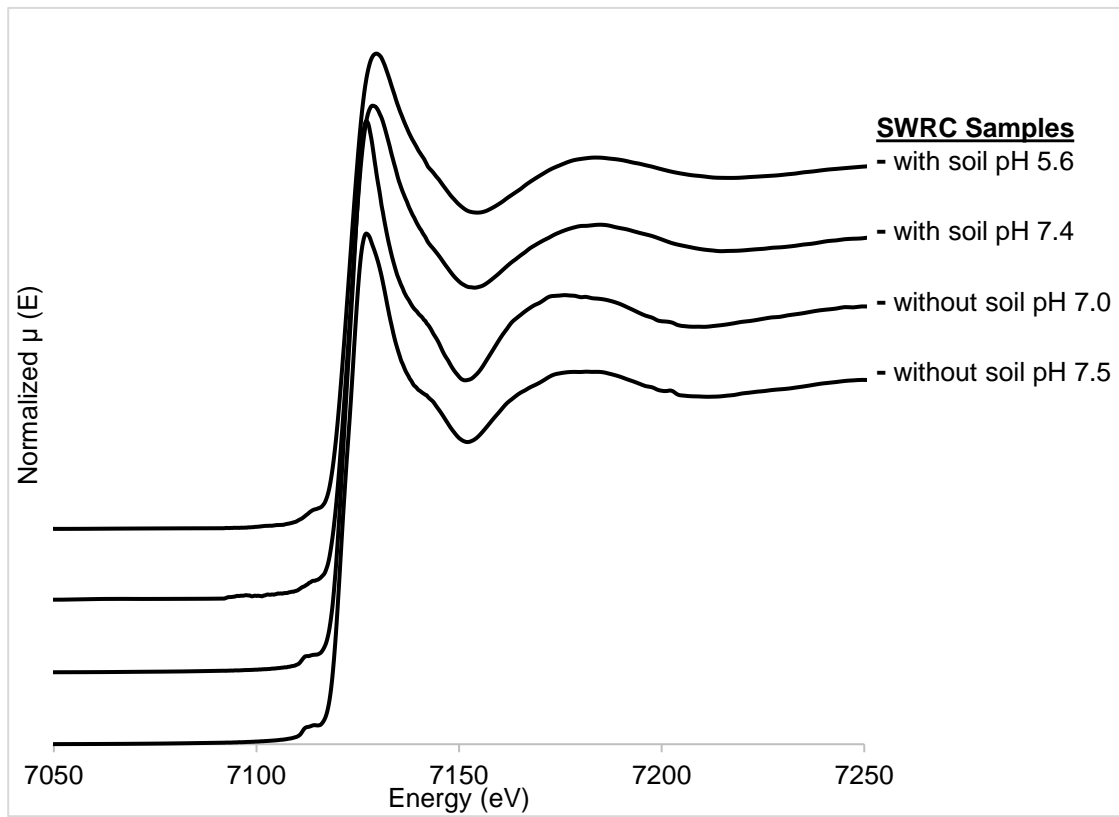


Figure 4.6: Fe *K* edge XANES spectra of SWRC reductive dissolution and γ -Al₂O₃ sorption samples

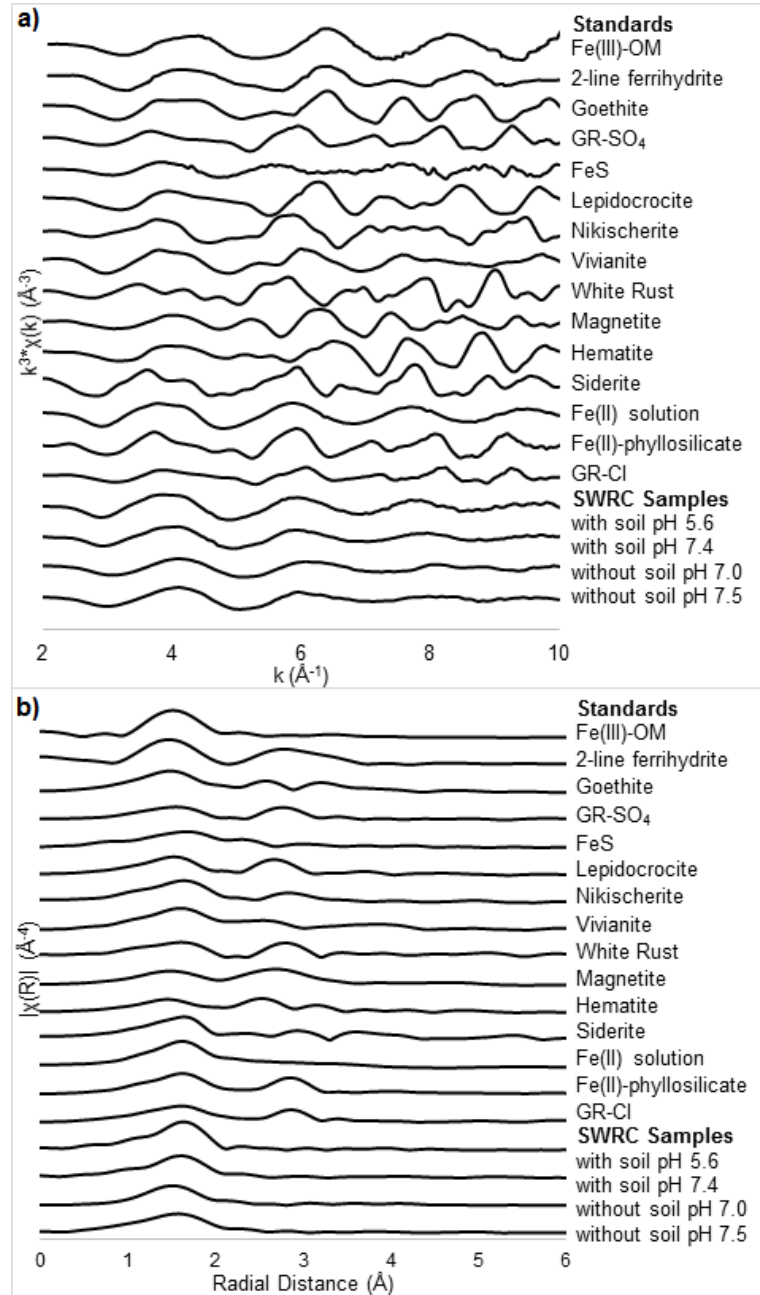


Figure 4.7: Fe *K* edge raw $k^3 \cdot \chi$ functions (a) and radial structure functions (RSF) (b) of SWRC reductive dissolution and $\gamma\text{-Al}_2\text{O}_3$ sorption samples and Fe standards.

Table 4.9: Fe K-Edge EXAFS Fitting Results of γ -Al₂O₃ Sorption Samples During Reductive Dissolution of SWRC soil^a

SWRC Sorption Samples	R-factor	Atomic Shell			ΔE (eV)	S_0^2	N_{ind}	N_{var}	χ^2	χ_v^2	k_{min}	k_{max}
		CN	R(\AA)	σ^2 (\AA^2)								
With soil												
pH 5.6	0.008	6.2	2.08	0.011	-4.85	0.85	4.48	3	995	672	3	10
pH 7.4	0.004	5.7	2.07	0.014	-1.92	0.85	4.48	3	818	553	3	10
Without soil												
pH 7.0	0.004	4.8	2.01	0.014	-2.79	0.85	4.48	3	3886	2627	3	10
pH 7.5	0.007	6.3	2.04	0.017	-2.00	0.85	4.48	3	2005	1355	3	10

^aR-factor is the absolute misfit between the data and theory (as defined by Artemis), CN is coordination number, R is interatomic radial distance, σ^2 is Debye-Waller factor, ΔE is energy shift, S_0^2 is amplitude reduction factor, N_{ind} is the number of independent points, N_{var} is the number of variables, χ^2 is chi square, χ_v^2 is reduced chi square, and k_{min} and k_{max} are the minimum and maximum values, respectively, of the region of k-space over which the RSF data was transformed for fitting.

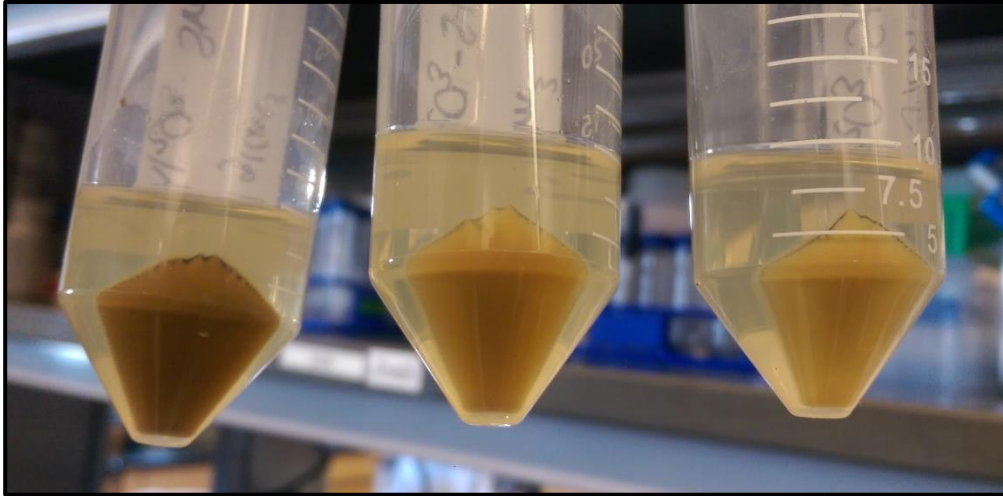


Figure 4.8: Image of dark precipitate formed during sorption of Stroud soil solutions to $\gamma\text{-Al}_2\text{O}_3$ in dialysis tubing with the following initial reaction conditions in soil solution: a) soil present in solution, pH 7.4; b) no soil in solution, pH 7.0; and c) no soil in solution, pH 7.5.

REFERENCES

- Abdelmoula, M.; Trolard, F.; Bourrie, G.; Génin, J.M.R. Evidence for the Fe(II)-Fe(III) green rust “Fougerite” mineral occurrence in a hydromorphic soil and its transformation with time and depth. *Hyperfine Interact.*, **1998**, 112:235-238; DOI 10.1023/A:1010802508927.
- Allada, R.K.; Peltier, E.; Navrotsky, A.; Casey, W.H.; Johnson, A.; Thompson-Berbeco, H.; Sparks, D.L. Calorimetric determination of the enthalpies of formation of hydrotalcite-like solids and their use in the geochemical modeling of metals in natural waters. *Clay Clay Miner.*, **2006**, 54:409–417.
- Andres, A.S.; Howard, C.S. Report of investigations no. 62: The Cypress Swamp Formation, Delaware. Delaware Geological Survey, 2000.
- Andres, A.S.; Howard, C.S. Report of investigations no. 64: Results of hydrogeologic studies of the Cypress Swamp Formation, Delaware. Delaware Geological Survey, 2002.
- Benke, M. B.; Mermut, A. R.; Shariatmadari, H. Retention of dissolved organic carbon from vinasse by a tropical soil, kaolinite, and Fe oxides. *Geoderma*, **1999**, 91:47-63; DOI 10.1016/S0016-7061(98)00143-8.
- Berner, R.A. A new geochemical classification of sedimentary environments. *J. Sediment. Res.*, **1981**, 51:359-365; DOI 10.1306/212F7C7F-2B24-11D7-8648000102C1865D.
- Borch, T.; Fendorf, S. Phosphate interactions with iron (hydr)oxides: Mineralization pathways and phosphorus retention upon bioreduction, In *Adsorption of Metals by Geomedia II: Variables, Mechanisms, and Model Applications*, Barnett, M.O; Kent, D.B, Eds. Elsevier: Amsterdam, NL, 2007.
- Bremner, J.M. Nitrogen-total, In *Methods of Soil Analysis. Part 3 Chemical Methods*; Sparks, D.L., Ed. American Society of Agronomy: Madison, WI, 1996. p. 1085-1121.
- Chen, C. Investigating organic matter-mineral interactions at a molecular scale: An integrated field and laboratory study. Ph.D. Dissertation, University of Delaware, Newark, DE, 2013.

- Christiansen, B.C.; Balic-Zunic, T.; Petit, P.O.; Frandsen, C.; Morup, S.; Geckeis, H.; Katerinopoulou, A.; Stipp, S.L.S. Composition and structure of an iron-bearing, layered double hydroxide (LDH) – Green rust sodium sulphate. *Geochim. Cosmochim. Acta*, **2009**, 73:3579-3592; DOI 10.1016/j.gca.2009.03.032.
- Connell, D. W. *Basic Concepts of Environmental Chemistry*. CRC Press: Boca Raton, FL, 2005.
- Cooper, D.C.; Picardal, F.; Rivera, J.; Talbot, C. Zinc immobilization and magnetite formation via ferric oxide reduction by *Shewanella putrefaciens*. *Environ. Sci. Technol.*, **2000**, 34:100-106; DOI 10.1021/es990510x.
- Cui, Y.; Weng, L. Arsenate and phosphate adsorption in relation to oxides composition in soils: LCD modeling. *Environ. Sci. Technol.*, **2013**, 47:7269-7276; DOI 10.1021/es400526q.
- Elzinga, E.J. Formation of layered Fe(II)-Al(III)-hydroxides during reaction of Fe(II) with aluminum oxide. *Environ. Sci. Technol.*, **2012**, 46:4894-4901; DOI 10.1021/es2044807.
- Feder, F.; Trolard, F.; Klingelhöffer, G.; Bourrie, G. In situ Mössbauer spectroscopy: Evidence for green rust (fougerite) in a gleysol and its mineralogical transformations with time and depth. *Geochim. Cosmochim. Acta*, **2005**, 69:4463-4483; DOI 10.1016/j.gca.2005.03.042.
- Fredrickson, J.K.; Zachara, J.M.; Kennedy, D.W.; Dong, H.L.; Onstott, T.C.; Hinman, N.W.; Li, S.M. Biogenic iron mineralization accompanying the dissimilatory reduction of hydrous ferric oxide by a groundwater bacterium. *Geochim. Cosmochim. Acta*, **1998**, 62:3239-3257; DOI 10.1016/S0016-7037(98)00243-9.
- Gambrell, R. P. Trace and toxic metals in wetlands - A review. *J. Environm. Qual.* **1994**, 23, 883-891; DOI 10.2134/jeq1994.00472425002300050005x.
- Gartley, K.L.; Sims, J.T.; Olsen, C.T.; Chu, P. 2002. Comparison of soil test extractants used in mid-Atlantic United States. *Commun. Soil Sci. Plan.*, **2002**, 33:873-895; DOI 10.1081/CSS-120003072.
- Hansel, C.M.; Benner, S.G.; Neiss, J.; Dohnalkova, A.; Kukkadapu, R.K.; Fendorf, S. Secondary mineralization pathways induced by dissimilatory iron reduction of ferrihydrite under advective flow. *Geochim. Cosmochim. Acta*, **2003**, 67:2977-2992; DOI 10.1016/S0016-7037(03)00276-X.

- Inskeep, W.P.; Bloom, P.R. Kinetics of calcite precipitation in the presence of water-soluble organic-ligands. *Soil Sci. Soc. Am. J.*, **1986**, 50:1167-1172; DOI 10.2136/sssaj1986.03615995005000050015x.
- Jackson, M.L. *Soil chemical analysis – Advanced course*. University of Wisconsin, Madison, WI, 1969.
- Jackson, M.L.; Lim, C.H.; Zelazny, L.W. Oxides, hydroxides, and aluminosilicates. In *Methods of Soil Analysis. Part 1 Physical and Mineralogical Chemical Methods*, 2nd ed, Klute, A., Ed. American Society of Agronomy: Madison, WI, 1986. p. 101-150.
- Jensen, D.L.; Boddum, J.K.; Tjell, J.C.; Christensen, T.H. The solubility of rhodochrosite (MnCO₃) and siderite (FeCO₃) in anaerobic aquatic environments. *Appl. Geochem.*, **2002**, 17:503-511; DOI 10.1016/S0883-2927(01)00118-4.
- Kaiser, K.; Guggenberger, G. Mineral surfaces and soil organic matter. *Eur. J. Soil Sci.*, **2003**, 54:219-236; DOI 10.1046/j.1365-2389.2003.00544.x.
- Kaiser, K.; Zech, W. Dissolved organic matter sorption by mineral constituents of subsoil clay fractions. *J. Plant Nutr. Soil Sci.*, **2000**, 163:531-535; DOI 10.1002/1522-2624(200010)163:5<531::AID-JPLN531>3.0.CO;2-N.
- Khaokaew, S.; Landrot, G.; Chaney, R.L.; Pandya, K.; Sparks, D.L. Speciation and release kinetics of zinc in contaminated paddy soils. *Environ. Sci. Technol.*, **2012**, 46:3957-3963; DOI 10.1021/es103971y.
- Kirk, G. *The Biogeochemistry of Submerged Soils*. John Wiley & Sons, Ltd: Chichester, 2004.
- Kunze, G.W.; Dixon, J.B. Pretreatment for mineralogical analysis. In *Methods of Soil Analysis. Part 1 Physical and Mineralogical Methods*, 2nd ed., Klute, A., Ed. American Society of Agronomy: Madison, WI, 1986. pp. 91-100.
- Leenheer, J. A.; Croué, J.-P. Characterizing aquatic dissolved organic matter. *Environ. Sci. Technol.*, **2003**, 37 (1):18A–26A; DOI 10.1021/es032333c.
- Li, W.; Livi, K.J.; Xu, W.; Siebecker, M.G.; Wang, Y.; Phillips, B.L.; Sparks, D.L. Formation of crystalline Zn-Al layered double hydroxide precipitates on γ -alumina: the role of mineral dissolution. *Environ. Sci. Technol.*, **2012**, 46(21):11670-11677, DOI 10.1021/es3018094.

- Loeppert, R.H.; Inskeep, W.P. Iron. In *Methods of Soil Analysis. Part 3 Chemical Methods*, Sparks, D.L., Ed. American Society of Agronomy: Madison, WI, 1996. p. 639-664.
- Louie, S. M.; Spielman-Sun, E. R.; Small, M. J.; Tilton, R. D.; Lowry, G. V. Correlation of the physicochemical properties of natural organic matter samples from different sources to their effects on gold nanoparticle aggregation in monovalent electrolyte. *Environ. Sci. Technol.*, **2015**, 49 (4):2188–2198; DOI 10.1021/es505003d.
- Lovley, D.R.; Phillips, E.J.P. Novel mode of microbial energy metabolism: Organic carbon oxidation coupled to dissimilatory reduction of iron or manganese. *Applied Env. Microbiol.*, **1988**, 54:1472-1480.
- Lovley, D.R.; Stolz, J.F.; Nord Jr., G.L.; Phillips, E.J.P. Anaerobic production of magnetite by a dissimilatory iron-reducing microorganism. *Nature*, **1987**, 330:252-254; DOI 10.1038/330252a0.
- McKeague, J.A.; Day, J.H. Dithionite- and oxalate-extractable Fe and Al as aids in differentiating various classes of soils. *Can. J. Soil Sci.*, **1966**, 46:13-22; DOI 10.4141/cjss66-003.
- McNear, D.H.; Chaney, R.L.; Sparks, D.L. The effects of soil type and chemical treatment on nickel speciation in refinery enriched soils: A multi-technique investigation. *Geochim. Cosmochim. Acta*, **2007**, 71(9):2190–2208; DOI 10.1016/j.gca.2007.02.006.
- Mehra, O.P.; Jackson, M.L. Iron oxide removal from soils and clays by a dithionite-citrate system buffered with sodium bicarbonate, In *Clays and Minerals*. Proceedings of the 7th National Congress: Pergamon, London, 1960.
- Mitsch, W. J.; Gosselink, J. G. *Wetlands*; John Wiley & Sons, Inc.: New York, 2000; p. 920.
- Mortimer, R.J.G.; Coleman, M.L. Microbial influence on the oxygen isotopic composition of diagenetic siderite. *Geochim. Cosmochim. Acta*, **1997**, 61:1705-1711; DOI 10.1016/S0016-7037(97)00027-6.
- Nachtegaal, M.; Marcus, M.A.; Sonke, J.E.; Vangronsveld, J.; Livi, K.J.T.; van der Lelie, D.; Sparks, D.L. Effects of in-situ remediation on the speciation and bioavailability of zinc in a smelter contaminated soil. *Geochim. Cosmochim. Acta*, **2005**, 69:4649–4664; DOI 10.1016/j.gca.2005.05.019.

- Nachtegaal, M.; Sparks, D.L. Nickel sequestration in a kaolinite-humic acid complex. *Environ. Sci. Technol.*, **2003**, 37(3):529-534; DOI 10.1021/es025803w.
- Nelson, D.W.; Sommers, L.E. Total carbon, organic carbon, and organic matter, In *Methods of Soil Analysis, Part 3: Chemical Methods*; Sparks, D.L., Ed.; American Society of Agronomy: Maddison, WI, 1996.
- Neupane, G.; Donahoe, R.J.; Arai, Y. Kinetics of competitive adsorption/desorption of arsenate and phosphate at the ferrihydrite-water interface. *Chem. Geol.*, **2014**, 368:31-38; DOI 10.1016/j.chemgeo.2013.12.020.
- Newbold, J. D.; Bott, R. L.; Kaplan L. A.; Sweeney, B. W.; Vannote, R. L. Organic matter dynamics in White Clay Creek, Pennsylvania, USA. *J. North Am. Benthol. Soc.*, **1997**, 16(1):46-50; DOI 10.2307/1468231.
- Nriagu, J. Stability of vivianite and ion-pair formation in the system $\text{Fe}_3(\text{PO}_4)_2\text{-H}_3\text{PO}_4\text{-H}_2\text{O}$. *Geochim. Cosmochim. Acta*, **1972**, 36:459-470; DOI 10.1016/0016-7037(72)90035-X.
- Nriagu, J.; Dell, C. Diagenetic formation of iron phosphates in recent lake sediments. *Am. Mineral.*, **1974**, 59:934-946.
- O'Day, P. A.; Rehr, J. J.; Zabinsky, S. I.; Brown, G. E. Extended X-ray absorption fine structure (EXAFS) analysis of disorder and multiple-scattering in complex crystalline solids. *J. Am. Chem. Soc.*, **1994**, 116:2938-2949, DOI 10.1021/ja00086a026.
- O'Loughlin, E.J.; Boyanov, M.I.; Flynn, T.M.; Gorski, C.A.; Hofmann, S.M.; McCormick, M.L; Scherer, M.M.; Kemner, K.M. Effects of bound phosphate on the bioreduction of lepidocrocite ($\gamma\text{-FeOOH}$) and maghemite ($\gamma\text{-Fe}_2\text{O}_3$) and formation of secondary minerals. *Environ. Sci. Technol.*, **2013**, 47:9157-9166; DOI 10.1021/es400627j.
- Parfitt, R.L.; Childs, C.W. Estimation of forms of Fe and Al: A review, and analysis of contrasting soils by dissolution and Moessbauer methods. *Aust. J. Soil Res.*, **1988**, 26:121-144; DOI 10.1071/SR9880121.
- Peltier, E.; Allada, R.; Navrotsky, A.; Sparks, D. L. Nickel solubility and precipitation in soils: A thermodynamic study. *Clay Clay Miner.* **2006**, 54(2):153-164; DOI 10.1346/CCMN.2006.0540202.
- Peltier, E.; Van Der Lelie, D.; Sparks, D.L. Formation and stability of Ni-Al hydroxide phases in soils. *Environ. Sci. Technol.*, **2010**, 44:302-308; DOI 10.1021/es902332b.

- Piccolo, A. The supramolecular structure of humic substances. *Soil Sci.* **2001**, 166(11):810–832; DOI 10.1097/00010694-200111000-00007.
- Ponnamperuma, F. N. The chemistry of submerged soils. *Adv. Agron.* **1972**, 24:29-96.
- Ravel, B.; Newville, M. Athena, Artemis, Hephaestus: Data analysis for X-ray absorption spectroscopy using IFEFFIT. *J. Synchrotron Radiation*, **2005**, 12:537-541; DOI 10.1107/S0909049505012719.
- Reddy, K.R.; DeLaune, R.D. *Biogeochemistry of Wetlands: Science and Applications*. Taylor & Francis Group, LLC: Boca Raton, 2008.
- Refait, P.; Abdelmoula, M.; Trolard, F.; Génin, J.M.R.; Ehrhardt, J.J.; Bourrié G. Mössbauer and XAS study of green rust mineral; the partial substitution of Fe²⁺ by Mg²⁺. *Am. Mineral.*, **2001**, 86:731-739; DOI 10.2138/am-2001-5-613.
- Roberts, D. R.; Scheidegger, A. M.; Sparks, D. L. Kinetics of mixed Ni-Al precipitate formation on a soil clay fraction. *Environ. Sci. Technol.*, **1999**, 33, 3749–3754; DOI 10.1021/es990235e.
- Roden, E.E.; Edmonds, J.W. Phosphate mobilization in iron-rich anaerobic sediments: Microbial Fe(III) oxide reduction versus iron-sulfide formation. *Arch. Hydrobiol.*, **1997**, 139:347-378.
- Roden, E.E.; Lovley, D.R. Dissimilatory Fe(III) reduction by the marine microorganism *Desulfuromonas acetoxidans*. *Applied Env. Microbiol.*, **1993**, 59:734-742.
- Rothe, M.; Frederichs, T.; Eder, M.; Kleeberg, A.; Hupfer, M. Evidence for vivianite formation and its contribution to long-term phosphorus retention in a recent lake sediment: A novel analytical approach. *Biogeosciences*, **2014**, 11:5169-5180; DOI 10.5194/bg-11-5169-2014.
- Scheinost, A.C.; Sparks, D.L. Formation of layered single- and double-metal hydroxides precipitates at the mineral/water interface: A multiple-scattering XAFS analysis. *J. Colloid Interface Sci.*, **2000**, 223:167-178, DOI 10.1006/jcis.1999.6638.
- Schwertmann, U. The differentiation of iron oxide in soils by a photochemical extraction with acid ammonium oxalate. *Z. Pflanzenernähr. Düng. Bodenkd.*, **1964**, 105:194-201.

- Shi, Z.; Peltier, E.; Sparks, D.L. Kinetics of Ni sorption in soils: Roles of soil organic matter and Ni precipitation. *Environ. Sci. Technol.*, **2012**, 46(4):2212-2219; DOI 10.1021/es202376c.
- Sims, J.T. Comparison of Mehlich 1 and Mehlich 3 extractants for P, K, Ca, Mg, Mn, Cu, and Zn in Atlantic coastal plain soils. *Commun. Soil Sci. Plan.*, **1989**, 20:17-18; DOI 10.1080/00103628909368178.
- Soil Survey Staff, Natural Resources Conservation Service, United States Department of Agriculture. 2014. Web Soil Survey. <http://websoilsurvey.nrcs.usda.gov/>. Accessed 6 May 2014.
- Sparks, D.L. *Environmental soil chemistry*, 2nd ed. Academic Press: San Diego, CA, 2003.
- Starcher, A.N.; Elzinga, E.J.; Kukkadapu, R.K.; Sparks, D.L. Evidence for the formation of Fe-layered hydroxides using spectroscopic techniques. 251st American Chemical Society National Meeting and Exposition, San Diego, CA, March 13-17, **2016**, poster presentation.
- Stumm, W.; Sulzberger, B. The cycling of iron in natural environments considerations based on laboratory studies of heterogeneous redox processes. *Geochim. Cosmochim. Acta*, **1992**, 56:3233-3257; DOI 10.1016/0016-7037(92)90301-X.
- Suzuki, S.; Shinoda, K.; Sato, M.; Fujimoto, S.; Yamashita, M.; Konishi, H.; Doi, T.; Kaminura, T.; Inoue, K.; Waseda, Y. Changes in chemical state and local structure of green rust by addition of copper sulphate ions. *Corros. Sci.*, **2008**, 50:1761-1765, DOI 10.1016/j.corsci.2008.02.022.
- Thoral, S.; Rose, J.; Garnier, J.M.; Van Geen, A.; Refait, P.; Traverse, A.; Fonda, E.; Nahon, D.; Bottero, J.Y. XAS study of iron and arsenic speciation during Fe(II) oxidation in the presence of As(III). *Environ. Sci. Technol.*, **2005**, 39:9478-9485, DOI 10.1021/es047970x.
- Trolard, F.; Génin, J.M.R.; Abdelmoula, M.; Bourrié, G.; Humbert, B.; Herbillon A. Identification of a green rust mineral in a reductomorphic soil by Mössbauer and Raman spectroscopies. *Geochim. Cosmochim. Acta*, **1997**, 61:1107-1111, DOI 10.1016/S0016-7037(96)00381-X.
- USEPA (U.S. Environmental Protection Agency). Method 3051A: Microwave Assisted Acid Digestion of Sediments, Sludges, Soils, and Oils. Washington, DC: USEPA, Office of Solid Waste, 2007.

- USEPA (U.S. Environmental Protection Agency). Method 6010C: Inductively Coupled Plasma-Atomic Emission Spectrometry. Washington, DC: USEPA, Office of Solid Waste, 2007.
- Violante, A.; Pigna, M. Competitive sorption of arsenate and phosphate on different clay minerals and soils. *Soil Sci. Soc. Am. J.*, **2002**, 66:1788-1796; DOI 10.2136/sssaj2002.1788.
- Von Tucher, S.; Schmidhalter, U. Lanthanum uptake from soil and nutrient solution and its effects on plant growth. *J. Plant Nutr. Soil Sci.*, **2005**, 168:574-580; DOI 10.1002/jpln.200520506.
- Walter, R. C.; Merritts, D. J. Natural streams and the legacy of water-powered mills. *Science*, **2008**, 319:299-304; DOI 10.1126/science.1151716.
- Whittig, L.D.; Allardice, W. R. X-ray diffraction techniques. In *Methods of Soil Analysis. Part 1 Physical and Mineralogical Methods*, 2nd ed.; A. Klute, Ed.; American Society of Agronomy, Madison, WI, 1986; pp. 331-362.
- Wilkin, R.T. Mineralogical preservation of solid samples collected from anoxic subsurface environments (EPA/600/R-06/112). USEPA (U.S. Environmental Protection Agency): Washington, D.C., 2006.
- Wolf, A.; Beegle, D. Recommended soil tests for macro and micronutrients, In *Recommended Soil Testing Procedures for the Northeastern United States*, 3rd ed. Northeast Regional Bulletin #493; Wolf, A. Ed.; p. 39-48; Agricultural Experiment Station, University of Delaware, Newark, DE, 2011.
- Wolthers, M.; Charlet, L.; Van Der Linde, P. R.; Rickard, D.; Van Der Weiden, C. H. Surface chemistry of disordered mackinawite (FeS). *Geochim. Cosmochim. Acta*, **2005**, 69:3469-3481; DOI 10.1016/j.gca.2005.01.027.
- Yu, K.; Rinklebe, J. Soil redox potential and pH controllers, In *Methods in Biogeochemistry of Wetlands*, DeLaune, R.D.; Reddy, K.R.; Richardson, C.J.; Megonigal, J.P., Eds. American Society of Agronomy: Madison, WI, 2013.
- Zachara, J.M.; Kukkadapu, R.K.; Fredrickson, J.K.; Gorby, Y.A.; Smith, S.C. Biomineralization of poorly crystalline Fe(III) oxides by dissimilatory metal reducing bacteria (DMRB). *Geomicrobiol. J.*, **2002**, 19:179-207; DOI 10.1080/01490450252864271.
- Zhu, Y.; Elzinga, E.J. Formation of layered Fe(II)-hydroxides during Fe(II) sorption onto clay and metal-oxide substrates. *Environ. Sci. Technol.*, **2014**, 48:4937-4945, DOI 10.1021/es500579p.

Zhu, Y.; Elzinga, E.J. Macroscopic and spectroscopic assessment of the cosorption of Fe(II) with As(III) and As(V) on Al-oxide. *Environ. Sci. Technol.*, **2015**, 49:13369-13377; DOI 10.1021/acs.est.5b04525.

Chapter 5

CONCLUSIONS, ENVIRONMENTAL IMPLICATIONS, AND FUTURE DIRECTIONS

5.1 Introduction

Previous studies have demonstrated Fe(II)-Al(III)-layered double hydroxide (LDH) phase formation from reactions of Al-oxides and phyllosilicates with Fe(II) in model geochemical systems (Elzinga, 2012; Zhu and Elzinga, 2014). This dissertation expands on the knowledge gained from those studies to show: 1) Fe(II)-Al(III)-LDH phase formation in the presence of Fe(III) and demonstrate the variability of Fe(II) phases that may form during sorption controlled by environmentally relevant factors; and 2) the formation of a mixed divalent metal layered hydroxide at conditions that are representative of those found in reducing natural environments (i.e. anoxic, circumneutral pH, environmentally relevant metal concentrations). This study also raises a series of questions to be examined further through systematic investigations and experiments on the environmental factors that can inhibit the formation of LDH phases in natural and laboratory systems.

5.2 Effects of Structural Fe(III) on Sorption Product

Chapter 2 of this dissertation examined the effects of structural Fe(III) presence in a phyllosilicate on Fe(II) sorption at circumneutral pH to determine impacts on LDH formation. This study demonstrated Fe(II)-Al-LDH formation in the systems examined and highlights the importance of coupling multiple analytical

techniques, such as X-ray absorption spectroscopy (XAS) and ^{57}Fe Mössbauer spectroscopy, to characterize sorption products formed. The net Fe(II) oxidation observed through Mössbauer spectroscopy, despite the absence of O_2 in the system, and the potential formation of a hybrid Fe(II)-Al(III)/Fe(III)-LDH phase merits further attention to elucidate the sorption mechanism. Further investigations of other Al-bearing minerals with higher Fe concentrations and a systematic study of aqueous Fe(III) concentrations on Fe(II) sorption should also be conducted to determine the effects of higher concentrations on LDH phase formation and to better understand their potential to form in the natural environment.

5.3 Effects of Sorbent Type

Results of Chapters 2 and 3 also discuss the importance of sorbent type on reaction products. Both studies demonstrate silica interlayer substitution at longer reaction times, which has been observed with the formation of other LDH phases (Ni, Zn, and Co) (Ford et al., 2001; Scheckel and Sparks, 2001; Scheckel et al., 2000). Such sorbents as Al-bearing oxides and phyllosilicates are ubiquitous in the environment and can release not only Al critical to the formation of LDH phases but also Si which has been shown to increase their stability (Li et al., 2012; Ford et al., 1999; Ford et al., 2001; Scheckel and Sparks, 2001; Scheckel et al., 2000; Scheidegger et al., 1998; Scheinost et al., 1999; Starcher et al., 2016; Zhu and Elzinga, 2014). The formation of Fe(II)-Al-LDH and Zn in inner-sphere complexation with $\gamma\text{-Al}_2\text{O}_3$ further iterates the importance of sorbent reactivity on LDH phase formation which has been demonstrated in other work (Li et al., 2012; Roberts et al., 2003). Understanding how these phases change with time in environmental systems is critical as these phases may

become more stable with aging due to Ostwald ripening and interlayer silication (Peltier et al., 2006).

5.4 Effects of Potentially Competing and Complexing Elements

Chapter 3 examined Fe/Zn co-sorption to an Al-oxide and a clay to better understand the importance of mixed divalent metal layered hydroxides in laboratory studies and natural systems and their abilities to affect the fate of contaminants in the natural environment, future research should examine the stability and dissolution of these phases as affected by changes in external conditions such as the impacts of: 1) sample aging; 2) acidification; and 3) changes in oxidation-reduction chemistry.

In Chapter 4, LDH phase formation was inhibited during the sorption of Fe released from the reductive dissolution of soils with different physicochemical properties. Low Fe concentrations in solution, lower pH, and high concentrations of C, P, S, Si, and OM are potential inhibitors of LDH phase formation. LDH phases are known to form in soils with circumneutral pH and sufficiently high concentrations of the divalent metal (McNear et al., 2007) and are typically more favorable phases over pure divalent metal hydroxide formation in phases that contain soluble aluminum (Allada et al., 2006; Peltier et al., 2006). However, sufficient thermodynamic data does not exist for comparisons of Fe(II)-Al-LDH phases with Fe(II) (oxy-hydr)oxides and should be examined in the future.

Future works should seek to understand the effects of potential inhibitors of Fe(II)-Al-LDH phase formation. OM has also been shown to inhibit the formation of other LDH phases (Nachtegaal, and Sparks, 2003; Peltier et al., 2010; Shi et al., 2012). In a recent study by Zhu and Elzinga (2015), high concentrations of As(V) were found to prevent Fe(II)-Al-LDH phase formation. The potential inhibition of Fe(II)-Al-LDH

phases by phosphate due to its similar reactivity to arsenate as well as the potential for vivianite formation in the presence of phosphates (Berner, 1981; Borch and Fendorf, 2007; Cui and Weng, 2013; Neupane et al., 2014; Nriagu, 1972; Nriagu and Dell, 1974; O'Loughlin et al., 2013; Roden and Edmonds, 1997; Violante and Pigna, 2002) make the examination of increasing phosphate concentrations on Fe(II)-Al-LDH formation an important study. Oxidation-reduction cycling is common in areas of flooding and periodic inundation, and Fe(II) is sensitive to oxidation. Understanding the redox effects on LDH stability and formation and potential links to green rust formation is also an important consideration (Starcher et al., 2016).

5.5 Conclusion

LDH phases form rapidly and extensively under conditions similar to those of riparian systems and are likely to occur in and impact Fe and trace metal geochemistry in such systems, having clear implications for the fate and speciation of Fe(II) in reducing geochemical environments. Determining the kinetics and thermodynamics of Fe(II)-Al-LDH and similar phases in the laboratory will lead to a better understanding of metal cycling in suboxic and anoxic geochemical systems. Future field investigations should look for soils with the following qualities: 1) circumneutral pH; 2) low concentrations of organic matter; 3) low concentrations of potentially inhibitive elements, such as As and P; and 4) sufficient Fe concentrations in forms that can undergo biotic reductive dissolution. Fully understanding Fe(II)-bearing mineral phases that may form in anoxic environments such as wetland soils is important due to the prevalence and reactivity of Fe phases in these environments.

REFERENCES

- Allada, R.K.; Peltier, E.; Navrotsky, A.; Casey, W.H.; Johnson, C.A.; Berbeco, H.T.; Sparks, D.L. Calorimetric determination of the enthalpies of formation of hydroxalite-like solids and their use in the geochemical modeling of metals in natural waters. *Clay Clay Miner.*, **2006**, 54(4):409–417; DOI 10.1346/CCMN.2006.0540401.
- Berner, R.A. A new geochemical classification of sedimentary environments. *J. Sediment. Res.*, **1981**, 51:359-365; DOI 10.1306/212F7C7F-2B24-11D7-8648000102C1865D.
- Borch, T.; Fendorf, S. Phosphate interactions with iron (hydr)oxides: Mineralization pathways and phosphorus retention upon bioreduction, In *Adsorption of Metals by Geomedia II: Variables, Mechanisms, and Model Applications*, Barnett, M.O; Kent, D.B, Eds. Elsevier: Amsterdam, NL, 2007.
- Cui, Y.; Weng, L. Arsenate and phosphate adsorption in relation to oxides composition in soils: LCD modeling. *Environ. Sci. Technol.*, **2013**, 47:7269-7276; DOI 10.1021/es400526q.
- Elzinga, E.J. Formation of layered Fe(II)-Al(III)-hydroxides during reaction of Fe(II) with aluminum oxide. *Environ. Sci. Tech.*, **2012**, 46:4894-4901; DOI 10.1021/es2044807.
- Ford, R.G.; Scheinost, A.C.; Scheckel, K.G.; Sparks, D.L. The link between clay mineral weathering and the stabilization of Ni surface precipitates. *Environ. Sci. Technol.* **1999**, 33(18):3140-3144, DOI 10.1021/es990271d.
- Ford, R.G.; Scheinost, A.C.; Sparks, D.L. Frontiers in metal sorption/precipitation mechanisms on soil mineral surfaces. *Advances in Agronomy*, **2001**, 74:41-62; DOI 10.1016/S0065-2113(01)74030-8.
- Li, W.; Livi, K.J.; Xu, W.; Siebecker, M.G.; Wang, Y.; Phillips, B.L.; Sparks, D.L. Formation of crystalline Zn-Al layered double hydroxide precipitates on γ -alumina: the role of mineral dissolution. *Environ. Sci. Technol.*, **2012**, 46(21):11670-11677, DOI 10.1021/es3018094.

- McNear, D.H.; Chaney, R.L.; Sparks, D.L. The effects of soil type and chemical treatment on nickel speciation in refinery enriched soils: A multi-technique investigation. *Geochim. Cosmochim. Acta*, **2007**, 71(9):2190–2208; DOI 10.1016/j.gca.2007.02.006.
- Nachtegaal, M.; Sparks, D.L. Nickel sequestration in a kaolinite-humic acid complex. *Environ. Sci. Technol.*, **2003**, 37(3):529-534; DOI 10.1021/es025803w.
- Neupane, G.; Donahoe, R.J.; Arai, Y. Kinetics of competitive adsorption/desorption of arsenate and phosphate at the ferrihydrite-water interface. *Chem. Geol.*, **2014**, 368:31-38; DOI 10.1016/j.chemgeo.2013.12.020.
- Nriagu, J. Stability of vivianite and ion-pair formation in the system $\text{Fe}_3(\text{PO}_4)_2\text{-H}_3\text{PO}_4\text{-H}_2\text{O}$. *Geochim. Cosmochim. Acta*, **1972**, 36:459-470; DOI 10.1016/0016-7037(72)90035-X.
- Nriagu, J.; Dell, C. Diagenetic formation of iron phosphates in recent lake sediments. *Am. Mineral.*, **1974**, 59:934-946.
- O'Loughlin, E.J.; Boyanov, M.I.; Flynn, T.M.; Gorski, C.A.; Hofmann, S.M.; McCormick, M.L.; Scherer, M.M.; Kemner, K.M. Effects of bound phosphate on the bioreduction of lepidocrocite ($\gamma\text{-FeOOH}$) and maghemite ($\gamma\text{-Fe}_2\text{O}_3$) and formation of secondary minerals. *Environ. Sci. Technol.*, **2013**, 47:9157-9166; DOI 10.1021/es400627j.
- Peltier, E.; Allada, R.; Navrotsky, A.; Sparks, D. L. Nickel solubility and precipitation in soils: A thermodynamic study. *Clay Clay Miner.* **2006**, 54(2):153–164; DOI 10.1346/CCMN.2006.0540202.
- Peltier, E.; Van Der Lelie, D.; Sparks, D.L. Formation and stability of Ni-Al hydroxide phases in soils. *Environ. Sci. Technol.*, **2010**, 44:302-308; DOI 10.1021/es902332b.
- Roberts, D.R.; Ford, R.G.; Sparks, D.L. Kinetics and mechanisms of Zn complexation on metal oxides using EXAFS spectroscopy. *J. Colloid Interface Sci.*, **2003**, 263:364-376; DOI 10.1016/S0021-9797(03)00281-9.
- Roden, E.E.; Edmonds, J.W. Phosphate mobilization in iron-rich anaerobic sediments: Microbial Fe(III) oxide reduction versus iron-sulfide formation. *Arch. Hydrobiol.*, **1997**, 139:347-378.

- Scheckel, K.G.; Scheinost, A.C.; Ford, R.G.; Sparks, D.L. Stability of layered Ni hydroxide surface precipitates: A dissolution kinetics study. *Geochim. Cosmochim. Acta*, **2000**, 64(16):2727–2735, DOI 10.1016/S0016-7037(00)00385-9.
- Scheckel, K.G.; Sparks, D.L. Dissolution kinetics of nickel surface precipitates on clay mineral and oxide surfaces. *Soil Sci. Soc. Am. J.*, **2001**, 65(3):685–694, DOI 10.2136/sssaj2001.653685x.
- Scheidegger, A.M.; Strawn, D.G.; Lamble, G.M.; Sparks, D.L. The kinetics of mixed Ni-Al hydroxide formation on clay and aluminum oxide minerals: a time-resolved XAFS study. *Geochim. Cosmochim. Acta*, **1998**, 62(13):2233-2245, DOI 10.1016/S0016-7037(98)00136-7.
- Scheinost, A.C.; Ford, R.G.; Sparks, D.L. The role of Al in the formation of secondary Ni precipitates on pyrophyllite, gibbsite, talc, and amorphous silica: A DRS study. *Geochim. Cosmochim. Acta*, **1999**, 63:3193-3203, DOI 10.1016/S0016-7037(99)00244-6.
- Shi, Z.; Peltier, E.; Sparks, D.L. Kinetics of Ni sorption in soils: Roles of soil organic matter and Ni precipitation. *Environ. Sci. Technol.*, **2012**, 46(4):2212-2219; DOI 10.1021/es202376c.
- Starcher, A.N.; Elzinga, E.J.; Kukkadapu, R.K.; Sparks, D.L. Evidence for the formation of Fe-layered hydroxides using spectroscopic techniques. 251st American Chemical Society National Meeting and Exposition, San Diego, CA, March 13-17, **2016**, poster presentation.
- Violante, A.; Pigna, M. Competitive sorption of arsenate and phosphate on different clay minerals and soils. *Soil Sci. Soc. Am. J.*, **2002**, 66:1788-1796; DOI 10.2136/sssaj2002.1788.
- Zhu, Y.; Elzinga, E.J. Formation of layered Fe(II)-hydroxides during Fe(II) sorption onto clay and metal-oxide substrates. *Environ. Sci. Technol.*, **2014**, 48:4937-4945, DOI 10.1021/es500579p.
- Zhu, Y.; Elzinga, E.J. Macroscopic and spectroscopic assessment of the cosorption of Fe(II) with As(III) and As(V) on Al-oxide. *Environ. Sci. Technol.*, **2015**, 49:13369-13377; DOI 10.1021/acs.est.5b04525.

Appendix A

SUPPORTING INFORMATION FROM CHAPTER 2

A.1 Pyrophyllite Preparation and Characterization

A.1.1 Clay Fractionation

Pyrophyllite was fractionated using centrifuge parameters calculated by Jackson (1985) and Gee and Or (2002). Briefly, the pyrophyllite was ground with a mortar and pestle and then ground dry in a porcelain ball mill with zirconia ball-shaped media. Separation of the zirconia media and the pyrophyllite was achieved using a plastic colander to prevent Fe contamination of the pyrophyllite. A slurry was then made with the ground pyrophyllite and DI water. The clay fraction ($<2\ \mu\text{m}$) was separated by centrifuging for 4 minutes at 1050 rpm. The supernatant containing the clay fraction was collected and centrifuged again for 20 minutes at 8080 rpm (10,000 g) to separate the clay fraction of pyrophyllite from the supernatant. The clay fraction was Na-saturated by rinsing in 0.5 M NaCl, sonicating for 1 minute, centrifuging at 10,000 g for 10 minutes, and discarding the supernatant. This procedure was completed in triplicate. The same procedure for Na-saturation was used with DI water to remove excess ions and was also completed in triplicate, and the Na-saturated pyrophyllite was then freeze-dried.

A.1.2 Iron Oxide Determination

Iron oxides were determined through the citrate-bicarbonate-dithionite method (Na-DCB) (Jackson et al., 1986; Loeppert and Inskeep, 1996; Mehra and Jackson, 1996). Briefly, 20 ml 0.3 M sodium citrate dehydrate and 2.5 ml 0.5 M sodium bicarbonate were each added to two centrifuge tubes containing 0.7 g pyrophyllite, and the slurries were raised to 80 °C in a water bath. Then 0.5 g sodium dithionite was added to each and reacted for 15 minutes, followed by centrifugation at 1600 rpm. A blank Na-DCB extractant was also prepared following the above procedure. The pyrophyllite Na-DCB extractants and blank were syringe-filtered with a 0.22 µm nitrocellulose filter membrane and analyzed at the University of Delaware Soil Testing Laboratory by inductively coupled plasma optical emission spectroscopy ICP-OES using a Thermo Elemental Intrepid II XSP Duo View (USEPA, 2007).

A.1.3 X-ray Diffraction Analysis

Pyrophyllite preparation for X-ray diffraction followed the methods by Jackson (1969) and Whittig and Allardice (1986). To Mg²⁺-saturate the pyrophyllite, a sample was sequentially washed in order with 2 M MgCl₂, 0.5 M Mg(OAc)₂, 0.5 M MgCl₂, 50% methanol, 95% methanol, and 95% acetone, repeating washings with 0.5 M Mg(OAc)₂, 0.5 M MgCl₂, and 95% acetone. K⁺-saturation was achieved by sequentially washing a pyrophyllite sample with 1 M KCl, 50% methanol, 95% methanol, and 95% acetone, performing the 1M KCl wash in triplicate and repeating the 95% acetone wash. After each washing, the samples were centrifuged at 1500 rpm for 5 minutes and the supernatants were discarded. Upon the completion of washings,

the Mg²⁺- and K⁺-saturated samples were allowed to air-dry prior to XRD analysis to achieve a random mounting orientation.

A.2 Accidental Oxidation

Although numerous precautions were taken to avoid accidental oxidation (strictly anoxic atmosphere during reaction time, transport, and analyses), Fe(III) was still found in the sorption products. Fe(III) presence in sorption products can be explained by several phenomena. First, it is possible that structural Fe(III) from pyrophyllite was released during mineral dissolution with Al and Si and was then incorporated into the sorption product during its formation. Second, electron transfer may have occurred between the structural Fe(III) still within the pyrophyllite and sorbed Fe(II) (Merola et al., 2007; Schaefer et al., 2011). Finally, surface-sorption-induced electron transfer has also been observed in anoxic systems between the mineral surface and sorbed Fe(II) (Géhin et al., 2007). The latter phenomena explains the Fe(III) concentrations in the sorption samples that are higher than expected from calculations with initial Fe(III) concentrations from pyrophyllite.

It is unlikely that accidental oxidation occurred as a result of reaction conditions or transportation environment. An Fe^{II}-Zn- γ -Al₂O₃ sorption sample for a separate study was prepared, transported, and examined by XAS at the same time as the sorption samples. This sample was stored out of the glovebox for 44 h prior to XAS data collection under the preservation conditions described above in the main text methods section. This sample had no initial Fe(III), as there was no Fe(III) was present at the start of the reaction, unlike the pyrophyllite sorption samples which contained structural Fe(III) within the mineral. This sample was shown through a

LCF of its $k^3 \cdot \chi$ function to not have become oxidized as a result of this treatment (Figure A3).

It is also unlikely that sorption samples contain Fe(III) as a result of accidental oxidation during spectroscopic analysis. Figure A.4 shows the near-edge Fe K edge XAS spectra for the first and tenth (last) scans of the Fe(II)-pyrophyllite sorption sample at 30 minutes of reaction time. There is no drift observed to higher energies for the last scan, which would be indicative of oxidation (Elzinga, 2012).

Table A.1: Modeled 77 K Mössbauer spectral parameters

Sample	Site	<CS>¹ mm/s	<QS>² mm/s	σ_{QSD}³ mm/s	Percent contribution⁴
3 mM Fe(II)/28d	Fe(III)	0.51	0.604	0.26	15
	Fe(II)	1.27	2.65	0.71	85
Fe(II)-Al-LDH std	Fe(II)	1.26	2.88	0.2	77
	Fe(II)	1.24	2.34	1.9	33
Green Rust std	Fe(III)	0.54	0.45	0.2	36
	Fe(II)	1.27	3.02	0.18	75

¹ average center shift; ² average quadrupole splitting parameter; ³ std dev of QS; ⁴ relative % contribution; Lorentzian half-width at half maximum = 0.097 mm/sec

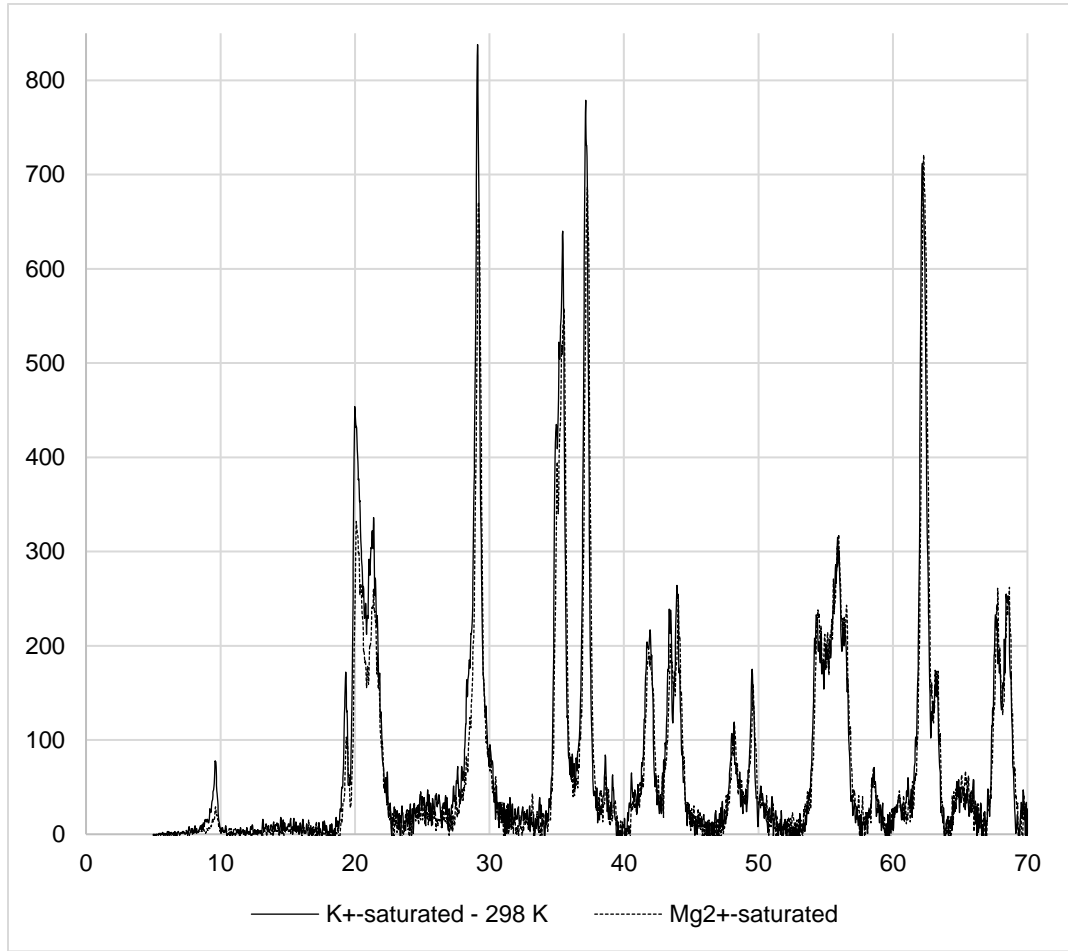


Figure A.1: Powder X-ray diffraction data of K⁺- (solid line) and Mg²⁺-saturated (dashed line) pyrophyllite at 298 K.

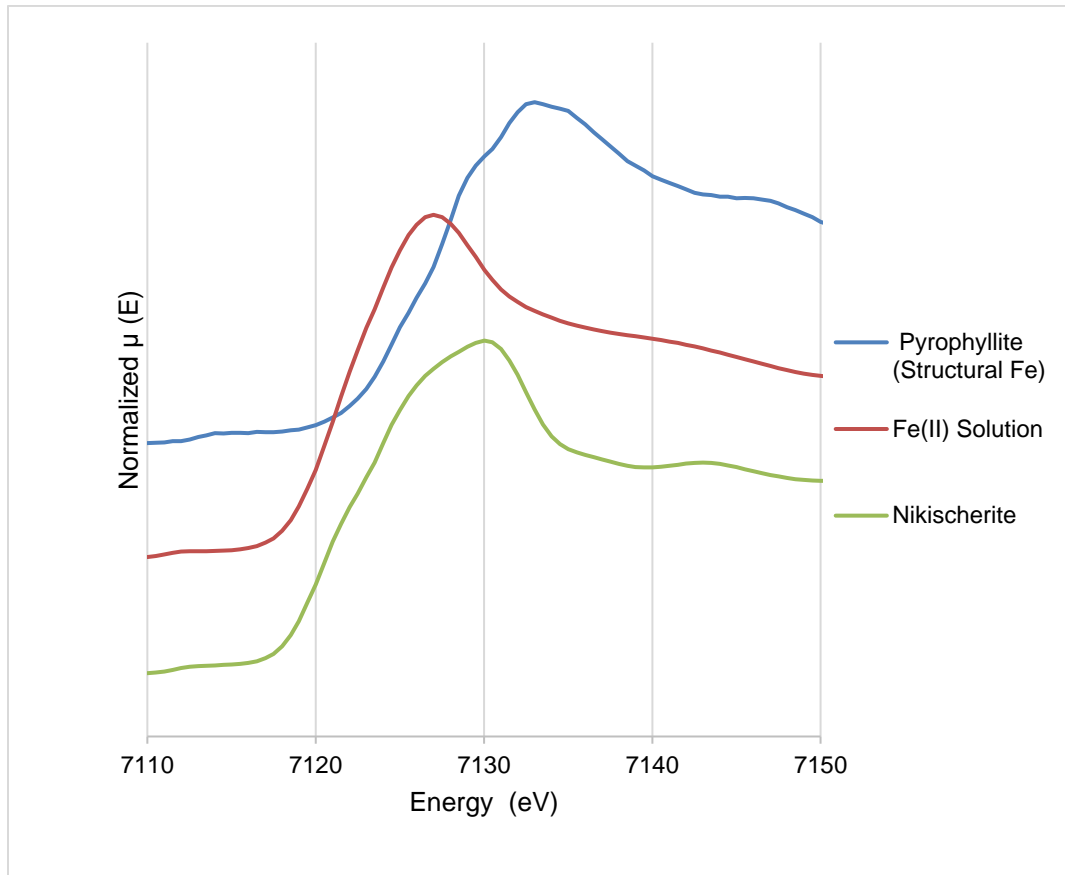


Figure A.2: Near-edge Fe *K* edge XAS spectra of pyrophyllite (with structural Fe(III)) and the Fe(II) standards Fe(II) solution and nikischerite (an Fe(II)-Al(III)-LDH).

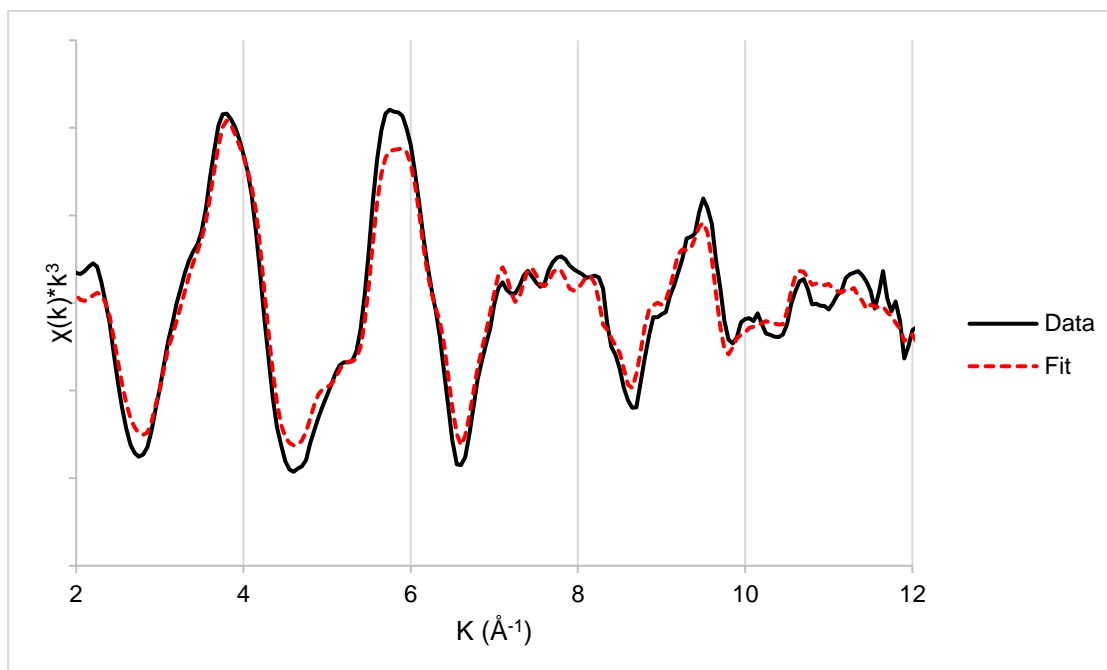


Figure A.3: Fe K edge EXAFS raw $k^3 \cdot \chi$ function of 4 week Fe(II)-Zn- γ - Al_2O_3 co-sorption sample (solid black line) and its corresponding linear combination fit (dashed red line). The LCF was performed on a k region of 3 to 10 \AA^{-1} , and yielded an R-factor of 0.0440. Standards used in fit contain no Fe(III).

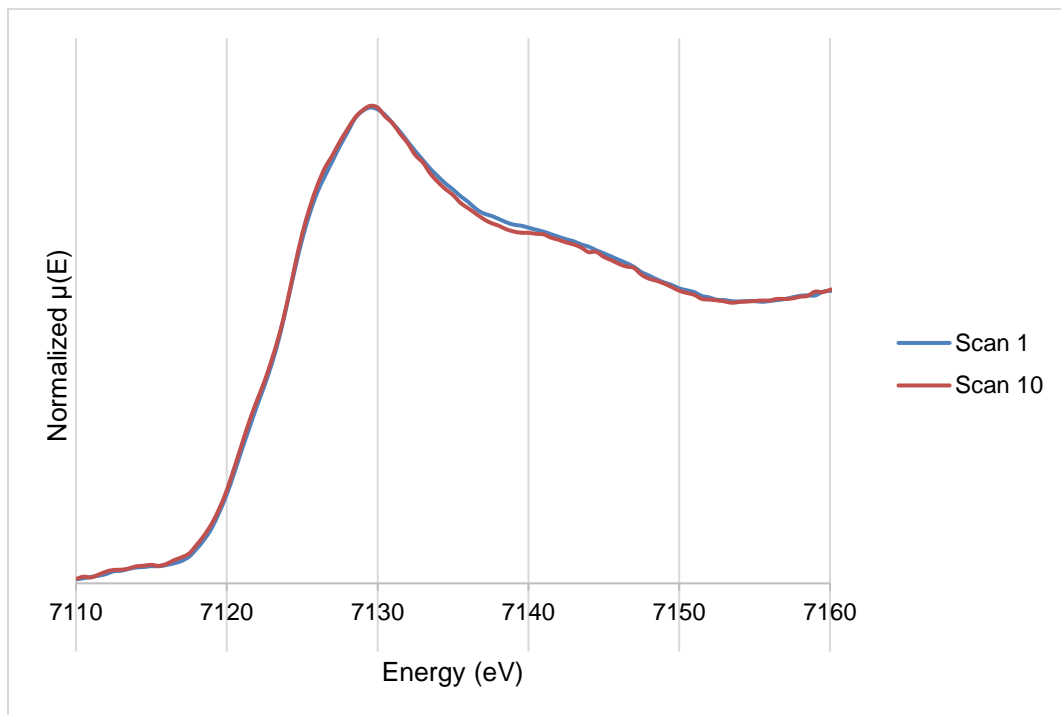


Figure A.4: Near-edge Fe *K* edge XAS spectra for the first and last (tenth) scans of Fe(II) sorption reaction with pyrophyllite at 30 minutes sample time.

Table A.2: Results of principal component analysis performed by SixPack with the bulk-EXAFS k^3 -weighted χ functions of Fe sorption reactions with pyrophyllite for 30 minutes to 4 weeks of reaction time.

Component	Eigenvalue	Variance	Cumulative Variance	IND*
1	70.781	0.591	0.591	0.48287
2	22.639	0.189	0.781	0.45940
3	11.497	0.096	0.877	0.58769
4	7.685	0.064	0.941	0.88157
5	4.025	0.033	0.975	2.94349
6	2.943	0.024	1	NA

*Empirical indicator function

Table A.3: Target transformation SPOIL values of selected standard spectra obtained by SixPack PCA with EXAFS spectra of Fe sorption reactions with pyrophyllite. SPOIL values indicate the following fits: <1.5 is excellent, 1.5-3 is good, 3-4.5 is fair, 4.5-6 is poor, and >6 is unacceptable (Malinowski, 1978).

References	SPOIL Values
2-line ferrihydrite	1.4552
Fe-phyllosilicate	11.0693
FeCl ₂ aqueous solution	2.5705
Goethite	2.1950
Hematite	2.0736
Hydroxychloride green rust (GR-Cl)	2.1443
Lepidocrocite	3.7704
Magnetite	4.8440
Nikischerite	2.2115
Pyrophyllite (with structural Fe(III))	0.7731
White Rust	3.2316

Table A.4: Fit parameters determined from linear combination fits of Fe-pyrophyllite sorption samples from 3-11 Å⁻¹. Fits were only included if they improved the R-factor or reduced chi square by 20% (Singh and Grafe, 2010).

Sample	R-factor^a	Standards	Weight
<hr/>			
3 mM Fe(II)			
28 d	0.0781	Nikischerite	0.964
		Pyrophyllite	0.036
7 d	0.0934	Nikischerite	0.923
		Pyrophyllite	0.077
1 d	0.1448	Nikischerite	0.754
		Pyrophyllite	0.246
4 h	0.1683	Nikischerite	0.647
		Pyrophyllite	0.353
1 h	0.1438	Nikischerite	0.663
		Pyrophyllite	0.337
0.5 h	0.1001	Nikischerite	0.618
		Pyrophyllite	0.382
<hr/>			
0.8 mM Fe(II)			
28 d	0.0786	Nikischerite	0.878
		Pyrophyllite	0.122
7 d	0.1827	Nikischerite	0.693
		Fe-phyllosilicate	0.307

^a*R-factor* is the absolute misfit between the data and theory as defined by Athena

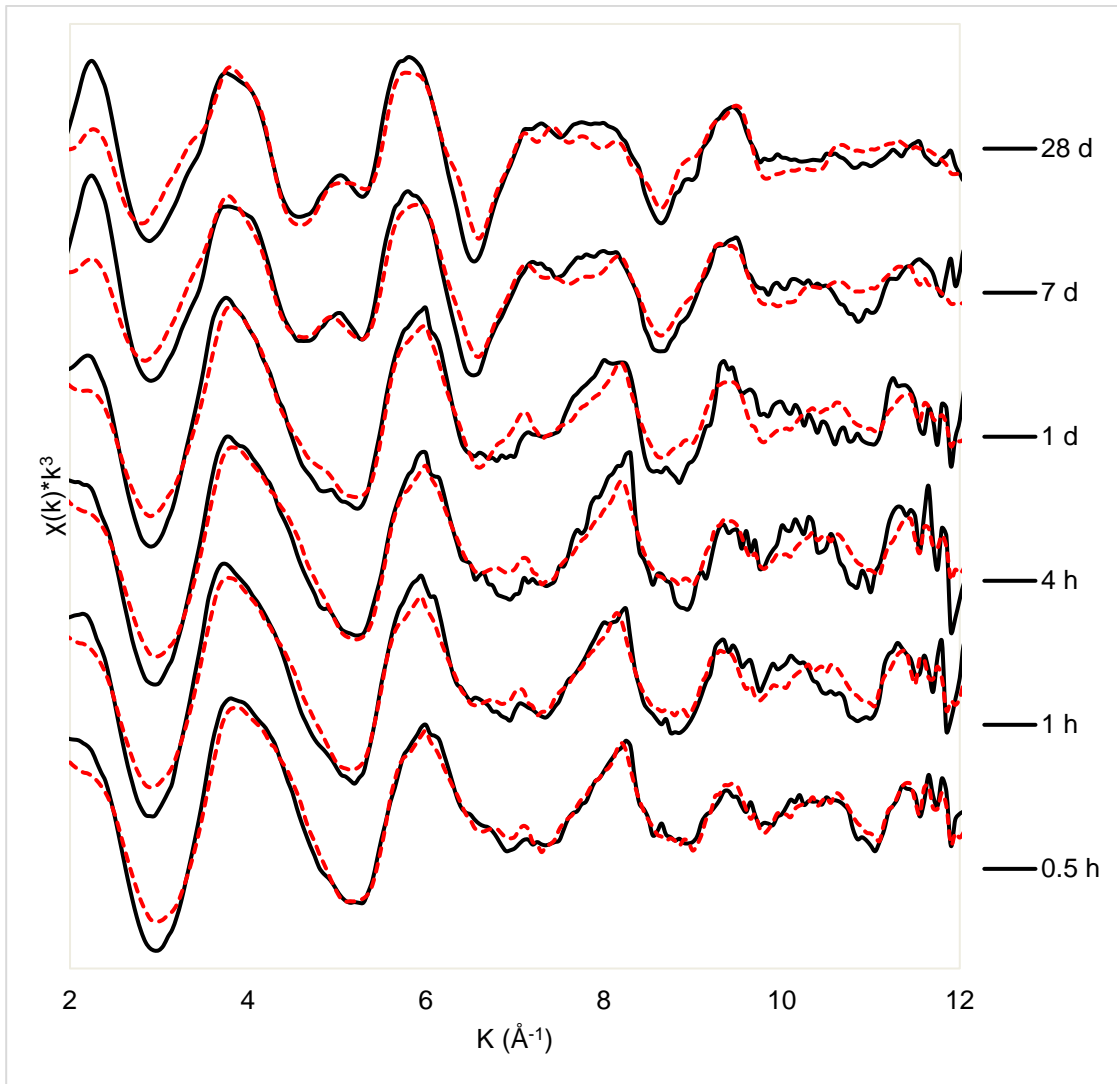


Figure A.5: Fe K edge EXAFS raw $k^3 \cdot \chi$ functions of 3 mM Fe-pyrophyllite sorption samples (solid black lines) and their corresponding linear combination fits (dashed red lines).

REFERENCES

- Elzinga, E.J. Formation of layered Fe(II)-Al(III)-hydroxides during reaction of Fe(II) with aluminum oxide. *Environ. Sci. Tech.*, **2012**, 46:4894-4901; DOI 10.1021/es2044807.
- Gee, G.W.; Or, D. Particle-size analysis, In *Methods of Soil Analysis, Part 4 Physical Methods*, Dane, C., Ed. Soil Science Society of America Book Series: Madison, Wisconsin, USA, 2002.
- Géhin, A.; Grenèche, J.-M.; Tournassat, C.; Brendlé, J.; Rancourt, D.G.; Charlet, L. Reversible surface-sorption-induced electron-transfer oxidation of Fe(II) at reactive sites on a synthetic clay mineral. *Geochim. Cosmochim. Acta*, **2007**, 71:863-876; DOI 10.1016/j.gca.2006.10.019.
- Jackson, M.L. *Soil chemical analysis – Advanced course*. University of Wisconsin, Madison, WI, 1969.
- Jackson, M.L. *Soil chemical analysis - Advanced course*. 2nd ed. University of Wisconsin, Madison, WI, 1985.
- Jackson, M.L.; Lim, C.H.; Zelazny, L.W. Oxides, hydroxides, and aluminosilicates. In *Methods of Soil Analysis. Part 1 Physical and Mineralogical Chemical Methods*, 2nd ed.; A. Klute, Ed.; American Society of Agronomy, Madison, WI, 1986; pp. 101-150.
- Loeppert, R.H.; Inskeep, W.P. Iron. In *Methods of Soil Analysis. Part 3 Chemical Methods*; D.L. Sparks, Ed.; American Society of Agronomy, Madison, WI, 1996; pp. 639-664.
- Malinowski, E.R. Theory of error for target factor analysis with applications to mass spectrometry and nuclear magnetic resonance spectrometry. *Anal. Chim. Acta*, **1978**, 103:339-354; DOI 10.1016/S0003-2670(00)00088-X.
- Mehra, O.P.; Jackson, M.L. Iron oxide removal from soils and clays by a dithionite-citrate system buffered with sodium bicarbonate. In *Clays and Minerals. Proceedings of the 7th National Congress*; Pergamon, London, 1996.

- Merola, R.B.; Fournier, E.D.; McGuire, M.M. Spectroscopic investigations of Fe²⁺ complexation on nontronite clay. *Langmuir*, **2007**, 23:1223-1226; DOI 10.1021/la062467e.
- Schaefer, M.V.; Gorski, C.A.; Scherer, M.M. Spectroscopic evidence for interfacial Fe(II)-Fe(III) electron transfer in a clay mineral. *Environ. Sci. Technol.*, **2011**, 45:540-545, DOI 10.1021/es102560m.
- Singh, B.; Grafe, M. *Synchrotron-based techniques in soils and sediments*, Elsevier: Amsterdam, NL, 2010.
- USEPA (U.S. Environmental Protection Agency). Method 6010C: Inductively Coupled Plasma-Atomic Emission Spectrometry. Washington, DC: USEPA, Office of Solid Waste, 2007.
- Whittig, L.D.; Allardice, W. R. X-ray diffraction techniques. In *Methods of Soil Analysis. Part 1 Physical and Mineralogical Methods*, 2nd ed.; A. Klute, Ed.; American Society of Agronomy, Madison, WI, 1986; pp. 331-362.

Appendix B

PERMISSIONS

ELSEVIER LICENSE TERMS AND CONDITIONS

Jul 18, 2016

This Agreement between Autumn N Starcher ("You") and Elsevier ("Elsevier") consists of your license details and the terms and conditions provided by Elsevier and Copyright Clearance Center.

License Number	3912070130349
License date	Jul 18, 2016
Licensed Content Publisher	Elsevier
Licensed Content Publication	Chemical Geology
Licensed Content Title	Fe(II) sorption on pyrophyllite: Effect of structural Fe(III) (impurity) in pyrophyllite on nature of layered double hydroxide (LDH) secondary mineral formation
Licensed Content Author	Autumn N. Starcher, Wei Li, Ravi K. Kukkadapu, Evert J. Elzinga, Donald L. Sparks
Licensed Content Date	7 November 2016
Licensed Content Volume Number	439
Licensed Content Issue Number	n/a
Licensed Content Pages	9
Start Page	152
End Page	160
Type of Use	reuse in a thesis/dissertation
Portion	full article
Format	both print and electronic
Are you the author of this Elsevier article?	Yes
Will you be translating?	No

Order reference number	
Title of your thesis/dissertation	Environmental Factors Impacting the Formation and Kinetics of Fe(II) Layered Hydroxides on Minerals and Soils
Expected completion date	Jul 2016
Estimated size (number of pages)	194
Elsevier VAT number	GB 494 6272 12
Requestor Location	Autumn N Starcher ISE Building 221 Academy Street 465 - AR NEWARK, DE 19716 United States Attn: Autumn N Starcher
Total	0.00 USD
Terms and Conditions	

INTRODUCTION

1. The publisher for this copyrighted material is Elsevier. By clicking "accept" in connection with completing this licensing transaction, you agree that the following terms and conditions apply to this transaction (along with the Billing and Payment terms and conditions established by Copyright Clearance Center, Inc. ("CCC"), at the time that you opened your Rightslink account and that are available at any time at <http://myaccount.copyright.com>).

GENERAL TERMS

2. Elsevier hereby grants you permission to reproduce the aforementioned material subject to the terms and conditions indicated.

3. Acknowledgement: If any part of the material to be used (for example, figures) has appeared in our publication with credit or acknowledgement to another source, permission must also be sought from that source. If such permission is not obtained then that material may not be included in your publication/copies. Suitable acknowledgement to the source must be made, either as a footnote or in a reference list at the end of your publication, as follows:

"Reprinted from Publication title, Vol /edition number, Author(s), Title of article / title of chapter, Pages No., Copyright (Year), with permission from Elsevier [OR APPLICABLE SOCIETY COPYRIGHT OWNER]." Also Lancet special credit - "Reprinted from The Lancet, Vol. number, Author(s), Title of article, Pages No., Copyright (Year), with

permission from Elsevier."

4. Reproduction of this material is confined to the purpose and/or media for which permission is hereby given.

5. Altering/Modifying Material: Not Permitted. However figures and illustrations may be altered/adapted minimally to serve your work. Any other abbreviations, additions, deletions and/or any other alterations shall be made only with prior written authorization of Elsevier Ltd. (Please contact Elsevier at permissions@elsevier.com)

6. If the permission fee for the requested use of our material is waived in this instance, please be advised that your future requests for Elsevier materials may attract a fee.

7. Reservation of Rights: Publisher reserves all rights not specifically granted in the combination of (i) the license details provided by you and accepted in the course of this licensing transaction, (ii) these terms and conditions and (iii) CCC's Billing and Payment terms and conditions.

8. License Contingent Upon Payment: While you may exercise the rights licensed immediately upon issuance of the license at the end of the licensing process for the transaction, provided that you have disclosed complete and accurate details of your proposed use, no license is finally effective unless and until full payment is received from you (either by publisher or by CCC) as provided in CCC's Billing and Payment terms and conditions. If full payment is not received on a timely basis, then any license preliminarily granted shall be deemed automatically revoked and shall be void as if never granted. Further, in the event that you breach any of these terms and conditions or any of CCC's Billing and Payment terms and conditions, the license is automatically revoked and shall be void as if never granted. Use of materials as described in a revoked license, as well as any use of the materials beyond the scope of an unrevoked license, may constitute copyright infringement and publisher reserves the right to take any and all action to protect its copyright in the materials.

9. Warranties: Publisher makes no representations or warranties with respect to the licensed material.

10. Indemnity: You hereby indemnify and agree to hold harmless publisher and CCC, and their respective officers, directors, employees and agents, from and against any and all claims arising out of your use of the licensed material other than as specifically authorized pursuant to this license.

11. No Transfer of License: This license is personal to you and may not be sublicensed, assigned, or transferred by you to any other person without publisher's written permission.

12. No Amendment Except in Writing: This license may not be amended except in a writing signed by both parties (or, in the case of publisher, by CCC on publisher's behalf).

13. Objection to Contrary Terms: Publisher hereby objects to any terms contained in any purchase order, acknowledgment, check endorsement or other writing prepared by you, which terms are inconsistent with these terms and conditions or CCC's Billing and Payment terms and conditions. These terms and conditions, together with CCC's Billing and Payment terms and conditions (which are incorporated herein), comprise the entire agreement between you and publisher (and CCC) concerning this licensing transaction. In the event of any conflict between your obligations established by these terms and conditions and those established by CCC's Billing and Payment terms and conditions, these terms and conditions shall control.

14. Revocation: Elsevier or Copyright Clearance Center may deny the permissions described in this License at their sole discretion, for any reason or no reason, with a full refund payable to you. Notice of such denial will be made using the contact information provided by you. Failure to receive such notice will not alter or invalidate the denial. In no event will Elsevier or Copyright Clearance Center be responsible or liable for any costs, expenses or damage incurred by you as a result of a denial of your permission request, other than a refund of the amount(s) paid by you to Elsevier and/or Copyright Clearance Center for denied permissions.

LIMITED LICENSE

The following terms and conditions apply only to specific license types:

15. **Translation:** This permission is granted for non-exclusive world **English** rights only unless your license was granted for translation rights. If you licensed translation rights you may only translate this content into the languages you requested. A professional translator must perform all translations and reproduce the content word for word preserving the integrity of the article.

16. **Posting licensed content on any Website:** The following terms and conditions apply as follows: Licensing material from an Elsevier journal: All content posted to the web site must maintain the copyright information line on the bottom of each image; A hyper-text must be included to the Homepage of the journal from which you are licensing at <http://www.sciencedirect.com/science/journal/xxxxx> or the Elsevier homepage for books at <http://www.elsevier.com>; Central Storage: This license does not include permission for a scanned version of the material to be stored in a central repository such as that provided by Heron/XanEdu.

Licensing material from an Elsevier book: A hyper-text link must be included to the Elsevier homepage at <http://www.elsevier.com> . All content posted to the web site must

maintain the copyright information line on the bottom of each image.

Posting licensed content on Electronic reserve: In addition to the above the following clauses are applicable: The web site must be password-protected and made available only to bona fide students registered on a relevant course. This permission is granted for 1 year only. You may obtain a new license for future website posting.

17. For journal authors: the following clauses are applicable in addition to the above:

Preprints:

A preprint is an author's own write-up of research results and analysis, it has not been peer-reviewed, nor has it had any other value added to it by a publisher (such as formatting, copyright, technical enhancement etc.).

Authors can share their preprints anywhere at any time. Preprints should not be added to or enhanced in any way in order to appear more like, or to substitute for, the final versions of articles however authors can update their preprints on arXiv or RePEc with their Accepted Author Manuscript (see below).

If accepted for publication, we encourage authors to link from the preprint to their formal publication via its DOI. Millions of researchers have access to the formal publications on ScienceDirect, and so links will help users to find, access, cite and use the best available version. Please note that Cell Press, The Lancet and some society-owned have different preprint policies. Information on these policies is available on the journal homepage.

Accepted Author Manuscripts: An accepted author manuscript is the manuscript of an article that has been accepted for publication and which typically includes author-incorporated changes suggested during submission, peer review and editor-author communications.

Authors can share their accepted author manuscript:

- – immediately
 - via their non-commercial person homepage or blog
 - by updating a preprint in arXiv or RePEc with the accepted manuscript
 - via their research institute or institutional repository for internal institutional uses or as part of an invitation-only research collaboration work-group
 - directly by providing copies to their students or to research

- collaborators for their personal use
 - for private scholarly sharing as part of an invitation-only work group on commercial sites with which Elsevier has an agreement
 - – after the embargo period
 - via non-commercial hosting platforms such as their institutional repository
 - via commercial sites with which Elsevier has an agreement

In all cases accepted manuscripts should:

- – link to the formal publication via its DOI
- – bear a CC-BY-NC-ND license - this is easy to do
- – if aggregated with other manuscripts, for example in a repository or other site, be shared in alignment with our hosting policy not be added to or enhanced in any way to appear more like, or to substitute for, the published journal article.

Published journal article (JPA): A published journal article (PJA) is the definitive final record of published research that appears or will appear in the journal and embodies all value-adding publishing activities including peer review co-ordination, copy-editing, formatting, (if relevant) pagination and online enrichment.

Policies for sharing publishing journal articles differ for subscription and gold open access articles:

Subscription Articles: If you are an author, please share a link to your article rather than the full-text. Millions of researchers have access to the formal publications on ScienceDirect, and so links will help your users to find, access, cite, and use the best available version.

Theses and dissertations which contain embedded PJAs as part of the formal submission can be posted publicly by the awarding institution with DOI links back to the formal publications on ScienceDirect.

If you are affiliated with a library that subscribes to ScienceDirect you have additional private sharing rights for others' research accessed under that agreement. This includes use for classroom teaching and internal training at the institution (including use in course packs and courseware programs), and inclusion of the article for grant funding purposes.

Gold Open Access Articles: May be shared according to the author-selected end-user license and should contain a [CrossMark logo](#), the end user license, and a DOI link to the formal publication on ScienceDirect.

Please refer to Elsevier's [posting policy](#) for further information.

18. **For book authors** the following clauses are applicable in addition to the above: Authors are permitted to place a brief summary of their work online only. You are not allowed to download and post the published electronic version of your chapter, nor may you scan the printed edition to create an electronic version. **Posting to a repository:** Authors are permitted to post a summary of their chapter only in their institution's repository.

19. **Thesis/Dissertation:** If your license is for use in a thesis/dissertation your thesis may be submitted to your institution in either print or electronic form. Should your thesis be published commercially, please reapply for permission. These requirements include permission for the Library and Archives of Canada to supply single copies, on demand, of the complete thesis and include permission for Proquest/UMI to supply single copies, on demand, of the complete thesis. Should your thesis be published commercially, please reapply for permission. Theses and dissertations which contain embedded PJAs as part of the formal submission can be posted publicly by the awarding institution with DOI links back to the formal publications on ScienceDirect.

Elsevier Open Access Terms and Conditions

You can publish open access with Elsevier in hundreds of open access journals or in nearly 2000 established subscription journals that support open access publishing. Permitted third party re-use of these open access articles is defined by the author's choice of Creative Commons user license. See our [open access license policy](#) for more information.

Terms & Conditions applicable to all Open Access articles published with Elsevier:

Any reuse of the article must not represent the author as endorsing the adaptation of the article nor should the article be modified in such a way as to damage the author's honour or reputation. If any changes have been made, such changes must be clearly indicated.

The author(s) must be appropriately credited and we ask that you include the end user license and a DOI link to the formal publication on ScienceDirect.

If any part of the material to be used (for example, figures) has appeared in our publication with credit or acknowledgement to another source it is the responsibility of the user to ensure their reuse complies with the terms and conditions determined by the rights holder.

Additional Terms & Conditions applicable to each Creative Commons user license:

CC BY: The CC-BY license allows users to copy, to create extracts, abstracts and new

works from the Article, to alter and revise the Article and to make commercial use of the Article (including reuse and/or resale of the Article by commercial entities), provided the user gives appropriate credit (with a link to the formal publication through the relevant DOI), provides a link to the license, indicates if changes were made and the licensor is not represented as endorsing the use made of the work. The full details of the license are available at <http://creativecommons.org/licenses/by/4.0>.

CC BY NC SA: The CC BY-NC-SA license allows users to copy, to create extracts, abstracts and new works from the Article, to alter and revise the Article, provided this is not done for commercial purposes, and that the user gives appropriate credit (with a link to the formal publication through the relevant DOI), provides a link to the license, indicates if changes were made and the licensor is not represented as endorsing the use made of the work. Further, any new works must be made available on the same conditions. The full details of the license are available at <http://creativecommons.org/licenses/by-nc-sa/4.0>.

CC BY NC ND: The CC BY-NC-ND license allows users to copy and distribute the Article, provided this is not done for commercial purposes and further does not permit distribution of the Article if it is changed or edited in any way, and provided the user gives appropriate credit (with a link to the formal publication through the relevant DOI), provides a link to the license, and that the licensor is not represented as endorsing the use made of the work. The full details of the license are available at <http://creativecommons.org/licenses/by-nc-nd/4.0>. Any commercial reuse of Open Access articles published with a CC BY NC SA or CC BY NC ND license requires permission from Elsevier and will be subject to a fee.

Commercial reuse includes:

- – Associating advertising with the full text of the Article
- – Charging fees for document delivery or access
- – Article aggregation
- – Systematic distribution via e-mail lists or share buttons

Posting or linking by commercial companies for use by customers of those companies.

20. Other Conditions:

v1.8

Questions? customer care@copyright.com or +1-855-239-3415 (toll free in the US) or +1-978-646-2777.

Appendix C

SUPPORTING INFORMATION FROM CHAPTER 4

C.1 Chemical Treatments to Determine Principal Forms of Soil Fe

Soil total “free” iron oxides were determined using the citrate-bicarbonate-dithionite method (Na-DCB) (Jackson et al., 1986; Loeppert and Inskeep, 1996; Mehra and Jackson, 1960). Briefly 2.5 g of <74 μm soil (passed through 200-mesh sieve) were reacted with 20 mL 0.3 M sodium citrate and 2.5 mL 1 M NaHCO_3 in a water bath 75-80°C for several minutes. Once the reaction temperature had equilibrated to 75-80 °C, 0.5 g $\text{Na}_2\text{S}_2\text{O}_4$ powder was added, and stirred over a 6-min period. Then a second 0.5-g portion of $\text{Na}_2\text{S}_2\text{O}_4$ powder was added to the vessel and intermittently stirred for 10 minutes. Upon the digestion completion, 5 mL saturated NaCl was added for flocculation, and the solution was centrifuged for 5 min at 2000 rpm. The supernatant was decanted and analyzed by ICP-OES at the University of Delaware Soil Testing Laboratory (USEPA, 2007).

Soil “active” or “amorphous” iron oxides were determined using the acid ammonium oxalate in darkness or Tamm’s reagent method (Schwertmann, 1964; McKeague and Day, 1966; Loeppert and Inskeep, 1996). Briefly, 50 mL of acidified 0.175 M ammonium oxalate and 0.1 M oxalic acid solution (pH 3.0) were added to 2.0 g of <200 μm composite soil from each sample site in a 50-mL centrifuge tube covered with foil. A light-proof container is used to prevent photoinduced oxalate decomposition and subsequent Fe oxide precipitation (Borggaard, 1988). The centrifuge tubes were then placed on a rotator, and after 2 h of reaction time, the

samples were centrifuged for 10 min at 10,000 g. The supernatant was syringe-filtered with a 0.22 μm nitrocellulose filter before being analyzed with ICP-OES by the University of Delaware Soil Testing Laboratory (USEPA, 2007).

C.2 Saturation Procedures for X-Ray Diffraction Analysis

The treated composite soil samples were separated into fractions sand/silt (>2 μm) and clay (<2 μm). The clay fractions were Mg^{2+} - and K^+ -saturated (Jackson, 1969; Whittig and Allardice, 1986). To Mg^{2+} -saturate the soil samples, samples were washed in order with 2 M MgCl_2 , 0.5 M $\text{Mg}(\text{OAc})_2$, 0.5 M MgCl_2 , 50% methanol, 95% methanol, and 95% acetone, repeating washings with 0.5 M $\text{Mg}(\text{OAc})_2$, 0.5 M MgCl_2 , and 95% acetone. K^+ -saturation was achieved by sequentially washing a pyrophyllite sample with 1 M KCl , 50% methanol, 95% methanol, and 95% acetone, performing the 1M KCl wash in triplicate and repeating the 95% acetone wash. After each washing, the samples were centrifuged at 1500 rpm for 5 minutes to separate the solids and the final Mg^{2+} - and K^+ -saturated samples were air-dried prior to XRD analysis to achieve a random mounting orientation.

C.3 Site Descriptions

From the GPS coordinates of the various sample points, the soil series of both sites at GCS were determined through the USDA Web Soil Survey to be combinations of Askecksy loamy sand (0-2% slopes) and Manahawkin muck (frequently flooded) (USDA Soil Survey Staff, 2014). The typical profile of Askecky loamy sand (0-2% slopes) is Oe - 0 to 3 inches: strongly acid, moderately decomposed plant material; A - 3 to 8 inches: strongly acid, loamy sand; Bg - 8 to 21 inches: strongly acid, loamy sand; Cg1 - 21 to 29 inches: extremely acid, sand; Cg2 - 29 to 80 inches: extremely

acid, sand (USDA Soil Survey Staff, 2014). The typical profile of Manahawkin muck (frequently flooded) is Oa1 - 0 to 8 inches: strongly acid, muck; Oa2 - 8 to 40 inches: extremely acid, muck, Cg - 40 to 80 inches: very strongly acid, sand (USDA Soil Survey Staff, 2014). Askecksy loamy sand (0-2%) and Manahawkin muck (frequently flooded) are considered to be poorly drained and very poorly drained, respectively (USDA Soil Survey Staff, 2014).

At the SWRC site, the soil series was classified by the USDA Web Soil Survey to be a Hatboro silt loam (frequently flooded) (USDA Soil Survey Staff, 2014). The typical profile of the Hatboro silt loam is Ap - 0 to 9 inches: silt loam; Bg - 9 to 44 inches: silt loam; Cg - 44 to 56 inches: sandy clay loam; and C - 56 to 70 inches: stratified gravelly sand to clay. The average pH of the Hatboro silt loam as described by the USDA Web Soil Survey is 6.0 (moderately acid) (USDA Soil Survey Staff, 2014).

Table C.1: Locations and site descriptions of soil samples from the Great Cypress Swamp in Frankford, DE, (GCS1 and GCS2) and Stroud Water Research Center in Avondale, PA (SWRC). Asterisks (*) indicate the field-oxidized soil samples.

Site	Sample Number	GPS Coordinates / Soil Series	Standing Water Depth (in)	Distance from Drained Soils (in)	Total Length of Soil (in)
GCS1	1	38.476120, -75.317215 ·Askecksy loamy sand, 0-2% slopes; ·Manahawkin muck, frequently flooded	7	126	41.0
	2		5	70	33.5
	3		7	114	34.5
	4		4	66	37.0
	5		9	144	35.5
GCS2	1	38.476604, -75.316078 ·Askecksy loamy sand, 0-2% slopes; ·Manahawkin muck, frequently flooded	5	70	41.0
	2*		3	52	39.5
	3*		5	30	32.0
	4		7	150	35.5
	5		9	150	34.0
SWRC	1*	39.870141, -75.785846 ·Hatboro silt loam, frequently flooded	N/A	N/A	5.0
	2*		N/A	N/A	5.0
	3*		N/A	N/A	5.0

REFERENCES

- Borggaard, O.K. Phase identification by phase dissolution techniques, In *Iron in soils and clay minerals*, Stucki, J.W., Ed. Reidel: Dordrecht, the Netherlands, 1988. p. 83-98.
- Jackson, M.L. *Soil chemical analysis – Advanced course*. University of Wisconsin, Madison, WI, 1969.
- Jackson, M.L.; Lim, C.H.; Zelazny, L.W. Oxides, hydroxides, and aluminosilicates. In *Methods of Soil Analysis. Part 1 Physical and Mineralogical Chemical Methods*, 2nd ed., Klute, A., Ed. American Society of Agronomy: Madison, WI, 1986. p. 101-150
- Loeppert, R.H.; Inskeep, W.P. Iron. In *Methods of Soil Analysis. Part 3 Chemical Methods*. Sparks, D.L., Ed. American Society of Agronomy: Madison, WI, 1996. p. 639-664
- McKeague, J.A.; Day, J.H. Dithionite- and oxalate-extractable Fe and Al as aids in differentiating various classes of soils. *Can. J. Soil Sci.*, **1966**, 46:13-22; DOI 10.4141/cjss66-003.
- Mehra, O.P.; Jackson, M.L. Iron oxide removal from soils and clays by a dithionite-citrate system buffered with sodium bicarbonate, In *Clays and Minerals*. Proceedings of the 7th National Congress: Pergamon: London, 1960.
- Schwertmann, U. The differentiation of iron oxide in soils by a photochemical extraction with acid ammonium oxalate. *Z. Pflanzenernähr. Düng. Bodenkd.*, **1964**, 105:194-201.
- Soil Survey Staff, Natural Resources Conservation Service, United States Department of Agriculture. 2014. Web Soil Survey. <http://websoilsurvey.nrcs.usda.gov/>. Accessed 6 May 2014.
- USEPA (U.S. Environmental Protection Agency). Method 6010C: Inductively Coupled Plasma-Atomic Emission Spectrometry. Washington, DC: USEPA, Office of Solid Waste, 2007.

Whittig, L.D.; Allardice, W. R. X-ray diffraction techniques. In *Methods of Soil Analysis. Part 1 Physical and Mineralogical Methods*, 2nd ed., Klute, A., Ed. American Society of Agronomy: Madison, WI, 1986. pp. 331-362.